



FACULTY OF SCIENCE AND TECHNOLOGY

MASTER'S THESIS

Study programme / specialisation: Petroleum Geosciences Engineering	The <i>(spring/autumn)</i> semester, <i>(year)</i> Spring 2023 Open
Author: Stine Aarthun Andreassen	
Supervisor at UiS: Christopher Townsend	
Thesis title: Testing the impact of standard geomodelling techniques	
Credits (ECTS): 30	
Keywords: Geomodelling Experimental design Parameter impact Petrel	Pages: 133 + appendix: 26 Stavanger, 15.06.23

Copyright
by
Stine Aarthun Andreassen
2023

Testing the impact of standard geomodelling techniques

by

Stine Aarthun Andreassen

Master thesis

Presented to the Faculty of Science and Technology

University of Stavanger

June 2022

Acknowledgements

First, I would like to express my sincere gratitude to my supervisor Chris Townsend for his expertise and guidance throughout this semester and thesis. For his suggestions, valuable feedback and answers to my many questions, it has been highly appreciated.

Further I would like to thank my classmates for the last five years. The time at the University would not have been the same without you.

Finally, I would like to thank my biggest supporters, my family. I could not have done this without your love or support during my time as a student.

Abstract

Geomodelling is an important tool in the oil and gas industry, it gives a visual 3D representation of the subsurface. In order to construct a 3D representation of the subsurface a comprehensive building process is required, and several modelling techniques is used. If these modelling techniques are not followed strictly, it can have significant impact on volume calculations. The construction of two geologically different models and several complex workflows will test the impact of standard and non-standard modelling techniques used for permeability, porosity, and water saturation to see the impact on the volume calculations, specifically pore volume, HCPV oil, HCPV gas, STOIP and GIIP. Different input parameters will be tested in Petrel using a full-factorial experimental design setup, and then compare the experiment models to the real-case models. The parameters tested are layering, the nr. of wells, most of vs. mid-point pick, vertical proportion curve (VPC), bias to facies on vs. off, Sequential Gaussian simulation (SGS) vs. Kriging, variogram range for porosity and permeability, with vs. without depth trend, the correlation coefficient for permeability, normal vs. asymmetric distribution and the saturation height function. The findings show that the tested parameters do have an impact on the calculated volumes. The impact varies from model to model and from parameter to parameter, and some parameters have a larger impact than others.

List of Abbreviations

Exp.	Experiment
GIIP	Gas initially in place
GOC	Gas oil contact
HCPV gas	Hydrocarbon pore volume gas
HCPV oil	Hydrocarbon pore volume oil
Nr.	Number
OWC	Oil water contact
Perm	Permeability
Por	Porosity
STOIIP	Stock tank oil initially in place
Sw	Water saturation
Vs.	Versus
VPC	Vertical Proportion Curve

Table of Contents

1. Introduction	1
1.1 Aim and Objectives	2
1.2 Geomodelling	3
1.3 Experimental Design	4
1.4 Workflows	6
2. Methodology	8
3. The Original Models	10
3.1 Model 1 (Fluvial).....	10
3.2 Model 2 (Turbidite).....	25
4. The Reservoir Models	31
5. The Experiments	34
5.1 Experiment set up.....	34
5.2 The Workflows.....	36
5.3 The Parameters	49
6. Results	52
6.1 Original Models vs. Experiment Models	53
6.2 Parameter Analysis.....	56
6.2.1 Model 1	56
6.2.2 Model 2A.....	59
6.2.3 Model 2B.....	61
6.3 Parameter Impact on STOIP and GIIP.....	63
6.4 Nr of Wells for Models 2A and 2B	64
6.4.1 Model 2A – 1 Well.....	65
6.4.2 Model 2A – 3 Wells	67
6.4.3 Model 2B – 1 Well.....	69

6.4.4 Model 2B – 3 Wells	71
6.4.5 Comparison tables for STOIP and GIIP for 1 Well and 3 Wells.....	73
6.5 Parameter Interactions.....	75
6.6 Comparing Models Results	76
7. Discussion	78
7.1 Real Cases (Original Models) vs. Reservoir Cases (Experiment Models)	78
7.2 The Models: Differences and Similarities.....	80
7.3 Parameter Analysis of STOIP and GIIP	82
7.4 Number of Wells Issue in Model 2A and 2B	83
7.5 Interaction Between Two Parameters	83
7.6 Other Remarks.....	84
8. Conclusion.....	85
9. References	87
Appendix	90
Appendix A	90
A.1 - Model 1 (Fluvial) parameter tables with sum, min, max, and avg	90
A.2 - Model 2A (Turbidite) parameter tables with sum, min, max, and avg.....	95
A.3 - Model 2B (Turbidite) parameter tables with sum, min, max, and avg	100
Appendix B	106
B.1 - Model 1 (Fluvial) Tornado plots of the impact of bulk volume, net volume, pore volume, HCPV oil, HCPV gas, STOIP, and gas on each parameter	106
B.2 - Model 2A (Turbidite) Tornado plots of the impact of bulk volume, net volume, pore volume, HCPV oil, HCPV gas, STOIP, and gas on each parameter	109
B.3 - Model 2B (Turbidite) Tornado plots of the impact of bulk volume, net volume, pore volume, HCPV oil, HCPV gas, STOIP, and gas on each parameter	113

List of Figures

Figure 1: Examples of fractional and full factorial setups for experimental design experiments (Allen 2020).	5
Figure 2: The planning process of an experimental design setup, modified from (Hanrahan et al. 2005).....	6
Figure 3: Workflow stages and components (ProcessStreet 2023).....	6
Figure 4: The study workflow of this thesis.....	8
Figure 5: Sketches of the conceptual models.....	9
Figure 6: Illustrates the building process for the two models step by step. It should be noted that Step 2 is only required for Model 1, as Model 2 does not include any faults. Step 10 involves constructing the porosity, permeability, and water saturation values for the models.	10
Figure 7: Steps in the construction of the polygon fault sticks.	11
Figure 8: How to open the spreadsheet.	11
Figure 9: The steps needed to convert the polygon fault sticks into actual faults sticks and how to merge the sticks to one fault.....	12
Figure 10: A is the procedure for constructing the grid boundary is depicted, along with an image of the completed boundary. B demonstrates the process of introducing points and identifying the fault blocks.....	12
Figure 11: How to make a surface. The “Main input” uses the points to make a surface, and it is important to insert the boundary into “Boundary”.	13
Figure 12: A is the original output of the top surface, while B depicts the desired appearance of the surface after eliminating the unnecessary parts.	14
Figure 13: 1. Illustrates how to eliminate the parts that do not belong to the layer. 2. Shows how to merge the different section surfaces into one surface. To remove specific parts of the surfaces it is necessary to create boundaries around each section and insert them into "The boundary" in the Step 1 window. Similarly, while combining the surfaces, it is crucial to add the newly merged surfaces into "Surface B" in the "Surface-Surface operations" folder.....	14
Figure 14: Shows how to create a 3D grid. It is important to check off “Make zig-zag type faults”.	15
Figure 15: 1. indicates where to add horizons, while 2. shows how to convert the horizons to points. A show the final horizons and B illustrates the horizons as points.	16

Figure 16: Illustrates how to create zones and layers, and shows which inputs are used.	17
Figure 17: Shows how to create the zone and segment index. A is an image of the zones while B is an image of the segments of the model.	17
Figure 18: Show the settings for facies modelling.	18
Figure 19: The facies model.	19
Figure 20: Shows the settings for the petrophysical modelling for porosity.	20
Figure 21: The Petrel calculator with the formulas used to create the porosity model with depth trend, the permeability model, and the water saturation model.	20
Figure 22: The porosity model with depth trend (A), the porosity model without depth trend (B), the permeability model (C), and the water saturation model (D).	21
Figure 23: The setting for the oil-water contact and the gas-oil contact, as well as the depths of the contacts. This process generates a contact set.	22
Figure 24: The construction of the contacts model using geometrical modelling and selecting “contacts,” and inserting the contact set created from the previous step.	22
Figure 25: The volume calculation process showing how to import the OWC and GOC as well as where to input Bo/Bg, net to gross and porosity.	23
Figure 26: How to create a well folder and the wells, and an image of the placement of the wells.	24
Figure 27: A shows how to make the logs using the settings for each well (check off the desired logs) and B displays the well logs and the 6 wells.	24
Figure 28: The workflow for Model 1 (Fluvial).	25
Figure 29: 1. Indicates how to define a model, 2. describes how to set up a boundary using “add points to polygon”, and 3. shows how to setup the points. B shows the points that will be used to construct the surfaces, while A shows the points and their depths in a 3D view.	26
Figure 30: The surfaces of Model 2.	26
Figure 31: A illustrates the zones, while B shows the segment of the model.	27
Figure 32: The method used in the turbidite modelling process, and how to edit and move the point to the desired positions.	28
Figure 33: The facies in Model 2.	28
Figure 34: The porosity model without depth trend (A), the porosity model with depth trend (B), the permeability model (C), and the water saturation model (D).	29
Figure 35: The contact model, red is the gas zone, green is the oil zone, and blue is the water.	29
Figure 36: Model 2’s workflow.	30

Figure 37: Layering for the coarser reservoir models. 0,60 is used as input for both models.	31
Figure 38: How to upscale the well logs by using “Create new”. The red box indicates where the desired logs are selected.	32
Figure 39: How to run the petrophysical modelling for the upscaled logs.	33
Figure 40: The different grids, their names, and contents for both models.	33
Figure 41: The experimental design set up with 1’s and -1’s.	35
Figure 42: The first line of the master workflow saves the project, while lines 2 and 3 assign the volumes created to a designated folder and removes the contents of the workflow if rerun. Lines 4 to 7 specify the location and naming conventions of the files on the computer. Lines 8 and 9 loads the files into Petrel in the Workflow and License tabs, respectively. Lines 11 to 17 execute the various workflows in a predefined loop, while line 18 saves the project when the run is complete.	37
Figure 43: Shows the License and Workflow tabs in Petrel. They are located in the “Output sheet” as shown with red boxes.....	37
Figure 44: The Read Data workflow. Lines 1 to 12 show the prop names for each parameter, what sheet Petrel needs to use (License), and which row and column to use from the experimental design setup from Figure 43. Line 14 starts the process of an if, else, and end statement of loading the assigned set values, which are also given prop names. This process needs to be set up for the 11 tested parameters, but Model 2 does not use VPC hence why it is shaded in this figure.	38
Figure 45: The Structure workflow where the first parameter, layering, is tested. The figure shows where to input the parameter in the “Layering” window. The window is opened by double-clicking on the “Layering” tab in the workflow.	39
Figure 46: The facies properties for each of the two models. Their names indicate the high (H) or low (L) values used for those particular facies’ models.....	40
Figure 47: The Facies workflow. Line 1 loads the 3D grid, lines 2 to 10 give the facies calculator names and the facies are inserted, and lines 12 to 19 are if/end statements where the parameters are tested. Lines 12 to 19 contain “Scale up well logs” which upscales the logs, “Facies modelling” which performs the facies modelling process, and a “Property calculator” which inserts the facies that is modelled to the FaciesTot model so that there are not thousands of facies models created. The resulting model will then always be shown in the FaciesTot model.	41
Figure 48: The “Scale up well logs” and “Facies modelling” windows. In the scale-up window number of wells is selected in the “Wells” setting as well as either most of or mid-	

point pick in the “Average method” setting. In the facies window the “Method for zone/facies” is selected and the active lithologies are moved to the right. 42

Figure 49: Vertical proportion curve off (A) or on (B) in the “Data Analysis” window..... 43

Figure 50: The Petrophysical workflow. Line 1 loads the 3D grid, lines 2 to 34 give calculator names and the porosity and permeability models are inserted using the blue arrows, and line 40 starts the if/end statements where the parameters are tested. Lines 40 to 53 contain “Scale up well logs” which upscales the logs, “Petrophysical modelling” which performs the petrophysical modelling process, and a “Property calculator” which inserts the porosity and permeability that is modelled to the PorTot and PermeabilityTot model so that there are not thousands of por/perm models created. The resulting model will then always be shown in the PorTot and PermeabilityTot model. 44

Figure 51: The porosity and permeability models for Model 1 and Model 2. Their names indicate the high (H) or low (L) values used for that particular model..... 44

Figure 52: The well log upscaling of porosity and permeability. In the upscaling of porosity, the “Use bias” is either on or off depending on the porosity model name BH (on) or BL (off) as marked with a red box. The upscaling of both porosity and permeability uses Arithmetic as the “Average method”. The permeability upscaling process does not use “Use bias”. 45

Figure 53: The petrophysical modelling process of the porosity with SGS as “Method for zone/facies”. In the Variogram tab, the variogram range parameter is tested by inserting \$VAL_Var to the “Anisotropy range” for Major dir. and Minor dir. Under the “Distribution” tab the “Seed number” is set to \$Seed+10 for sand, \$Seed+20 for fine sand and \$Seed+30 for the sand in the next zone. 46

Figure 54: The petrophysical modelling process for permeability with SGS “Method for zone/facies”. In the Variogram tab, the variogram range parameter is tested by inserting \$VAL_Var to the “Anisotropy range” for Major dir. and Minor dir. Under the Distribution tab the “Seed number” is set to \$Seed+40 for the fine sand, \$Seed+50 for sand and \$Seed+60 for the sand in the next zone. In the Co-kriging tab, the correlation coefficient is tested by inserting \$VAL_CC to the “Collocated co-kriging” setting, and the corresponding porosity model to the permeability is inserted to the “Volumes” setting..... 46

Figure 55: The petrophysical modelling process for porosity and permeability when the “Method for zone/facies” is Kriging and where to insert \$VAL_Var for variogram range and VAL_CC for collocated co-kriging..... 47

Figure 56: The Data Analysis for porosity and permeability with depth trend and normal distribution. A show the data analysis for permeability, and it uses “Logarithmic” for depth

trend and has a normal score. To achieve normal score, one has to select “Estimate” twice and then the settings marked with two small red boxes. B shows the data analysis for porosity with directional data trend (depth trend) and it is important to select the distorted cube in the Z direction in the “Coordinate system”, and C shows the normal score distribution for porosity.

.....	47
Figure 57: The Data Analysis for porosity (A) and permeability (B) with asymmetric distribution and no depth trend. For asymmetric distribution, the “Estimate” button is selected twice, and then the “mountain” button is used as marked with a little red box.	48
Figure 58: The volume workflow.	48
Figure 59: Real-case volumes compared to P10-P90 for Model 1. The real-case values are shown with a red dot.	55
Figure 60: Real-case volumes compared to P10-P90 for Model 2A. The real-case values are shown with a red dot.	55
Figure 61: Real-case volumes compared to P10-P90 for Model 2B. The real-case values are shown with a red dot.	55
Figure 62: Tornado plot for the % difference in pore volume for Model 1. The % difference values are taken from Table 14.	57
Figure 63: Tornado plot for the % difference in HCPV oil for Model 1. The % difference values are taken from Table 14.	57
Figure 64: Tornado plot for the % difference in HCPV gas for Model 1. The % difference values are taken from Table 14.	57
Figure 65: Tornado plot for the % difference in STOIP for Model 1. The % difference values are taken from Table 14.	58
Figure 66: Tornado plot for the % difference in GIIP for Model 1. The % difference values are taken from Table 14.	58
Figure 67: Tornado plot for the % difference in pore volume for Model 2A. The % difference values are taken from Table 15.	59
Figure 68: Tornado plot for the % difference in HCPV oil for Model 2A. The % difference values are taken from Table 15.	59
Figure 69: Tornado plot for the % difference in HCPV gas for Model 2A. The % difference values are taken from Table 15.	60
Figure 70: Tornado plot for the % difference in STOIP for Model 2A. The % difference values are taken from Table 15.	60

Figure 71: Tornado plot for the % difference in GIIP for Model 2A. The % difference values are taken from Table 15.	60
Figure 72: Tornado plot for pore volume Model 2B. The % difference values are taken from Table 16.....	61
Figure 73: Tornado plot for HCPV oil Model 2B, The % difference values are taken from Table 16.....	61
Figure 74: Tornado plot for HCPV gas Model 2B. The % difference values are taken from Table 16.....	62
Figure 75: Tornado plot for STOIIP Model 2B. The % difference values are taken from Table 16.....	62
Figure 76: Tornado plot for GIIP Model 2B. The % difference values are taken from Table 16.....	62
Figure 77: Tornado plot for the % difference in pore volume for Model 2A with 1 well.	65
Figure 78: Tornado plot for the % difference in HCPV oil for Model 2A with 1 well.	65
Figure 79: Tornado plot for the % difference in HCPV gas for Model 2A with 1 well.	66
Figure 80: Tornado plot for the % difference in STOIIP for Model 2A with 1 well.....	66
Figure 81: Tornado plot for the % difference in GIIP for Model 2A with 1 well.	66
Figure 82: Tornado plot for the % difference in pore volume for Model 2A with 3 wells.....	67
Figure 83: Tornado plot for the % difference in HCPV oil for Model 2A with 3 wells.....	67
Figure 84: Tornado plot for the % difference in HCPV gas for Model 2A with 3 wells.....	68
Figure 85: Tornado plot for the % difference in STOIIP for Model 2A with 3 wells.	68
Figure 86: Tornado plot for the % difference in GIIP for Model 2A with 3 wells.....	68
Figure 87: Tornado plot for the % difference in pore volume for Model 2B with 1 well.	69
Figure 88: Tornado plot for the % difference in HCPV oil for Model 2B with 1 well.....	69
Figure 89: Tornado plot for the % difference in HCPV gas for Model 2B with 1 well.	70
Figure 90: Tornado plot for the % difference in STOIIP for Model 2B with 1 well.....	70
Figure 91: Tornado plot for the % difference in GIIP for Model 2B with 1 well.....	70
Figure 92: Tornado plot for the % difference in pore volume for Model 2B with 3 wells.....	71
Figure 93: Tornado plot for the % difference in HCPV oil for Model 2B with 3 wells.	71
Figure 94: Tornado plot for the % difference in HCPV gas for Model 2B with 3 wells.....	72
Figure 95: Tornado plot for the % difference in STOIIP for Model 2B with 3 wells.	72
Figure 96: Tornado plot for the % difference in GIIP for Model 2B with 3 wells.	72
Figure 97: The facies statistics for Model 2A and shows that there is a sampling issue when using only 1 or 3 wells.	74

Figure 98: The Real-Case Model Facies and Porosity vs. the Experiment Model Facies and Porosity..... 79

List of Tables

Table 1: Lithologies and porosity values for Model 1 (Fluvial).	9
Table 2: Lithologies and porosity values for Model 2 (Turbidite).....	9
Table 3: The depths of each layer in their section.....	15
Table 4: Lists the different methods, settings, layouts, sections, levees, and trends used to run the facies modelling process.	18
Table 5: The depths and segmetns for the OWC and GOC.	21
Table 6: The X and Y locations of the wells.....	24
Table 7: Lists the methods, facies and geometry used to run the facies modelling for the turbidite system, the shale and the sandstone base.....	27
Table 8: The depths of the OWC and GOC for Model 2.	29
Table 9: The X and Y position of the three wells.	30
Table 10: The assigned values for all the parameters in the experimental design setup.....	35
Table 11: The real-case data vs. the experiment data from Model 1.	54
Table 12: The real-case data vs. the experiment data from Model 2A.	54
Table 13: The real-case data vs. the experiment data from Model 2B.....	54
Table 14: A summary table of the % difference of average high and average low for each parameter in Model 1 on pore volume, HCPV oil, HCPV gas, STOIP, and GIIP.	56
Table 15: A summary table of the % difference of average high and low for each parameter in Model 2A on pore volume, HCPV oil, HCPV gas, STOIP, and GIIP.....	59
Table 16: A summary table of the % difference of average high and low for each parameter in Model 2B on pore volume, HCPV oil, HCPV gas, STOIP, and GIIP.....	61
Table 17: The parameter impact on STOIP and GIIP for all three models, they are ranked from most to least importance. Abbreviations are used in this table; bias to facies (BtF), normal vs. asymmetric distribution (NA), depth trend (DT), nr of wells (W), SGS vs. Kriging (SK), saturation height function (SHF), correlation coefficient (CC), layering (LAY), vertical proportion curve (VPC), variogram range (VR), and most of vs. mid-point pick (MM). X* in Model 2A and 2B indicates that there is no VPC in those models.	64
Table 18: A summary table of the difference of average high and low for each parameter on pore volume, HCPV oil, HCPV gas, STOIP, and GIIP for 1 well in Model 2A.....	65
Table 19: A summary table of the difference of average high and low for each parameter on pore volume, HCPV oil, HCPV gas, STOIP, and GIIP for 3 wells in Model 2A.	67

Table 20: A summary table of the difference of average high and low for each parameter on pore volume, HCPV oil, HCPV gas, STOIP, and GIIP for 1 well in Model 2B.	69
Table 21: A summary table of the difference of average high and low for each parameter on pore volume, HCPV oil, HCPV gas, STOIP, and GIIP for 3 wells in Model 2B.	71
Table 22: Comparison of STOIP and GIIP for 1 well vs. 3 wells for Model 2A.	73
Table 23: Comparison of STOIP and GIIP for 1 well vs. 3 wells for Model 2B.	73
Table 24: Parameter interaction impact of bias to facies and normal vs. asymmetric distribution on Model 1.	75
Table 25: The impact of each parameter on STOIP and GIIP ranked in a high, medium and low order for all models.	76
Table 26: Comparison of Model 2A with 1 well and 3 wells. Where STOIP and GIIP are ranked in a high, medium and low order for all models.	77
Table 27: Comparison of Model 2B with 1 well and 3 wells. Where STOIP and GIIP are ranked in a high, medium and low order for all models.	77
Table 28: Real-Case model data vs. the most “correct” and “incorrect” model data for Models 2A and 2B.	81

1. Introduction

The oil and gas industry requires a vast amount of information and data to effectively explore and produce oil and gas fields. This information includes seismic data, well logs, core samples, and geochemical data, among others. Geoscientists use this data to develop geological models, which are 3D grid representations of geological structures. These grids are populated properties that represent geological features such as layers, faults, lithologies/facies, petrophysical values, and other relevant geological structures. Software programs, such as Petrel and RMS, create 3D models where the models are based on seismic interpretations, wells, other field data, and geological concepts. The data used in Petrel and RMS is commonly used to convert geological maps or gathered data into 3D models (Wellmann et al. 2019).

Geological models offer a digital representation of the subsurface, including its structures, formations, lithologies, and facies. The models are usually constrained by real input data (including wells), with inter-well representations that are constrained by the use of geological conceptual models which helps build realistic configurations. In this thesis, conceptual models will be constructed and used for the experiments using Petrel software (Thornton, Mariethoz, and Brunner 2018). Petrel provides a comprehensive range of tools to solve complex stratigraphic and structural problems. Usually, the focus of these models is creating realistic input for reservoir simulation and volumetric estimates. The problems these models address can range from regional exploration to reservoir development studies. Petrel allows geoscientists to conduct geological workflows from seismic and stratigraphic interpretation to geocellular property modelling and production simulation (Schlumberger 2023a).

In geomodelling, the modeller often uses workflows when constructing models. There are many options available on how to set up a workflow, but even though there is a “standard” workflow. In practice, not all geomodels are built to the standard which is thought to be due to a lack of detailed knowledge and experience among industry practitioners.

This thesis will involve the construction of two different models which will test the impact of standard and non-standard modelling techniques used for permeability, porosity, and water saturation on volume calculations. Different input parameters will be tested in Petrel using an

experimental design setup, and then compared to the real-case model. Standard modelling techniques in the oil and gas industry are not always strictly followed, which may influence the resulting geological models and their volumes. This can lead to miscalculations in the simulation of oil and gas reserves and, consequently, affect investment decisions. Non-stationary states in the model input data may also significantly impact these calculations because models are not always run in a non-stationary state. Therefore, this thesis aims to determine the impacts of different input parameters by conducting several experiments on the constructed models.

1.1 Aim and Objectives

The objective of this thesis and research is to construct a series of model scenarios to examine the effects of standard modelling techniques and missing out on specific steps in the modelling process, to establish their influence on permeability, porosity, and water saturation and their subsequent impact on volume calculations. A sensitivity analysis of geological models with respect to specific parameters will be executed to evaluate the significance of each parameter and quantify its impact, utilizing an experimental design methodology, and comparing the results with the real-case models. The study will include two distinct conceptual models in order to confirm if the parameter impacts are possibly universal or case-specific.

The main objectives for the thesis are:

- Do we represent real reservoir volumetrics in our geological models by comparing the modelled results with the real-case model?
- What effect do the changes in parameters, standard modelling techniques, have on the output of permeability, porosity, water saturation, and volume calculations?
- Which parameters have the largest and smallest impact on volume calculations?
- When does the greatest impact on permeability, porosity, water saturation, and volume calculations occur?
- In the case where several parameters have not been modelled correctly what is the cumulative effect on volume calculations?

- Determine if the results are case-specific or if they could be universal across several different geological situations.

1.2 Geomodelling

Geomodelling, the creation, and understanding of a three-dimensional (3D) digital representation of the subsurface geology of a specific area is a fundamental tool and process in the earth sciences, and geomodelling has been used in the industry for over 20 years. The process integrates various types of geological data, such as seismic data, conceptual models, well logs, and cores, to build a 3D model that can be analysed and visualized to better understand the subsurface and its geological structures. The resulting model can be used to simulate geological processes and make predictions about behaviour over time (Mallet 2002; Pyrcz and Deutsch 2014; Wellmann and Caumon 2018; Wellmann et al. 2019).

The use of geological models is not limited to the oil and gas industry, as they also have wide-ranging applications in fields such as environmental assessment, mineral exploration, and groundwater management. They are utilized in decision-making processes to determine if the region is economically feasible for exploration, development, and production (Mallet 2002).

While geomodelling is an important tool, it is not without challenges and limitations. The accuracy of the 3D geological models depends on the quantity and quality of the data used in the construction of the model. Geological models are based on predicting and interpolating geological features for a modelled area with limited data. They also allow for uncertainties related to unknown inter-well locations and errors in the input data that occur throughout the modelling process (Frank, Tertois, and Mallet 2007; Li et al. 2023; Ortiz 2013).

Conceptual models are crucial in the geomodelling process, as they serve as a guide for realistic and robust models. The geoscientist or geologist should have a mental image of how the model and reservoir should look; the conceptual model is used to constrain the geomodel. The model building process consists of various steps with the main steps include developing a model concept, structural and stratigraphic framework with model elements, property modelling, upscaling, and handling modelling uncertainties (Ringrose and Bentley 2021).

The structural and stratigraphic framework of a reservoir model uses a combination of structural and stratigraphic inputs. The structural inputs are surfaces and faults interpreted from seismic data, while the stratigraphic inputs are used to define geological layers within the model. Building a model, especially a fault model, is a time-consuming process, and it is important to consider the stratigraphic inputs in the model, such as hierarchy and correlation. The model input elements are facies, lithofacies, facies associations, and genetic units (Ringrose and Bentley 2021).

Property modelling is a crucial step in the geomodelling process, as it forms the basis for engineering decisions and reservoir evaluation. As Ringrose and Bentley (2021) said, the purpose of building a reservoir model is “*to capture knowledge of the subsurface in a quantitative form in order to evaluate and engineer the reservoir*”. It is in the property modelling process that porosity, permeability, and water saturation models are built. The volume calculations, such as bulk volume, STOIP, and GIIP, are calculated after the property modelling process has been completed. Property modelling can be divided into three main processes: geometrical modelling, facies modelling, and petrophysical modelling (Schlumberger 2023b).

1.3 Experimental Design

Allen (2020) said, “*Experimental design is the fastest way to find out the most about a system*”. Experimental design involves the systematic planning of experiments in order to obtain the most relevant information with the least amount of time effort or resources. It is a method of controlling the effects of variation in factors and identifying which factors have the largest impact on the outcome. Instead of testing variables randomly, a specific set of high and low values are selected together for the tests. Different experimental designs can be utilized, such as testing one variable at a time, a fractional factorial design, or a full factorial design. In a full factorial design, all possible combinations of high and low values for each variable are tested, while in a one-at-a-time design, the variables are adjusted one at a time from the lowest value to the highest value but this setup is not very reliable (Allen 2020). See Figure 1 for a visual representation.

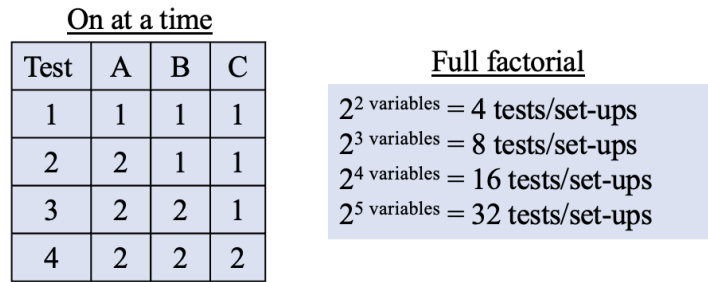


Figure 1: Examples of fractional and full factorial setups for experimental design experiments (Allen 2020).

In a full-factorial design, all the different parameter combinations are used. Therefore, the number of runs= 2^x , where x is the number of parameters to be investigated. Fractional factorial designs can also be used to increase the efficiency of an experiment whereby specific parameter combinations are selected (Allen 2020; Box, Hunter, and Hunter 2005). In this thesis, a full-factorial design was used. The model building and corresponding volume calculations ran relatively quickly and did not impose severe time restrictions even though 2048 runs were used for each experiment. If a one-at-a-time design had been used it would possibly have taken much longer and the reliability of the result would have been impacted, because it would be hard to keep track of which experiment is being run and mistakes could happen more easily.

Experimental design involves a systematic and objective approach to understanding and evaluating the factors or parameters that influence a system using statistical methods. The ultimate goal is to maximize precision and draw conclusions about the hypothesis being tested. It combines theoretical knowledge of experimental design with knowledge of the factors or parameters under investigation. The design setup is dependent on the number of factors or parameters being investigated and the experiment's objectives. The planning process of an experimental design is illustrated in Figure 2. (Hanrahan et al. 2005; Bell 2009; Box, Hunter, and Hunter 2005). This thesis will use a full factorial test with 2048 test/set-ups since there are 11 parameters being tested (2^{11} variables = 2048).

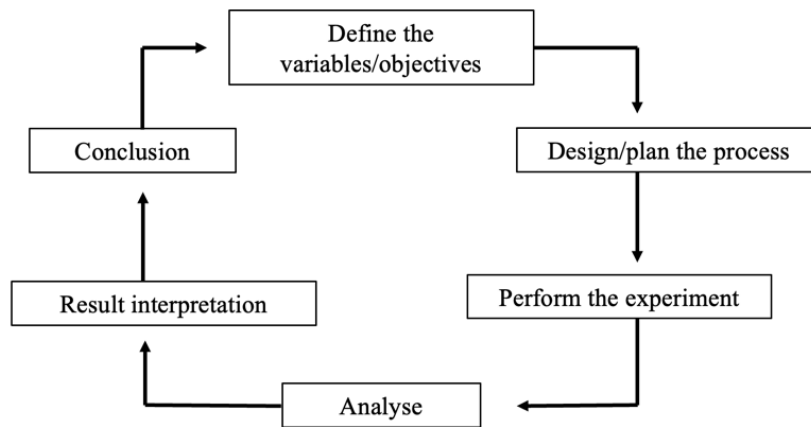


Figure 2: The planning process of an experimental design setup, modified from (Hanrahan et al. 2005).

1.4 Workflows

In the context of data processing, a workflow refers to a systematic process consisting of a set of interrelated tasks designed to guide data processing along a specific path from initiation to completion. The main purpose of a workflow is to facilitate the execution of a series of steps necessary to accomplish a specific objective. Workflows can be divided into different stages, and typically consist of three basic components: the trigger, the tasks, and the result (Fig. 3). These components are integrated and interconnected to form a cohesive workflow that can be used to efficiently and effectively process data (ProcessStreet 2023).

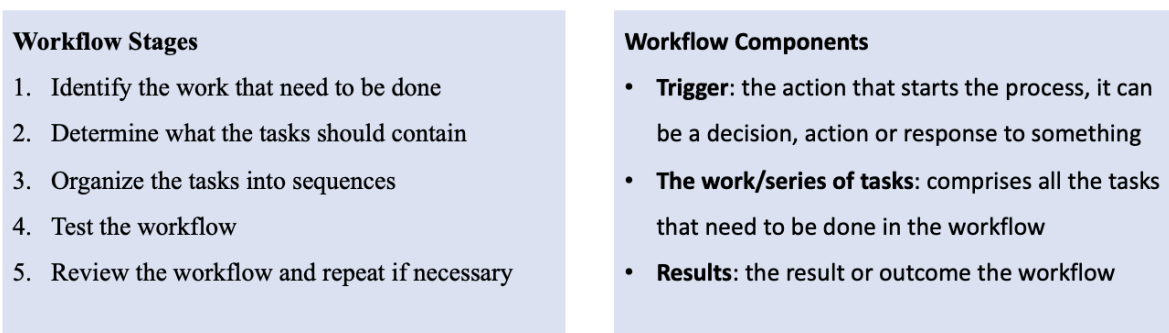


Figure 3: Workflow stages and components (ProcessStreet 2023).

In Petrel, a workflow is a series of stages and components that guide the processing of data in a specific path, from initiation to completion, similar to other workflows. Specifically, in Petrel, a workflow can describe and produce an entire geomodelling process, including

loading data, generating surfaces and horizons, performing structural and property modelling, calculating volumes, and closing desired loops. This workflow can be easily re-run and customized to fit the process that the modeller wants, such as running a geological model several times for testing a particular parameter or planning a well trajectory. A standard workflow in Petrel for geomodelling typically includes data import, seismic interpretation, well correlation, fault modelling, pillar gridding, horizons, zones and layering, geometrical modelling, log upscaling, facies modelling, petrophysical modelling, contacts modelling, and volume calculation. These stages allow for a comprehensive and efficient approach to geomodelling, which can be tailored to meet the specific objectives of the project (Petrofaq.org 2019; Schlumberger 2023b; Nemes 2022). Several workflows will be constructed for this thesis to test the impact of standard modelling techniques on porosity, permeability, water saturation, and volume calculations.

2. Methodology

This study uses an experimental design setup to analyse the impact of high and low values of various parameters on porosity, permeability, water saturation, and volume calculations. The workflow of the study is depicted in Figure 4. There are multiple steps needed to achieve the results, including constructing two Original Models and then two Reservoir Models from synthetic wells which are sampled from these Original Models. The Original Models are conceptual (synthetic) models and are based on different geological concepts.

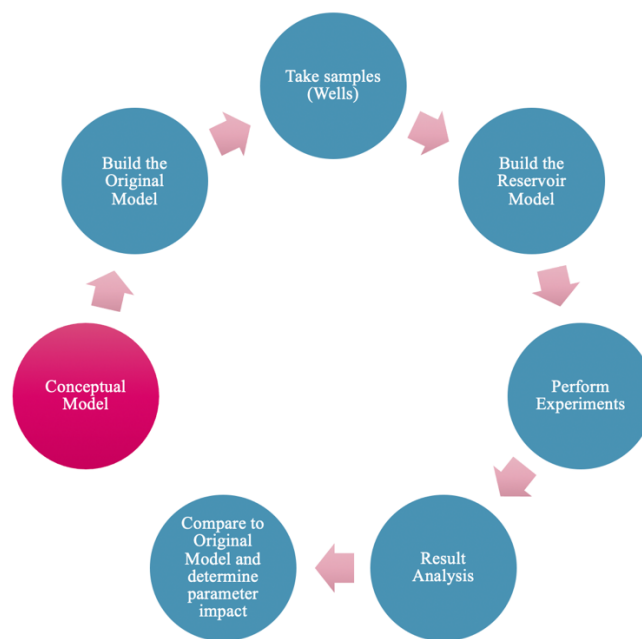


Figure 4: The study workflow of this thesis.

The two Original Models are very detailed and aim to represent possible real reservoir situations. The models are then sampled using synthetic wells, which in-turn are used as the input data to create typical oil-field Reservoir Models. The study will then compare the actual Reservoir Models with the Original Models. To begin the construction of the two models in Petrel conceptual models were first drawn for both of them (Fig. 5). Model 1 (Fluvial) was based on figures from Cao et al. (2021) and Mukhopadhyay, Mazumdar, and van Loon (2016), while the Model 2 (Turbidite) was based on figures from Huang (2018) and Vargas Grajales et al. (2020).

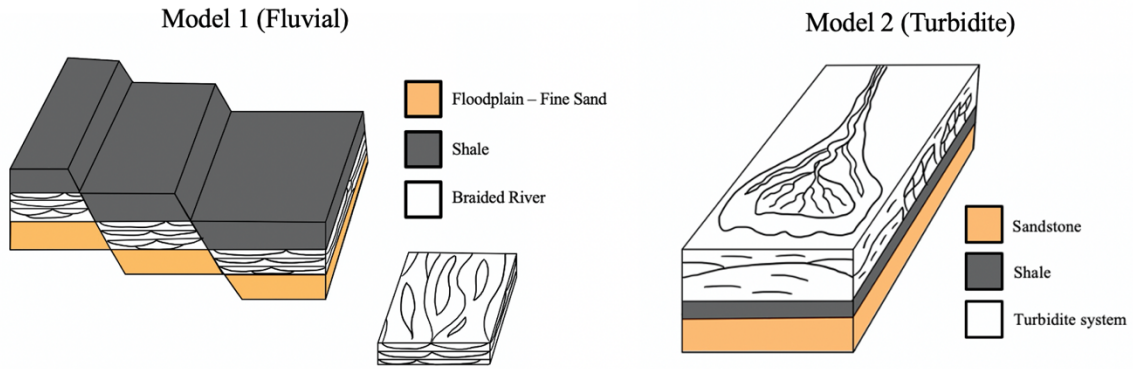


Figure 5: Sketches of the conceptual models.

Model 1 (Fluvial) consists of a braided river system with a shale top layer, a braided river in the middle, and a floodplain as the base. On the other hand, Model 2 (Turbidite) comprises a turbidite system as the top layer, a shale in the middle, and a sandstone base. Both models have assigned minimum and maximum porosity values, the values for Model 1 are listed in Table 1 and the values for Model 2 are in Table 2.

Zone	Lithology	Min	Max	Mean	Std
1. Top Shale	Shale	0.05	0.10	0.07	0.20
2. Braided River System	Fine sand	0.15	0.20	0.17	0.20
	Coarse sand	0.25	0.30	0.27	0.20
	Shale	0.05	0.10	0.07	0.20
3. Floodplain	Fine sand	0.15	0.20	0.17	0.20

Table 1: Lithologies and porosity values for Model 1 (Fluvial).

Zone	Lithology	Min	Max	Mean	Std
1. Turbidite System	Fine sand	0.20	0.30	0.25	0.20
	Sand	0.14	0.20	0.18	0.20
	Shale	0.03	0.09	0.05	0.20
2. Shale Layer	Shale	0.03	0.09	0.05	0.20
3. Base Sand	Sand	0.20	0.30	0.25	0.20

Table 2: Lithologies and porosity values for Model 2 (Turbidite).

The models' construction process is accomplished using Petrel's "Structural Modelling" and "Property Modelling" functionalities. Structural modelling involves building the structures of the models, including faults, while property modelling involves setting up the models' properties, such as facies modelling, petrophysical modelling, and geometrical modelling.

Geometrical modelling generates pre-defined system variables such as segment index, zone index, and contact property (Schlumberger 2023b). Various processes within the structural and petrophysical modelling will be utilized during the construction of the models. Figure 6 briefly summarizes the construction steps needed to develop the Original models for both the turbidite and fault models. These Original models are then used to create the Reservoir Models, which are utilized in the experimental design.

- | | |
|----------------------------|-----------------------------|
| 1. Define a Model | 8. Geometrical Modelling |
| 2. Create the Faults | 9. Facies Modelling |
| 3. Create a Boundary | 10. Petrophysical Modelling |
| 4. Make Surfaces | 11. Create Contacts |
| 5. Pillar Gridding | 12. Volume Calculations |
| 6. Make Horizons | 13. Create Wells |
| 7. Create Zones and Layers | 14. Set up Workflow |

Figure 6: Illustrates the building process for the two models step by step. It should be noted that Step 2 is only required for Model 1, as Model 2 does not include any faults. Step 10 involves constructing the porosity, permeability, and water saturation values for the models.

3. The Original Models

This section of the thesis will describe how the Original Models are constructed. The first model built is Model 1, which is a fluvial system that contains braided rivers. The second model is Model 2, and that model is a turbidite system that contains one turbidite fan. The construction of the models is a step by step process as Figure 6 lists.

3.1 Model 1 (Fluvial)

The initial step in constructing a model involves defining a model using the "Define model" function (Step 1 in Figure 6), followed by creating a polygon to establish the fault using "Add points to polygon" in a 3D window (Fig. 7) which indicated Step 2 in Figure 6. The polygon is duplicated four times to create four fault sticks. This process is then repeated to generate the second fault. As shown in Figure 8, the values for the x, y, and z directions of each

polygon fault stick are modified in the spreadsheet to match the conceptual model. This step may require some adjustment to properly align the fault sticks.

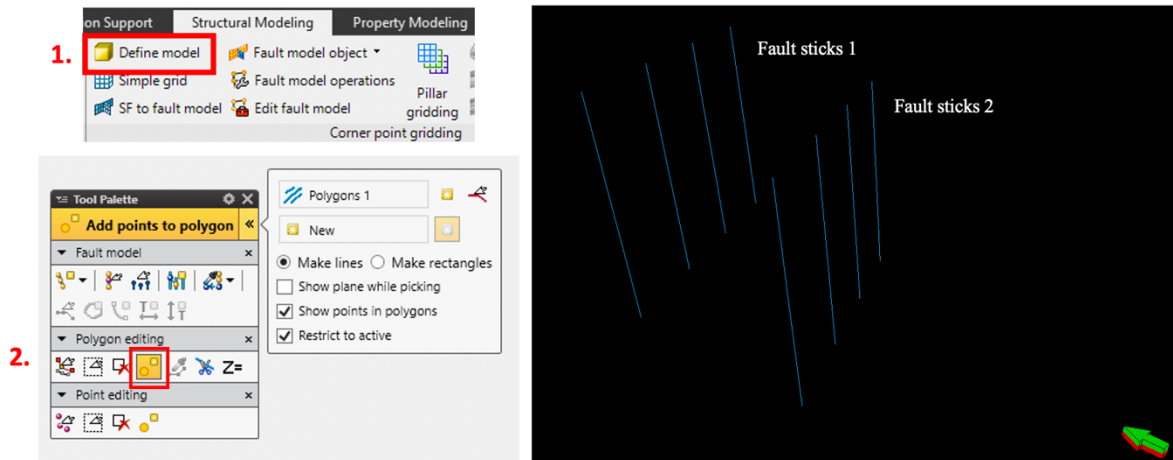


Figure 7: Steps in the construction of the polygon fault sticks.

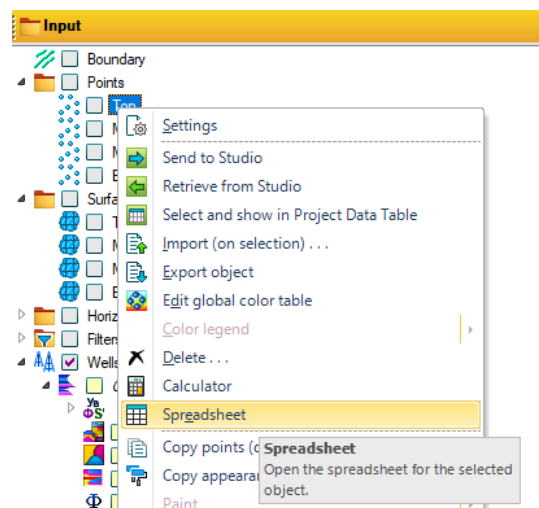


Figure 8: How to open the spreadsheet.

The polygon fault sticks were aligned and then converted to genuine fault pillars through the "Convert to fault sticks in fault model" function. Afterwards, they were combined into a single fault as illustrated in Figure 9. This procedure was executed for both faults.

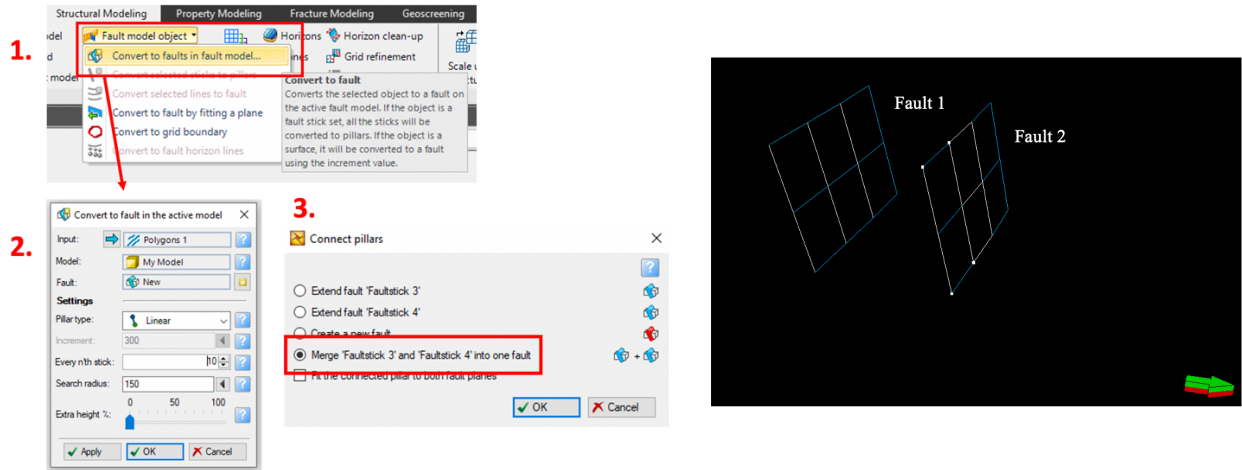


Figure 9: The steps needed to convert the polygon fault sticks into actual faults sticks and how to merge the sticks to one fault.

The subsequent phase, step 3 (Fig. 6), involves generating a boundary surrounding the pair of faults via the "Create external grid boundary" function, as illustrated in Figure 10A. It is critical to ensure that the faults extend beyond the boundary so that the model is sub-divided into separate compartments.

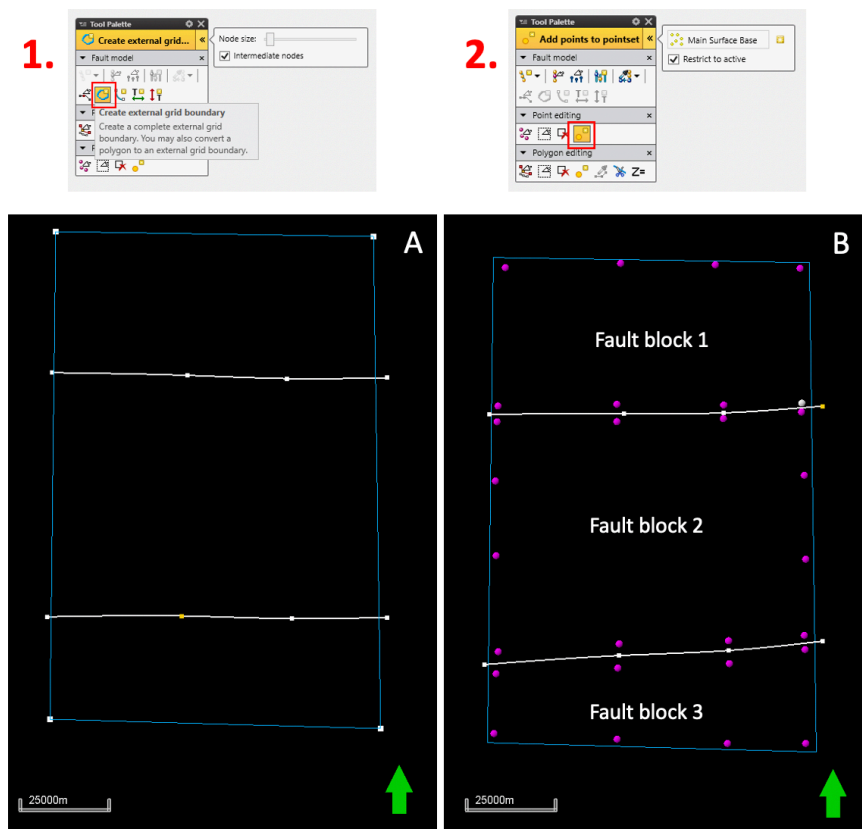


Figure 10: A is the procedure for constructing the grid boundary is depicted, along with an image of the completed boundary. B demonstrates the process of introducing points and identifying the fault blocks.

Seismic horizons were constructed by inserting points into each fault block, see Figure 10B. The depth of each point was edited in the spreadsheet, with a 500m difference in depth for each fault block. Specifically, fault block 1 is located at a depth of -1000m, fault block 2 at -1500m, and fault block 3 at -2000m. The points were then used as input to generate surfaces, using the “make surface option in Petrel utilizing points, polygons, interpretations, or wells tops. Step 4 (Fig. 6) is to create surfaces representing each horizon. Surfaces were created using the three point sets for each fault block from the prior step (Figure 11). The resulting surfaces are displayed in Figure 12A. It is necessary to remove the portions that don't pertain to each fault block and retain solely the fault block containing points. For instance, in fault block 1, the parts from fault blocks 2 and 3 should be eliminated, and so on. The correct surface can be seen in Figure 12B. This was accomplished by accessing the surface settings, navigating to operations, selecting "eliminate where," and then choosing "eliminate outside” (Fig. 13) This operation was repeated for each fault block of every layer.

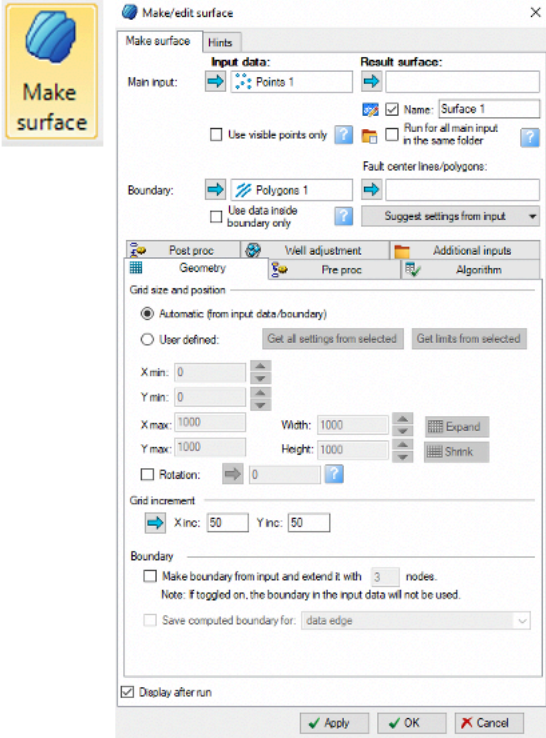


Figure 11: How to make a surface. The “Main input” uses the points to make a surface, and it is important to insert the boundary into “Boundary”.

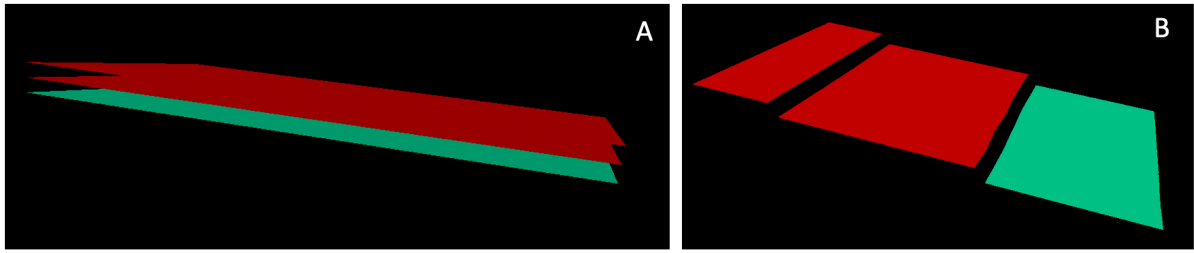


Figure 12: A is the original output of the top surface, while B depicts the desired appearance of the surface after eliminating the unnecessary parts.

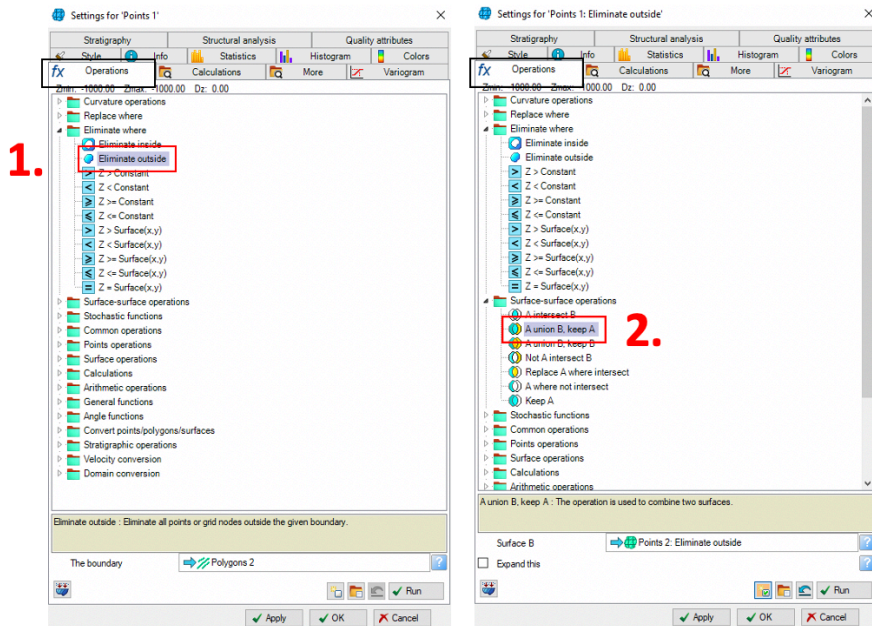


Figure 13: 1. Illustrates how to eliminate the parts that do not belong to the layer. 2. Shows how to merge the different section surfaces into one surface. To remove specific parts of the surfaces it is necessary to create boundaries around each section and insert them into "The boundary" in the Step 1 window. Similarly, while combining the surfaces, it is crucial to add the newly merged surfaces into "Surface B" in the "Surface-Surface operations" folder.

To create the combined surface, the individual fault block surfaces need to be merged, as illustrated in Figure 9. Firstly, section surface 1 should be merged with section surface 2, resulting in the combined section surface 1+2. Afterwards, the new combined section surface 1+2 should be merged with section surface 3 to form the combined surface. This merging process needs to be repeated three times, once for each of the horizons in the model. Copying the points from the first layer and adjusting the depths in the spreadsheet is the method used to accomplish this. To achieve this, the new points must be moved 500m downward, as shown in Table 3 and new surfaces need to be created and adjusted as the previous surface was.

Layer	Depth: Section 1	Depth: Section 2	Depth: Section 3
Top	-1000	-1500	-2000
Middle	-1500	-2000	-2500
Bottom	-2000	-2500	-3000
Base	-2500	-3000	-3500

Table 3: The depths of each layer in their section.

The model has 3 zones and therefore requires 4 horizons which are described further down. The 3 other surfaces were constructed in the same manner as the first surface, but they have different depths as outlined in Table 3.

The subsequent stage, step 5 (Fig. 6), is the implementation of pillar gridding, which establishes the framework for a 3D grid. To enable pillar gridding, the active fault model must be activated in a 2D window, and then the "Apply" and "OK" buttons should be clicked. This process generates a 3D grid, as depicted in Figure 14.

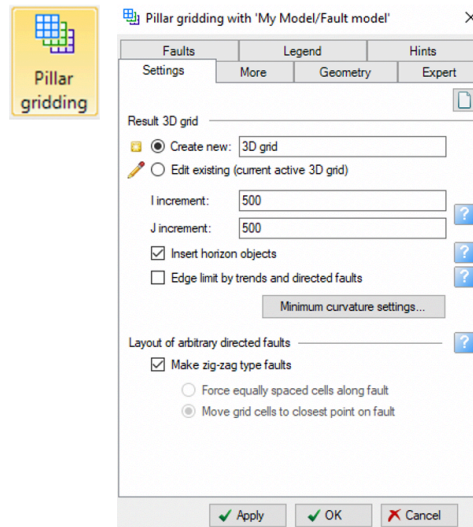


Figure 14: Shows how to create a 3D grid. It is important to check off "Make zig-zag type faults".

Once the 3D grid has been generated, the next step, step 6 (Fig.6), involves inserting the seismic horizons into the grid. To do so, select the "Horizons" tab, which will prompt a new window to appear. Initially, the horizons are created using the surfaces as input parameters. Later on, these horizons are converted to points to eliminate any unwanted points that cause unevenness in the horizons. After verifying that the horizon points appear satisfactory, new

horizons are constructed using these points. The procedure for creating horizons is illustrated in Figure 15.

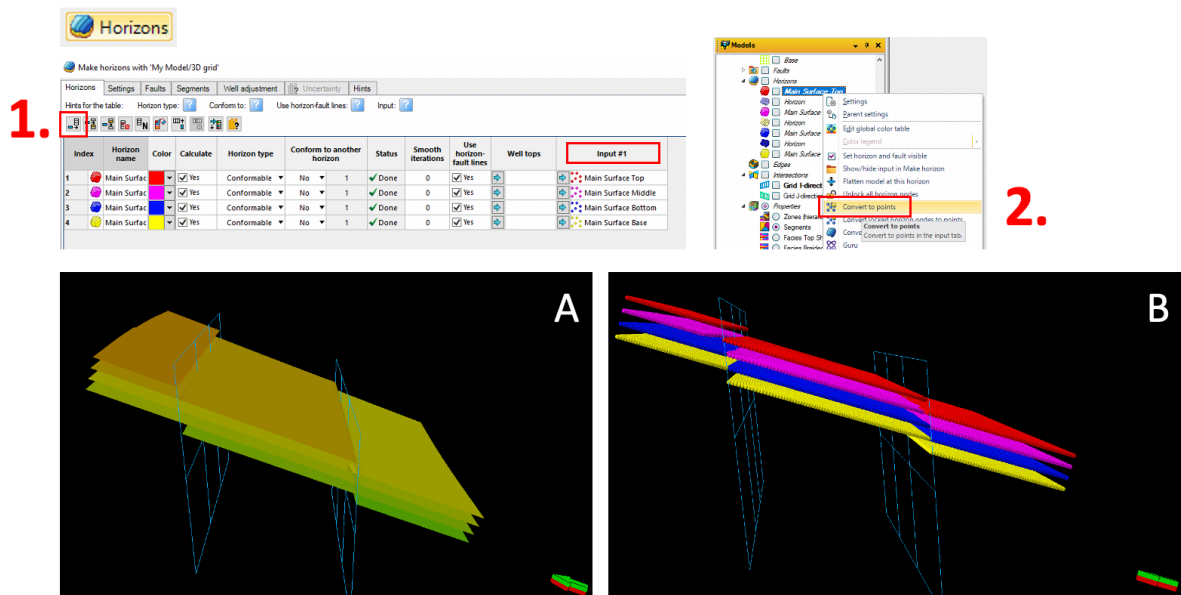


Figure 15: 1. indicates where to add horizons, while 2. shows how to convert the horizons to points. A show the final horizons and B illustrates the horizons as points.

The subsequent step is to construct zones and layers, and then proceed with the geometrical modelling (Steps 7 and 8 in Figure 6). The four horizons created previously were sufficient for this model's zones, although the creation of "Zones" is normally used in model building. "Layering" (Fig. 16) was used for this model and generates layers to achieve the final cell thickness (Schlumberger, 2023). After the layers have been created, the geometrical modelling must be run (Fig. 17). It is critical to apply the geometrical modelling after layering to ensure proper running and display. Performing the geometrical modelling for the zones index and segment index before the zones and layering are established will result in an incomplete display. In Figure 16, the layering was set to "Cell thickness" to establish a cell thickness of 15cm. A cell thickness of 15cm is the optimal value for the wells that will be created later. 15cm is the sampling scale of typical well-log sampling and is therefore used in the layering process.

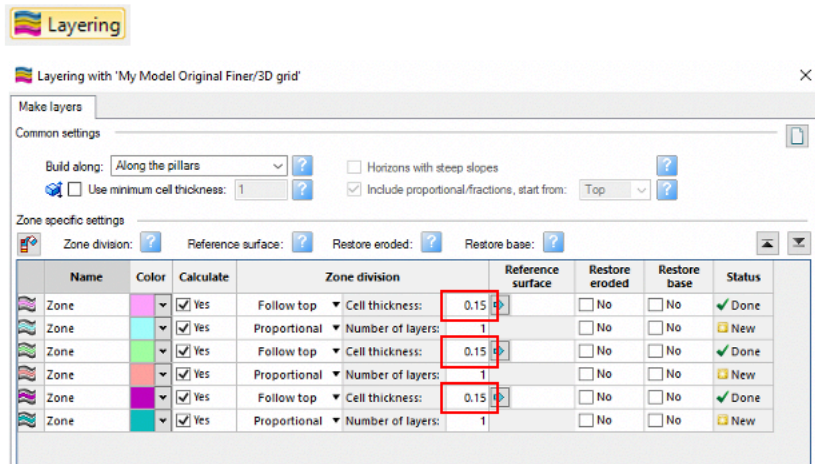


Figure 16: Illustrates how to create zones and layers, and shows which inputs are used.

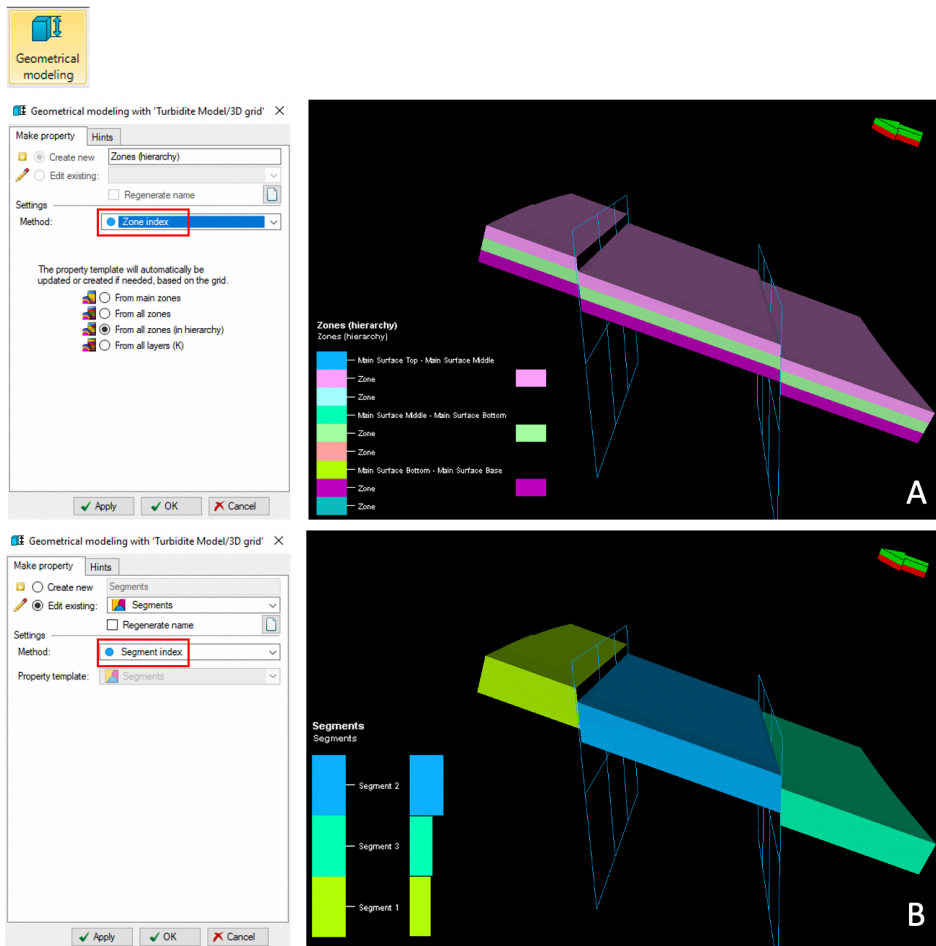


Figure 17: Shows how to create the zone and segment index. A is an image of the zones while B is an image of the segments of the model.

Once the structural modelling is finished, the next step is to perform the property modelling processes. The facies modelling and petrophysical modelling for porosity, permeability, and water saturation are the next steps (Steps 9 and 10 in Figure 6). The facies modelling procedure fills the 3D grid with discrete data which attempts to represent geological rock types with similar petrophysical data and other characteristics. The facies modelling process utilizes both deterministic and stochastic methods. The inputs utilized for the fault model are listed in Table 4.

Parameters	Braided River	Top Shale	Base Floodplain
Method	Object Modeling - Adaptive channels	Assign values	Assign values
Settings	Fraction: 58%	Constant: Shale	Constant: Fine sand
Layout	Orientation (12,30,60) Amplitude (600,800,1000) Wavelength (1000,1500,2000)		
Section	Width Normal (500,500)		
Levee	Default		
Trends	Default		

Table 4: Lists the different methods, settings, layouts, sections, levees, and trends used to run the facies modelling process.

During the facies modelling process, it is essential to select the "zone" being modelled, along with the "Method for zones/facies." These selections are highlighted in red boxes in Figure 18. Once the zone and method are determined, the types of channels can be selected, and the settings for layout, section, levee, and trends can be set using the tabs marked with black boxes in Figure 18. The finished facies modelling for the fault model is displayed in Figure 19.

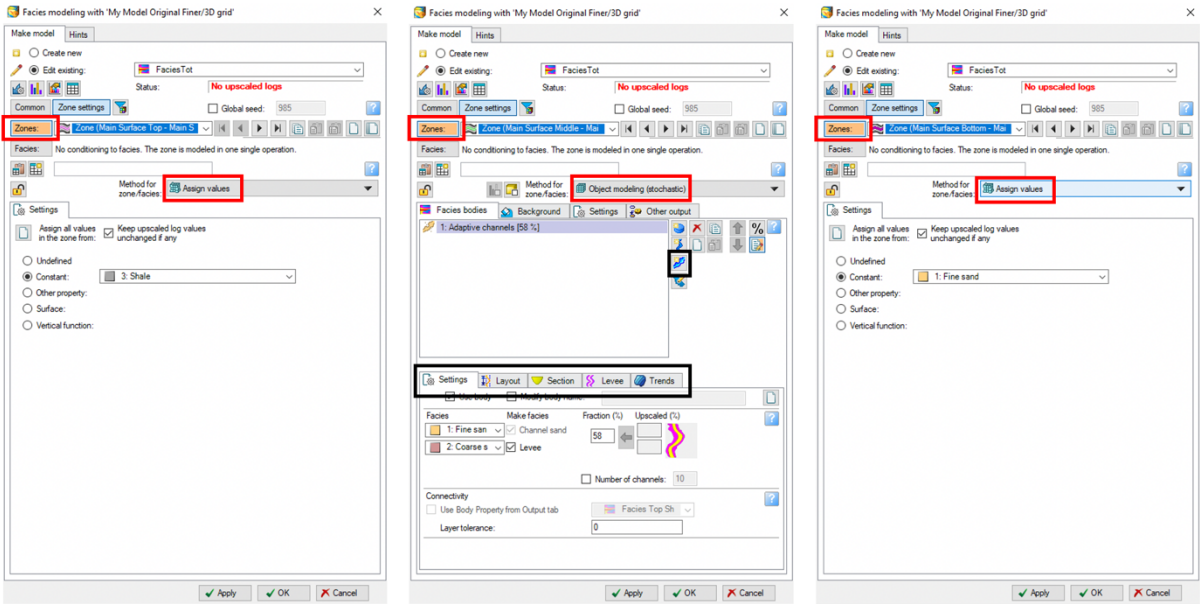


Figure 18: Show the settings for facies modelling.

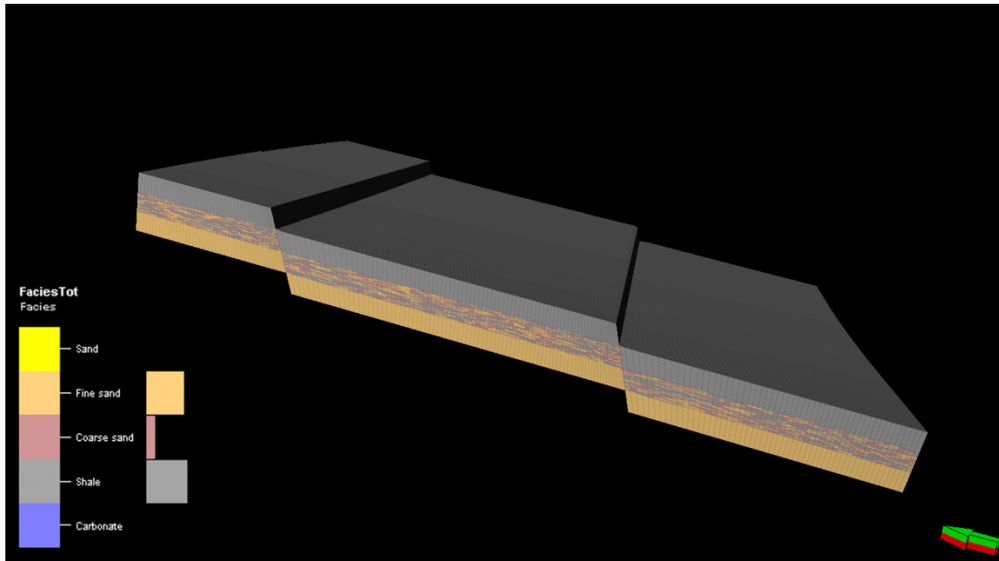


Figure 19: The facies model.

To create the porosity model, the Petrel software uses deterministic and stochastic methods to populate the 3D grid with continuous data such as porosity and permeability. The input data used for the porosity model is listed in Table 2, and the modelling type used for the model is “Gaussian random function Simulation”.

To set up the petrophysical modelling of the porosity, the “Property Modelling” section of the Petrel header is selected and opens a window where the porosity log is selected. The user needs to select the zone that is going to be modelled and assign the facies and the right lithology for the zone. It is essential to model all the different lithologies for each zone.

Figure 20 displays the settings for the petrophysical modelling of the porosity, where the crucial steps are marked with red boxes. The input values for the porosity are inserted in the areas marked with black boxes. Once the porosity modelling process is complete, the porosity model is displayed in Figure 22B.

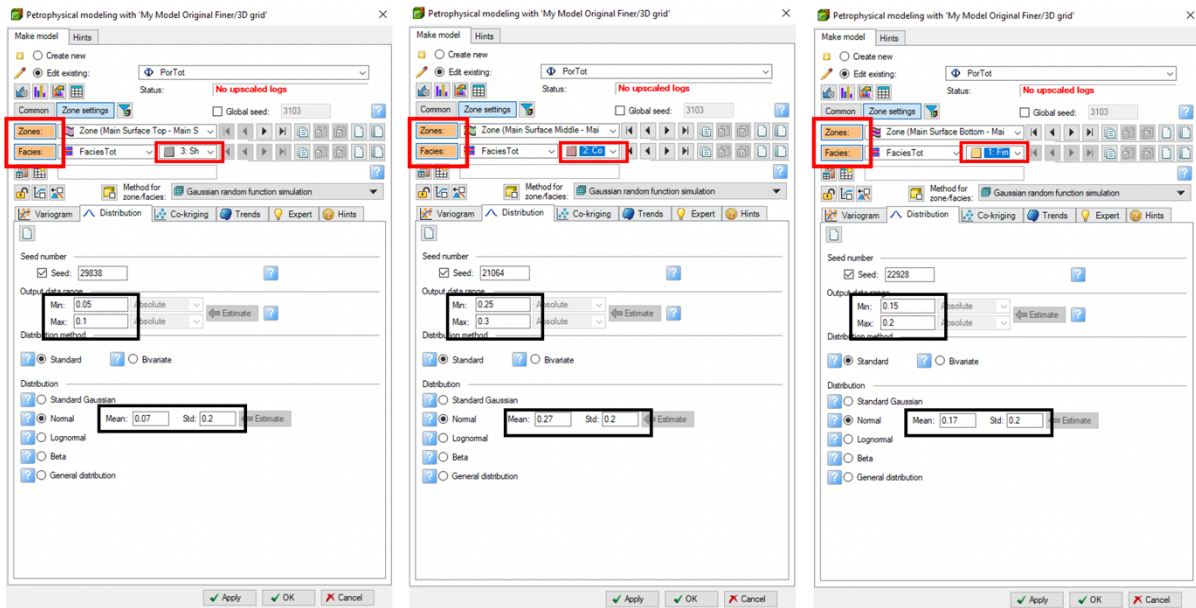


Figure 20: Shows the settings for the petrophysical modelling for porosity.

A porosity model with a depth trend was created based on the previous model, where the porosity decreases with depth due to compaction and cementation as it would in real life. The model was developed using the formula $y=mx+c$, which needed to be re-written as $x=(y-c)/m$ "the old porosity" because x is the unknown variable and the new porosity relies on data from the old porosity. An "Elevation general" depth was created, which represents the y variable in the formula, and was done by using the "Geometrical modelling" tool in Petrel. The "c" and "m" values were calculated using Excel, and the Petrel calculator was used to construct the porosity model (Fig. 21). The resulting porosity model with a depth trend is illustrated in Figure 22A.

```

PorDepthTrend = ((Elevation_general+2700)/10000)+PorTot
Permeability = 0.0549*Exp(25.252*PorDepthTrend)
Sw = Pow(10,-0.04695-(1.65077*PorDepthTrend))*Pow(Sqrt(Permeability/PorDepthTrend)*(0.076146*500^22/53.4)-0.185826)-0.0623748
  
```

Figure 21: The Petrel calculator with the formulas used to create the porosity model with depth trend, the permeability model, and the water saturation model.

The permeability (Fig. 22C) and water saturation (Fig. 22D) models were generated using the Petrel calculator (Fig. 21), as they rely on the porosity model as an input. Since the permeability model is a function of porosity, it needs to be calculated using a mathematical formula. Similarly, the Sw model requires input from both porosity and permeability models, and hence, the Petrel calculator is used for its creation.

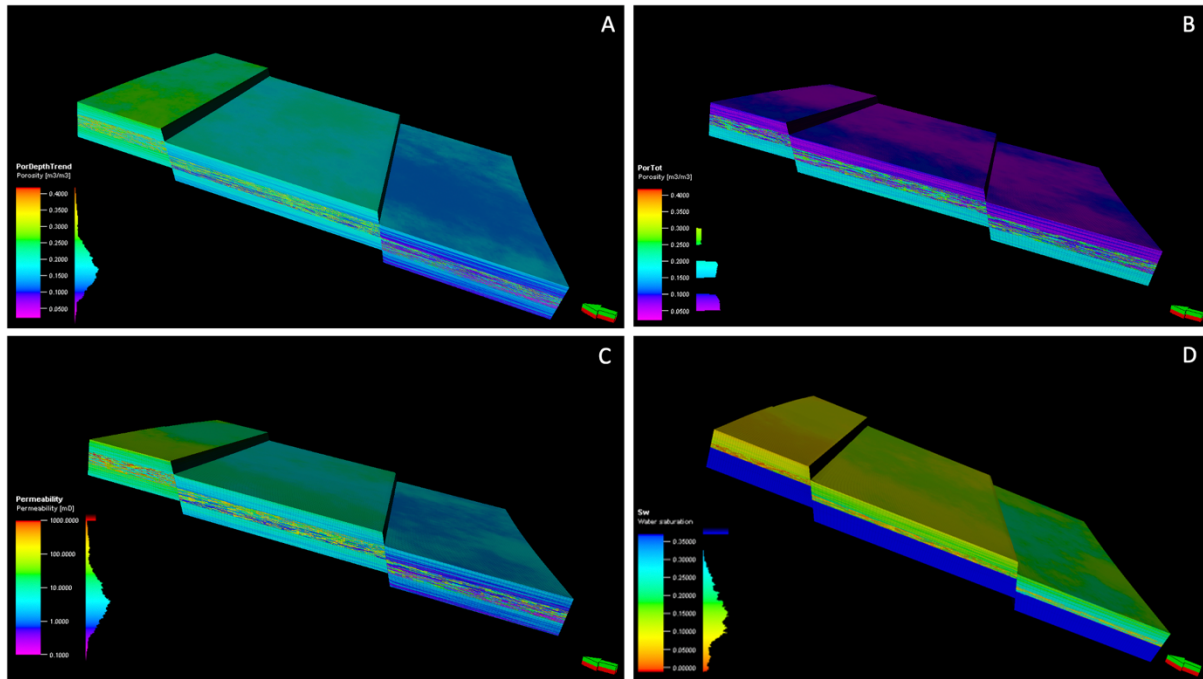


Figure 22: The porosity model with depth trend (A), the porosity model without depth trend (B), the permeability model (C), and the water saturation model (D).

The subsequent step involves creating the contacts that establish the fluid interfaces in the 3D grid (Step 11 in Figure 6). Table 5 provides the depths used for the model, and the oil-water contact (OWC) and gas-oil contact (GOC) depths were selected based on the facies and lithologies of the model. The contacts were established utilizing the "Contacts" tab in Petrel, and the OWC and GOC were set as depicted in Figure 23. Finally, the contact model was constructed using geometrical modelling as illustrated in Figure 24.

Segment	1	2	3
GOC	-1500	-2000	-2500
OWC	-1700	-2200	-2700

Table 5: The depths and segments for the OWC and GOC.

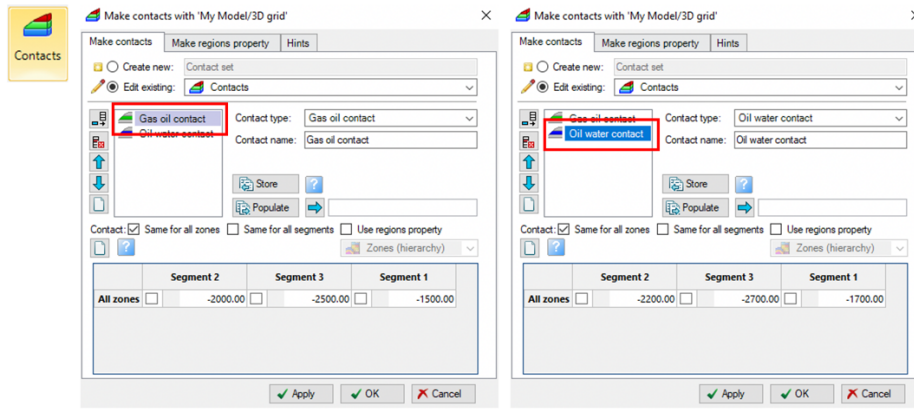


Figure 23: The setting for the oil-water contact and the gas-oil contact, as well as the depths of the contacts. This process generates a contact set.

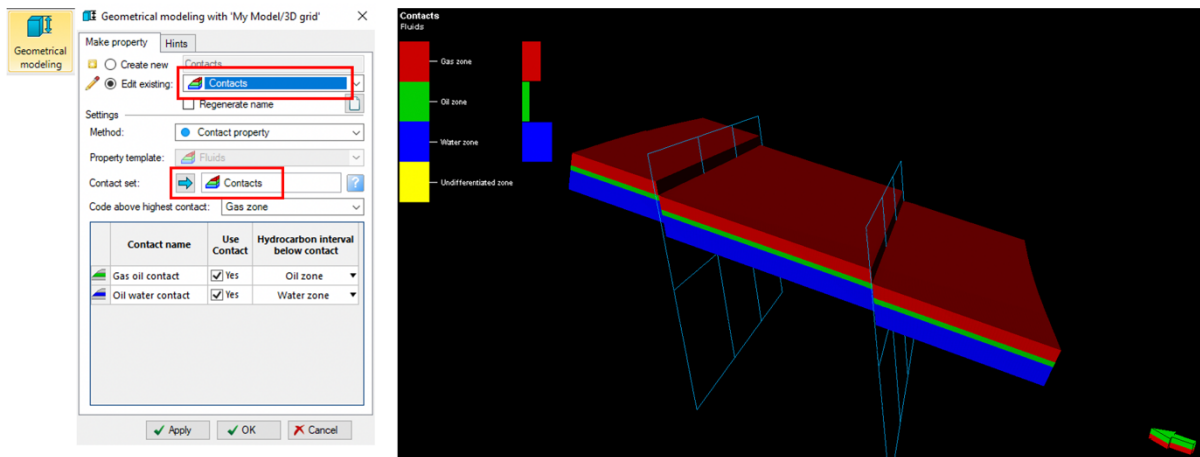


Figure 24: The construction of the contacts model using geometrical modelling and selecting "contacts," and inserting the contact set created from the previous step.

The next step is to perform the volume calculations, step 12 in Figure 6. The volume calculation considers the reservoir properties and the geometry of the reservoir and provides an estimate of the total volume of hydrocarbons present in the reservoir. The "Volumes" tab is used to calculate the volume of the reservoir. Initially, the contacts are imported by following the steps illustrated in Figure 25. Next, the net-to-gross ratio is set, and the porosity to be used in the calculations and the formation volume factor for oil and gas is chosen, as shown in Figure 25 with small red boxes.

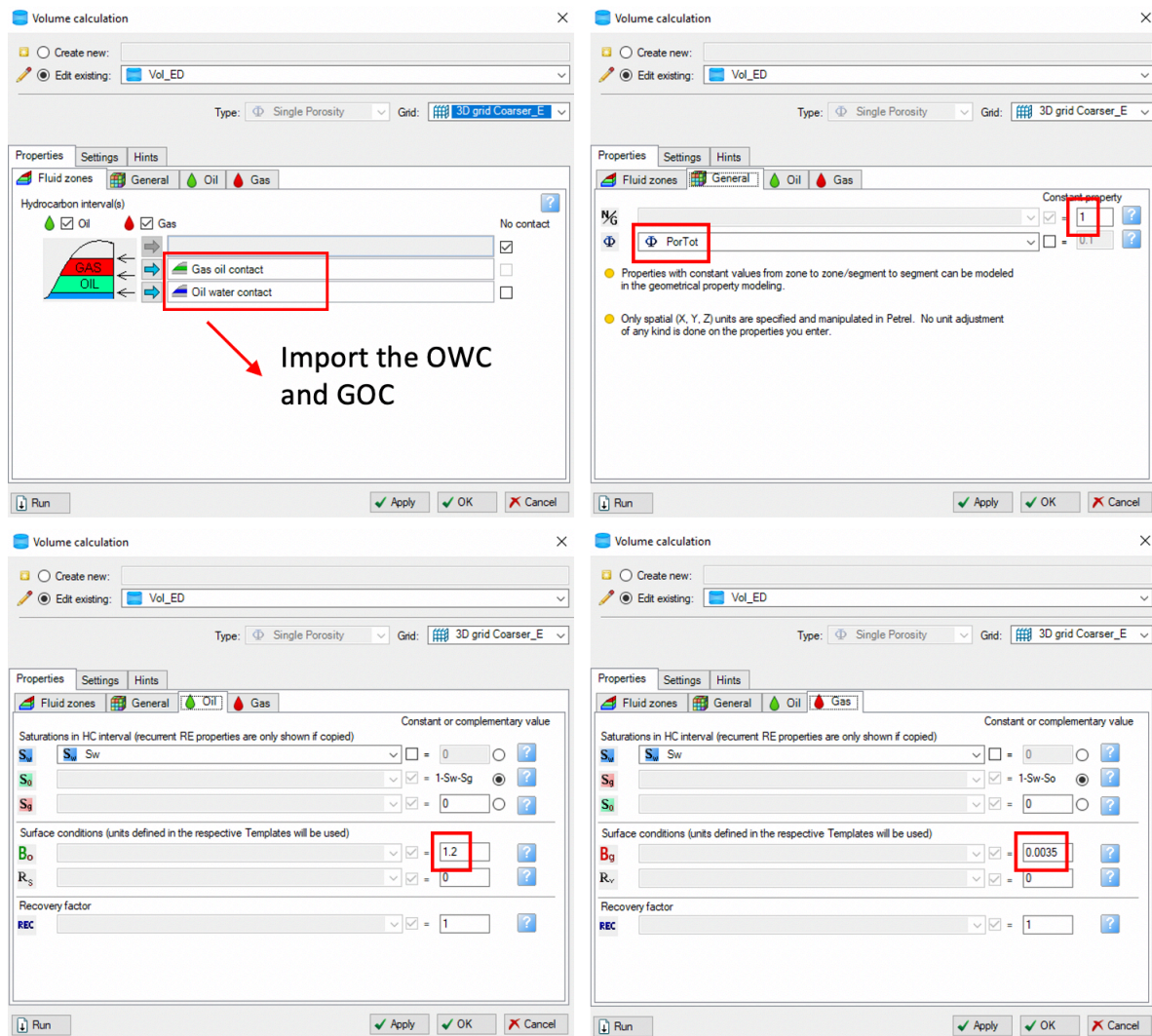


Figure 25: The volume calculation process showing how to import the OWC and GOC as well as where to input B_o/B_g , net to gross and porosity.

The last step (Step 13) in the building process of the Original Model is to set up the wells and generate synthetic well logs which are to be used as input for the Reservoir Model. To create wells, a well folder is set up and the option “create new well” is selected, as shown in Figure 26. The wellhead location coordinates X and Y are provided in Table 6. Once the well is created, the logs for the well can be generated by opening the settings and selecting the desired logs, followed by clicking “Make logs” as indicated with a red box in Figure 27.

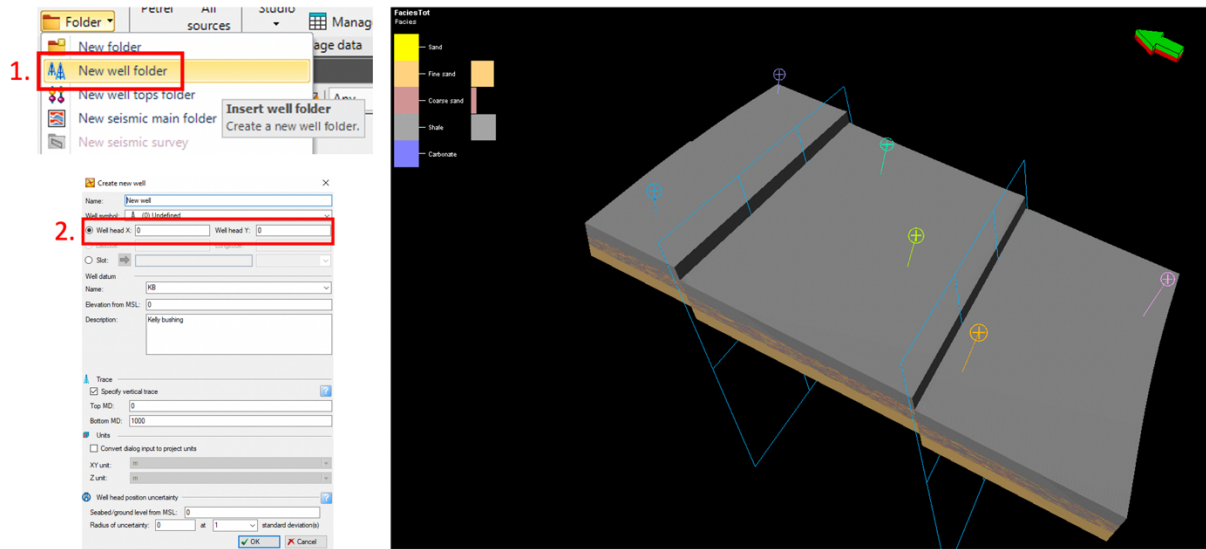


Figure 26: How to create a well folder and the wells, and an image of the placement of the wells.

Well	X location	Y location
1	10063	120486
2	48365	94990
3	26895	79153
4	12433	62260
5	43729	37393
6	56720	125065

Table 6: The X and Y locations of the wells.

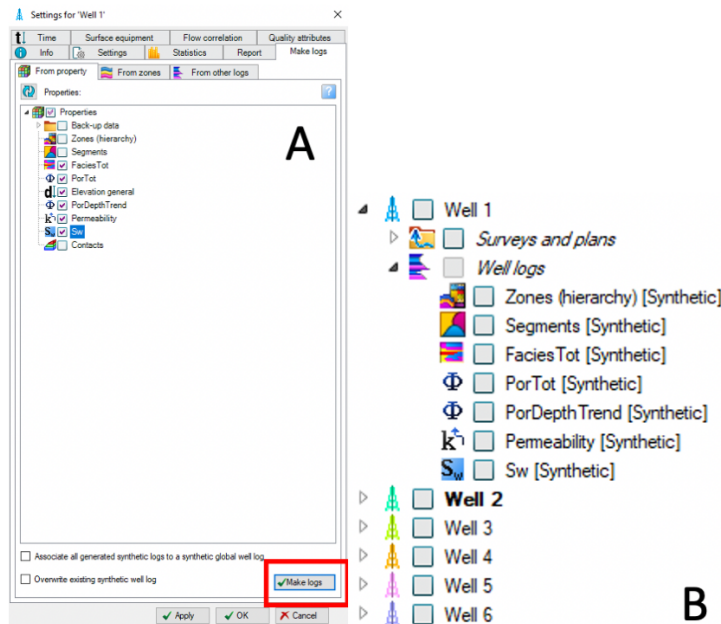


Figure 27: A shows how to make the logs using the settings for each well (check off the desired logs) and B displays the well logs and the 6 wells.

The construction process is completed by setting up a workflow (Fig. 28) that runs through the entire process (Step 14 in Figure 6). This workflow enables any necessary edits to be made to the model, such as for example the facies modelling, and allows for the entire building process to be executed in one go.

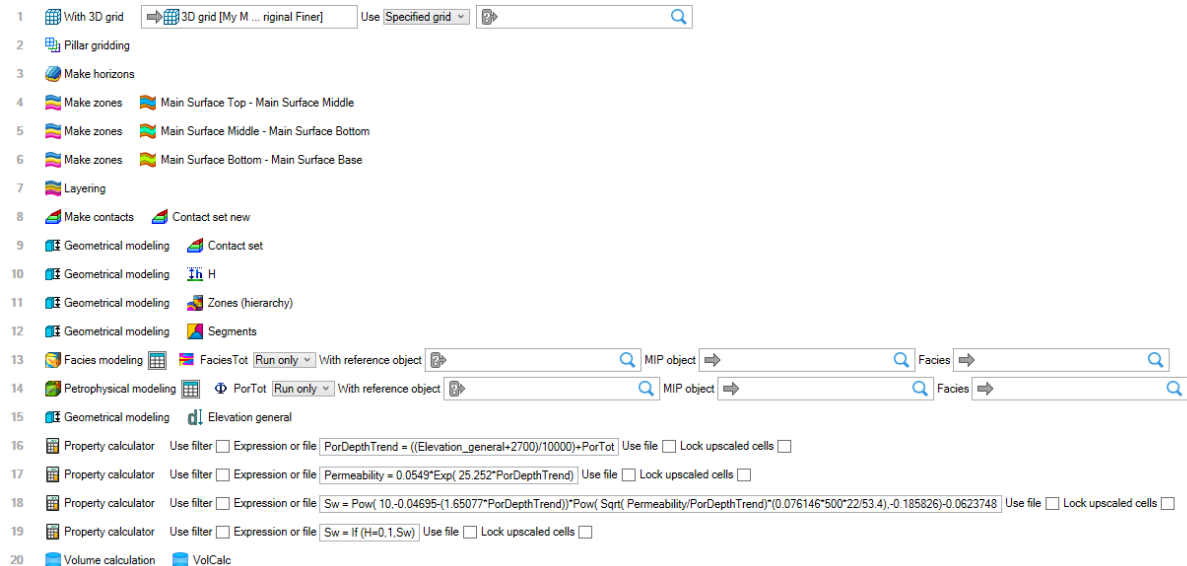


Figure 28: The workflow for Model 1 (Fluvial).

3.2 Model 2 (Turbidite)

The procedure for building the turbidite model is similar to that of the fault model, so only the main differences will be highlighted in this section. In Model 2 (Turbidite) no faults are present, so the grid building stage is simplified. The initial step involves defining the model, as shown in Figure 29, followed by digitizing up a boundary using "Add points to polygon". The input points for each surface were added using "Add points to pointset" (Fig. 29A). For each point set, the points were copied, and the depths were modified in the spreadsheet, to represent the depth of each horizon (Fig. 29B & 30).

The model construction was the same as used for the fault model horizon, zones, layers, and geometrical modelling. The only difference was that the surfaces did not need to be edited to account for the fault displacements. The zones and segment index are displayed in Figure 31.

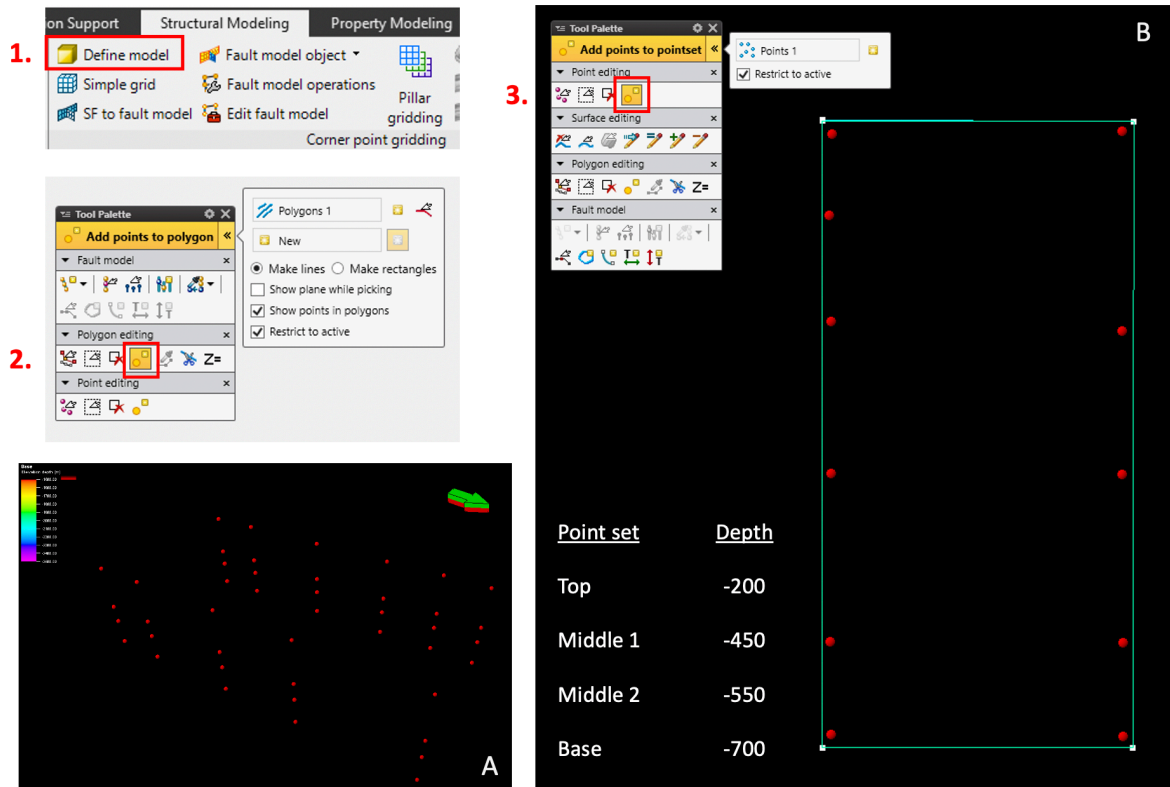


Figure 29: 1. Indicates how to define a model, 2. describes how to set up a boundary using “add points to polygon”, and 3. shows how to setup the points. B shows the points that will be used to construct the surfaces, while A shows the points and their depths in a 3D view.

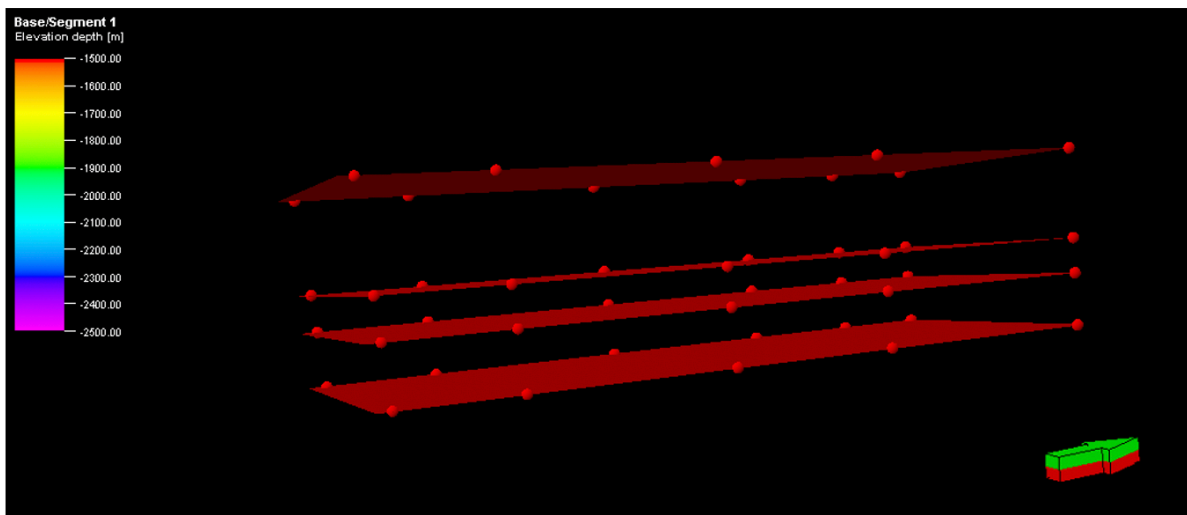


Figure 30: The surfaces of Model 2.

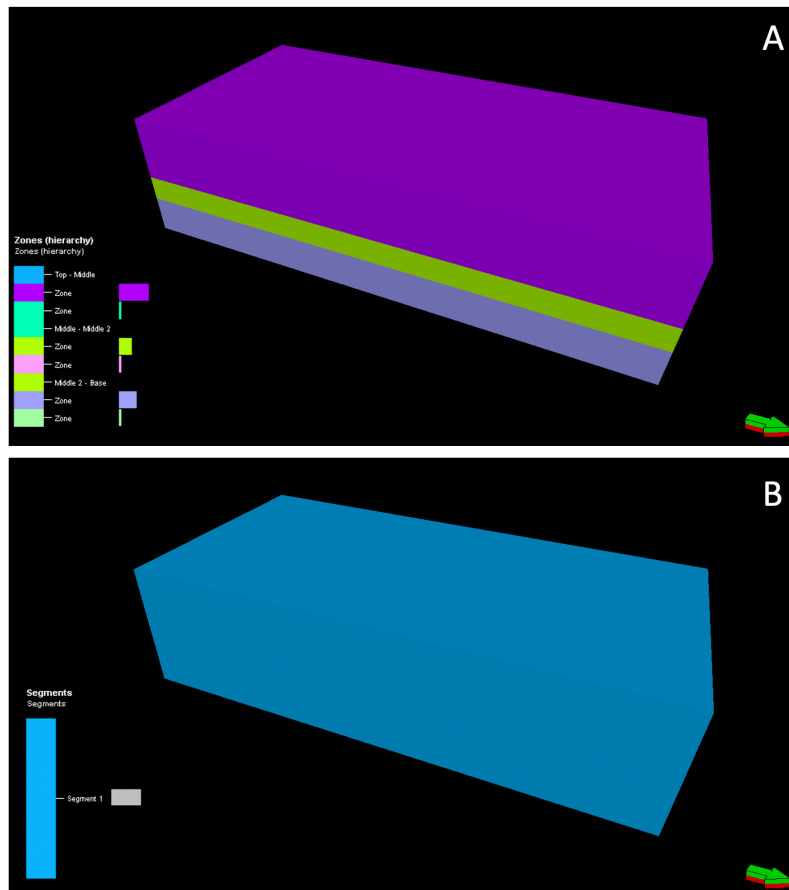


Figure 31: A illustrates the zones, while B shows the segment of the model.

Following the structural modelling, the property modelling phase begins with facies modelling, for which the input data is listed in Table 7.

Parameters	Turbidite	Shale	Base Sandstone
Method	Truncated Gaussian with trends	Assign values	Assign values
Facies	Sand, Fine sand and Shale	Constant: Shale	Constant: Sand
Geometry	Edited in Petrel to illustrate a turbidite system by using "point source"		

Table 7: Lists the methods, facies and geometry used to run the facies modelling for the turbidite system, the shale and the sandstone base.

The "Truncated Gaussian with trends" method is used for the turbidite facies modelling. This method allows the modeller to shape the desired facies into complex body shapes using "point source". It also allows for pro- and retro-grading sequences. In this method, the points in the geometry can be moved and edited as needed, as shown in Figure 32. The complete facies modelling process is displayed in Figure 33.

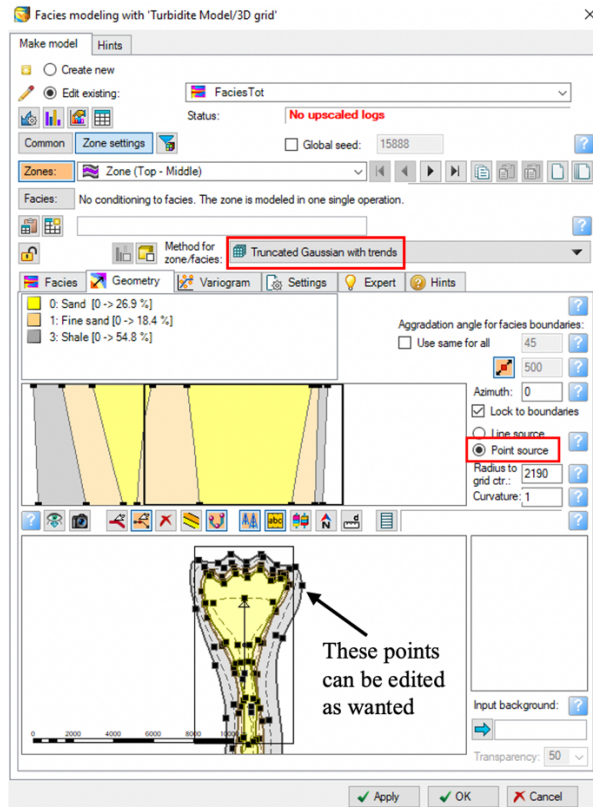


Figure 32: The method used in the turbidite modelling process, and how to edit and move the point to the desired positions.

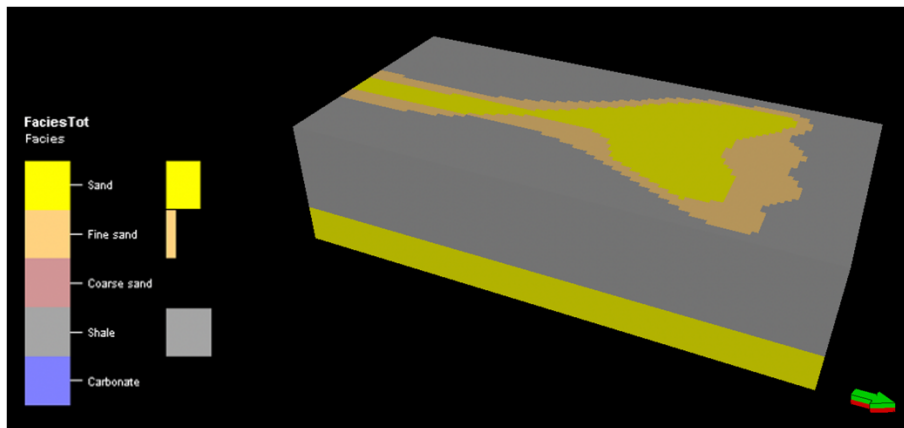


Figure 33: The facies in Model 2.

Like Model 1, the permeability and water saturation models were created using the Petrel calculator, and the porosity values used for the porosity model are derived from Table 2. The resulting models are shown in Figure 34. The contacts were also established using a similar process but with different depths for the oil-water and gas-oil contacts as listed in Table 8. The resulting contact model is displayed in Figure 35.

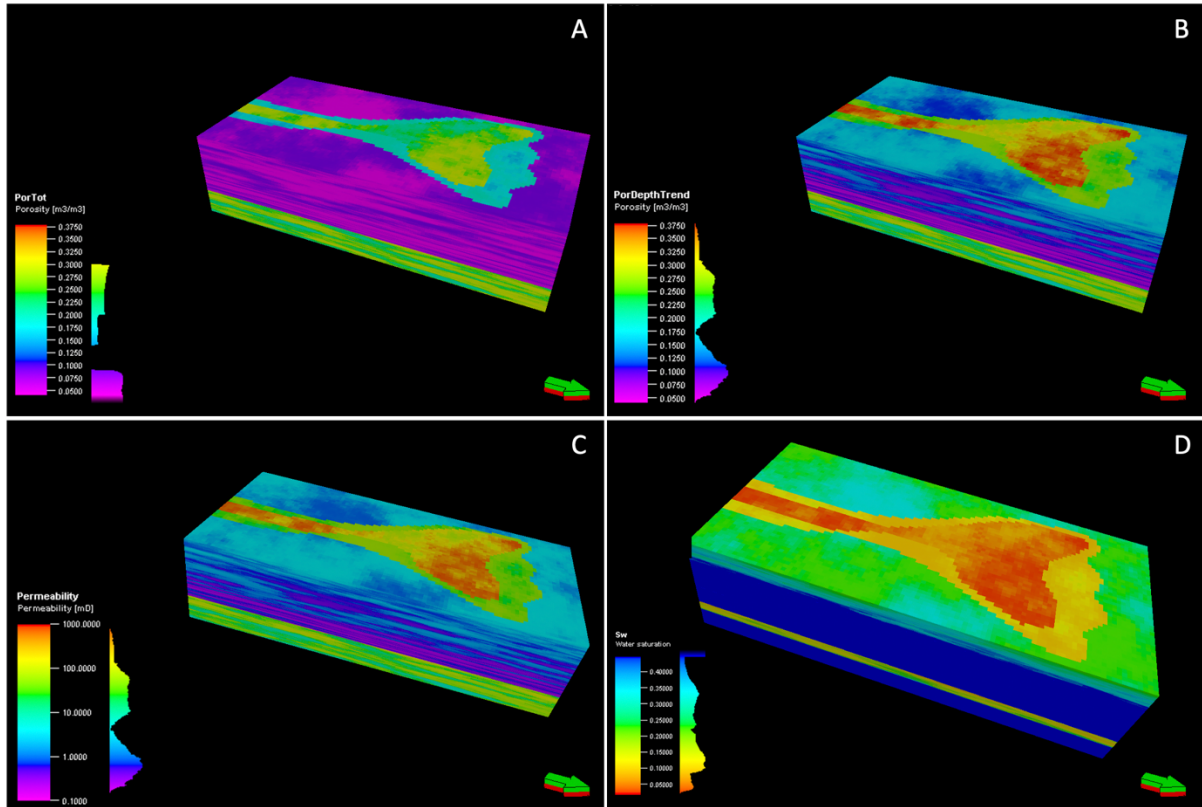


Figure 34: The porosity model without depth trend (A), the porosity model with depth trend (B), the permeability model (C), and the water saturation model (D).

Zone	1	7
GOC	-250	-550
OWC	-300	-450 and -600

Table 8: The depths of the OWC and GOC for Model 2.

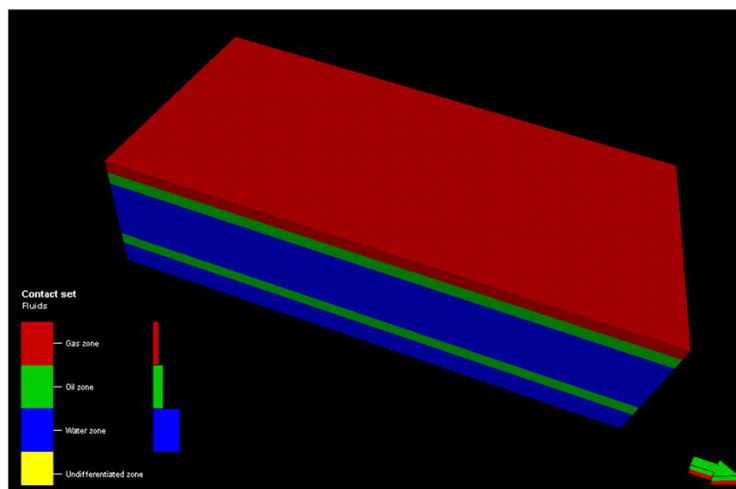


Figure 35: The contact model, red is the gas zone, green is the oil zone, and blue is the water.

The final steps of the turbidite model construction involve setting up the wells, performing volume calculations, and establishing a workflow. The well creation process is similar to the fault model, with the exception that there are only three wells in the turbidite model. The locations of the wells are specified in Table 9. The volume calculations are performed using the same methods and values as for the fault model, as shown in Figure 25. Finally, the workflow is established in the same manner as for the fault model, as illustrated in Figure 36.

Well	X	Y
1	3451	998
2	1194	4211
3	3209	7615

Table 9: The X and Y position of the three wells.

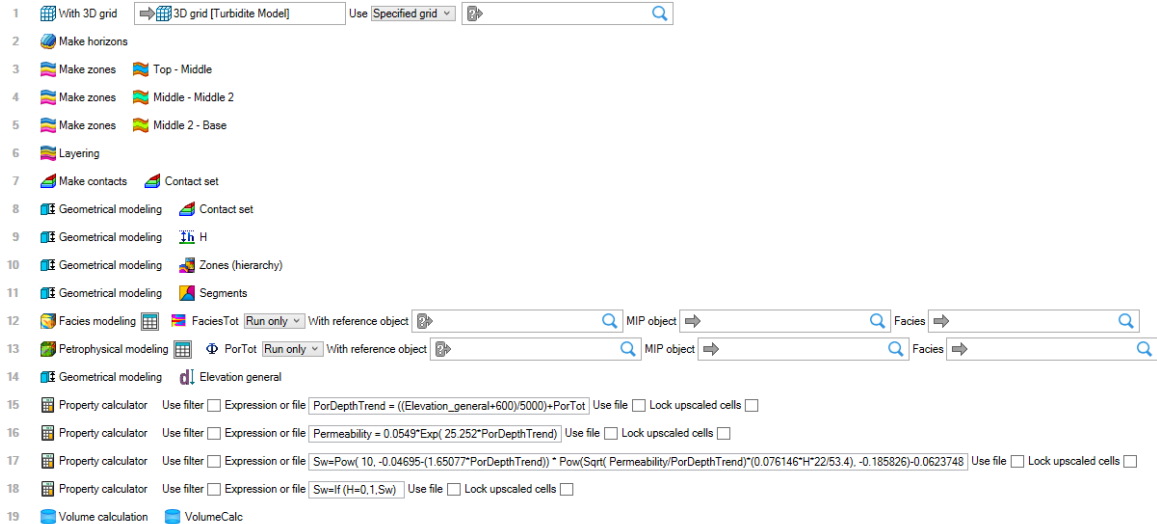


Figure 36: Model 2's workflow.

4. The Reservoir Models

After completing the Original Models, which include Model 1 and Model 2, samples are collected from the wells to create the coarser reservoir models. The Original Models have a cell thickness of 15cm, whereas the new Reservoir Models have a coarser cell thickness of 60cm. To construct the coarser reservoir models, a new 3D grid is created for both models. The horizons, zones, layers, and contacts are then run again, but with 0,60 as the input in the “Layering” tab (Fig. 37). The horizons, zones, and contacts are set up in the same manner as the Original Models.

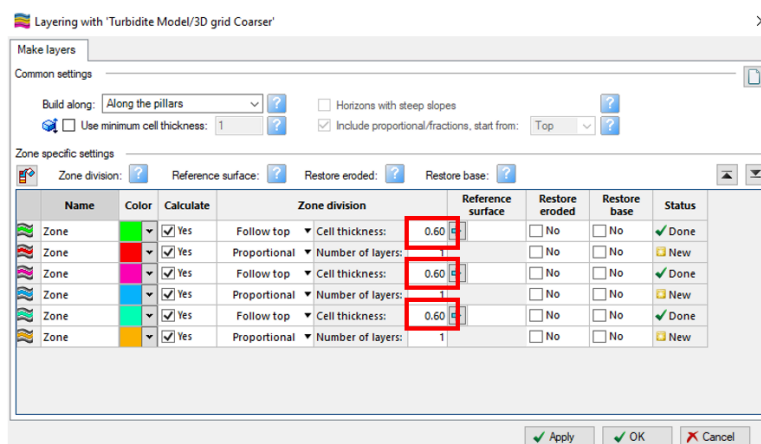


Figure 37: Layering for the coarser reservoir models. 0,60 is used as input for both models.

The subsequent step in the construction of the coarser Reservoir Models involves upscaling the well logs to enable facies modelling and property modelling. Upscaling refers to the process in which Petrel identifies the 3D grid cells that the well intersects. Subsequently, for each grid cell, log values that fall within that cell are averaged using an algorithm chosen to produce one log value for that cell. The extent to which each well intersects cells and the number of cells it penetrates is dictated by the resolution and layout of the 3D grid. The upscaling of well logs represents the first step towards disseminating petrophysical values to all cells within the model (Schlumberger 2023). The upscaled logs in this study include facies and porosity logs (Fig. 38), whereas the calculator is utilized to generate permeability and water saturation logs, as demonstrated in Figure 21.

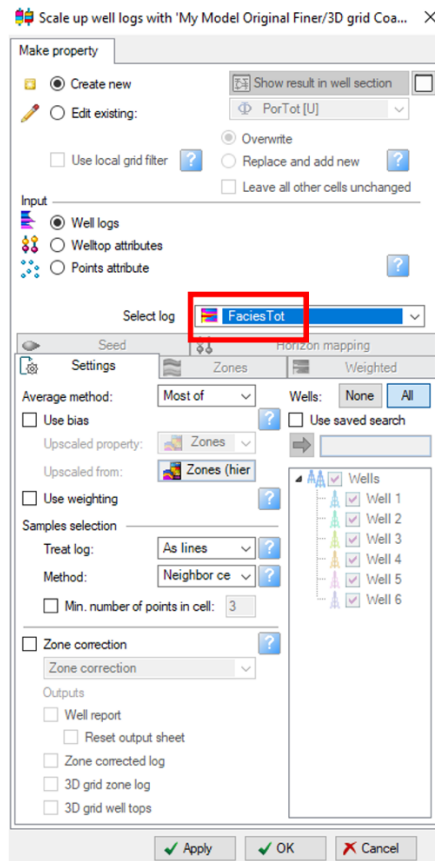


Figure 38: How to upscale the well logs by using "Create new". The red box indicates where the desired logs are selected.

Once the well logs are upscaled, the facies modelling and petrophysical modelling can be initiated. The facies modelling process follows the same methodology as the Original Model, utilizing the "Truncated Gaussian with trends" technique and shifting the active lithologies towards the right to simulate the geometry of a turbidite system. The facies distribution is adjusted by manipulating the "point source" feature. During the petrophysical modelling process, the PorTot and PorDepthTrend are selected, and it is imperative to ensure that the distribution chosen is "From upscaled logs," as depicted in Figure 39. The volume calculation for the coarser models is performed using the same parameters as the Original Models. Workflows are also designed for the coarser reservoir models.

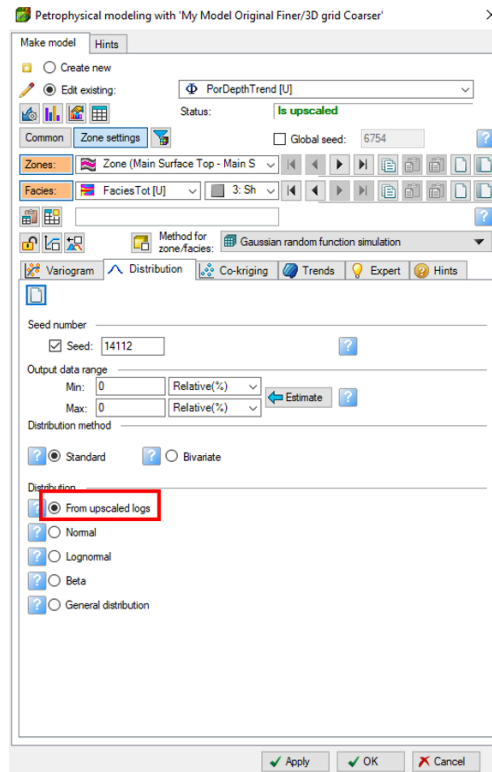


Figure 39: How to run the petrophysical modelling for the upscaled logs.

The process of constructing the coarser Reservoir Models is carried out for both Model 1 and Model 2. The newly generated coarser grids are duplicated and assigned new names to ensure the preservation of the coarser reservoir grids just in case a new coarser grid is needed (as shown in Figure 40).



Figure 40: The different grids, their names, and contents for both models.

5. The Experiments

In this chapter of the thesis the setup of the experiments and an explanation of each parameter will be described. The experiments for both models use an experimental design setup, and several workflows in Petrel will be used to conduct the experiments.

5.1 Experiment set up

In the grids "3D grid Coarser_ED" and "3D grid Coarser ExD" (Fig. 40), experiments are conducted through the implementation of workflows that iterate through the parameters being tested. An experimental design is employed, which utilizes set values of 1 and -1 as shown in Table 10. The intention of the experiments is to examine several modelling parameters, and there are different choices on how to do so. In experimental design, there is a full factorial and a fractional factorial setup, as mentioned before. Experimental design with a full factorial setup is utilized over other experiment types because with experimental design one can use relatively high and low values for each parameter that is tested. It is also efficient, and one can easily analyze the results to determine the impact of each parameter and look at interactions between the parameters.

A table and an Excel sheet are constructed in order to perform the experiments using experimental design. Table 10 is structured so that when the experimental design employs a value of 1, the layering is set to 1.5, whereas when a value of -1 is employed, the layering is set to 0.6. The experimental design is illustrated in Figure 41. Initially, the first row of the design contains only 1's. Subsequently, in the second row, the last number in column K is changed to -1. The two rows are then copied and pasted, with the two 1s in column J replaced by -1's. The four rows are then copied and pasted, with the two 1s in column I replaced by -1s- This process is repeated until column A is reached.

	Fault Model		Turbidite Model		Variable	Prop Name
	H	L	H	L		
Layering	1.5 (1)	0.6 (-1)	1.5 (1)	0.6 (-1)	Lay	Lay
Nr. of wells	2 (1)	6 (-1)	1 (1)	3 (-1)	Wells	W
Most of vs Mid-point pick	Most of (1)	Mid-point pick (-1)	Most of (1)	Mid-point pick (-1)	MO	M
VPC	With VPC (1)	Without VPC (-1)	With VPC (1)	Without VPC (-1)	VPC	VPC
Bias to facies	On (1)	Off (-1)	On (1)	Off (-1)	BF	BF
SGS vs Kriging	SGS (1)	Kriging (-1)	SGS (1)	Kriging (-1)	SK	SK
Variogram Por/Perm	1000 (1)	250 (-1)	1000 (1)	250 (-1)	Var	Var
Depth trend	On (1)	Off (-1)	On (1)	Off (-1)	DT	DT
Correlation Coefficient for permeability	0.9 (1)	0.6 (-1)	0.9 (1)	0.6 (-1)	CC	CC
Normal vs Asymmetric distribution	Normal (1)	Asymmetric (-1)	Normal (1)	Asymmetric (-1)	NS	NS
Saturation hight function	0.075 (1)	0.025 (-1)	0.075 (1)	0.025 (-1)	Sat	Sat

Table 10: The assigned values for all the parameters in the experimental design setup.

	A	B	C	D	E	F	G	H	I	J	K
	Layering	Nr. of wells	Most of/Midpoint pick	VPC	Bias to facies	SGS/Kriging	Variogram Por/Perm	Depth trend	Corr. Coeff. Perm	Normal/Asymmetric	Saturation high func
1	1	1	1	1	1	1	1	1	1	1	1
2	1	1	1	1	1	1	1	1	1	1	-1
3	1	1	1	1	1	1	1	1	1	1	-1
4	1	1	1	1	1	1	1	1	1	-1	1
5	1	1	1	1	1	1	1	1	1	-1	-1
6	1	1	1	1	1	1	1	1	-1	1	1
7	1	1	1	1	1	1	1	1	-1	1	-1
8	1	1	1	1	1	1	1	1	-1	-1	1
9	1	1	1	1	1	1	1	1	-1	-1	-1
10	1	1	1	1	1	1	1	1	-1	1	1
11	1	1	1	1	1	1	1	-1	1	1	-1
12	1	1	1	1	1	1	1	-1	1	-1	1
13	1	1	1	1	1	1	1	-1	1	-1	-1
14	1	1	1	1	1	1	1	-1	-1	1	1
15	1	1	1	1	1	1	1	-1	-1	1	-1
16	1	1	1	1	1	1	1	-1	-1	-1	1
17	1	1	1	1	1	1	1	-1	-1	-1	-1
18	1	1	1	1	1	1	-1	1	1	1	1
19	1	1	1	1	1	1	-1	1	1	1	-1
20	1	1	1	1	1	1	-1	1	1	-1	1
21	1	1	1	1	1	1	-1	1	1	-1	-1
22	1	1	1	1	1	1	-1	1	-1	1	1
23	1	1	1	1	1	1	-1	1	-1	1	-1
24	1	1	1	1	1	1	-1	1	-1	-1	1
25	1	1	1	1	1	1	-1	1	-1	-1	-1
26	1	1	1	1	1	1	-1	-1	1	1	1
27	1	1	1	1	1	1	-1	-1	1	1	-1
28	1	1	1	1	1	1	-1	-1	1	-1	1
29	1	1	1	1	1	1	-1	-1	-1	-1	-1
30	1	1	1	1	1	1	-1	-1	-1	1	1
31	1	1	1	1	1	1	-1	-1	-1	1	-1
32	1	1	1	1	1	1	-1	-1	-1	-1	1
33	1	1	1	1	1	1	-1	-1	-1	-1	-1
34	1	1	1	1	1	-1	1	1	1	1	1
35	1	1	1	1	1	-1	1	1	1	1	-1
36	1	1	1	1	1	-1	1	1	1	-1	1
37	1	1	1	1	1	-1	1	1	1	-1	-1
38	1	1	1	1	1	-1	1	1	-1	1	1
39	1	1	1	1	1	-1	1	1	-1	1	-1
40	1	1	1	1	1	-1	1	1	-1	-1	1
41	1	1	1	1	1	-1	1	1	-1	-1	-1

Figure 41: The experimental design set up with 1's and -1's.

To conduct experiments, workflows are created in Petrel to execute the specific parameters along with their corresponding values for each modelling process. While some of the parameters are tested during the facies modelling process, others are tested during the petrophysical modelling process, and the rest during the data analysis. There are two experiments conducted, one on each of the models. The same parameters and experimental design setup are used for both models, with the exception that the vertical proportion curve (VPC) is not used in Model 1 (Turbidite). After analyzing the results, a slight mistake was discovered. The porosity models were built using normal distribution but should have been built using non-normal (asymmetric) distribution, so a third experiment on Model 2 (turbidite) was run. There are now two sets of results for Model 2, now named Model 2A and Model 2B.

5.2 The Workflows

After the experiment set-up is completed, the workflows are created to execute the specific parameters with their assigned values for each modelling process. There are six workflows for each model, and they are all created in the same way. The first workflow is the master workflow, which executes the entire experiment in one go. The master workflow loads the experimental design setup as well as the set values for the 1's and -1's. It then assigns the set values to the appropriate parameters and runs through the structure of the model, including the horizons, zones, layering, contacts, and geometrical modelling. The master workflow also runs the facies and petrophysical modelling processes, where several parameters are tested. Finally, the master workflow performs volume calculations. Figure 42 shows the structure of the master workflow. It is within each of the different workflows that the parameters are assigned prop names and then the read data workflow assigns the values.

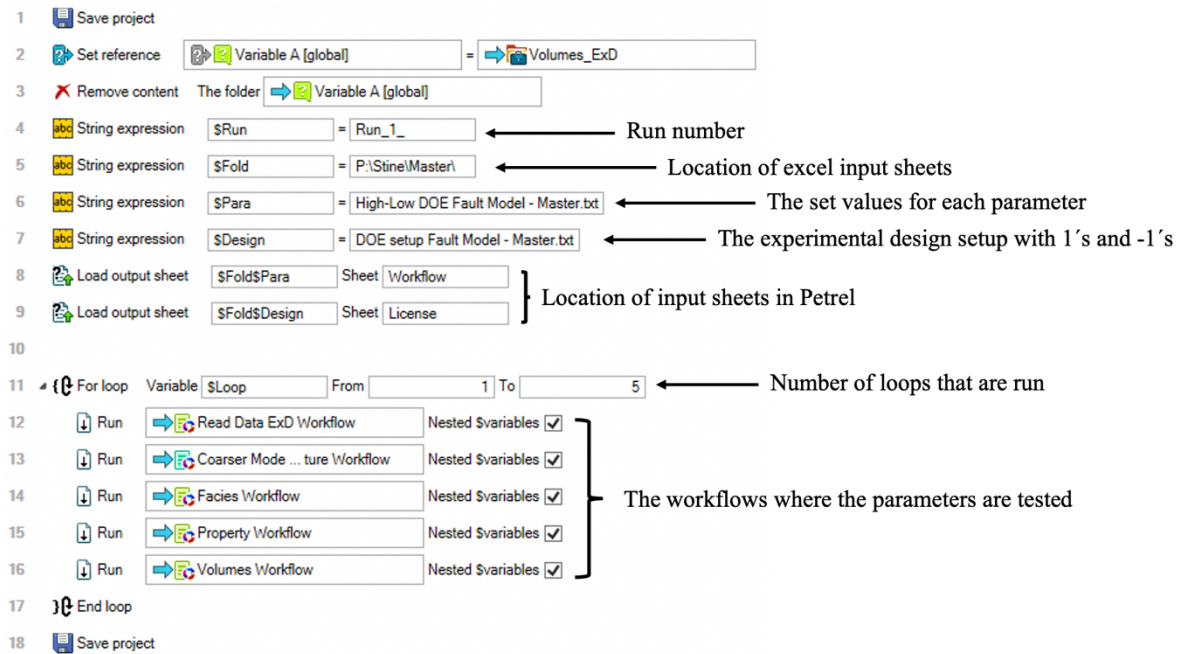


Figure 42: The first line of the master workflow saves the project, while lines 2 and 3 assign the volumes created to a designated folder and removes the contents of the workflow if rerun. Lines 4 to 7 specify the location and naming conventions of the files on the computer. Lines 8 and 9 loads the files into Petrel in the Workflow and License tabs, respectively. Lines 11 to 17 execute the various workflows in a predefined loop, while line 18 saves the project when the run is complete.

The Read Data workflow plays a crucial role in the experiment as it reads input data from Excel sheets and loads it into the Petrel Workflow and License sheets, as shown in Figure 43. It is designed to ensure that each row and column in the Workflow and License sheets are correctly read by Petrel, and the appropriate input data is utilized for each parameter, as depicted in Figure 44. To facilitate input into other workflows, the input parameters are assigned prop names in the Read Data workflow, as illustrated in Figure 44.

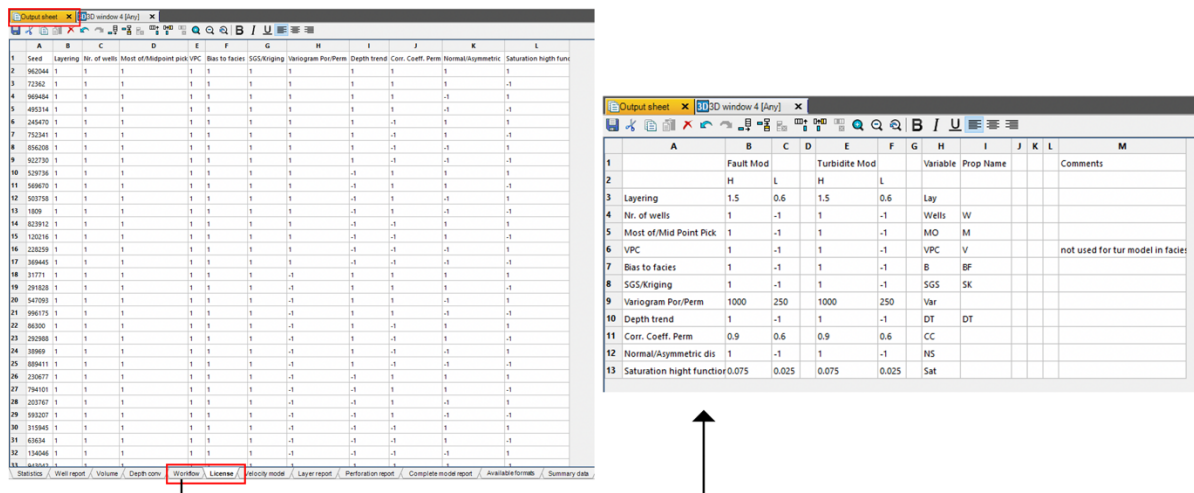


Figure 43: Shows the License and Workflow tabs in Petrel. They are located in the "Output sheet" as shown with red boxes.

1		Read output sheet	\$Seed	Row	\$Loop+1	Column	1	Sheet	License	Evaluate	<input type="checkbox"/>	
2		Read output sheet	\$LV_Lay	Row	\$Loop+1	Column	2	Sheet	License	Evaluate	<input type="checkbox"/>	
3		Read output sheet	\$LV_Wells	Row	\$Loop+1	Column	3	Sheet	License	Evaluate	<input type="checkbox"/>	
4		Read output sheet	\$LV_MO	Row	\$Loop+1	Column	4	Sheet	License	Evaluate	<input type="checkbox"/>	
5		Read output sheet	\$LV_VPC	Row	\$Loop+1	Column	5	Sheet	License	Evaluate	<input type="checkbox"/>	
6		Read output sheet	\$LV_BF	Row	\$Loop+1	Column	6	Sheet	License	Evaluate	<input type="checkbox"/>	
7		Read output sheet	\$LV_SK	Row	\$Loop+1	Column	7	Sheet	License	Evaluate	<input type="checkbox"/>	
8		Read output sheet	\$LV_Var	Row	\$Loop+1	Column	8	Sheet	License	Evaluate	<input type="checkbox"/>	
9		Read output sheet	\$LV_DT	Row	\$Loop+1	Column	9	Sheet	License	Evaluate	<input type="checkbox"/>	
10		Read output sheet	\$LV_CC	Row	\$Loop+1	Column	10	Sheet	License	Evaluate	<input type="checkbox"/>	
11		Read output sheet	\$LV_NS	Row	\$Loop+1	Column	11	Sheet	License	Evaluate	<input type="checkbox"/>	
12		Read output sheet	\$LV_Sat	Row	\$Loop+1	Column	12	Sheet	License	Evaluate	<input type="checkbox"/>	
13												
14		If	\$LV_Lay=1									
15		Read output sheet	\$VAL_Lay	Row		Column	3	5	Sheet	Workflow	Evaluate	<input type="checkbox"/>
16		Else										
17		Read output sheet	\$VAL_Lay	Row		Column	3	6	Sheet	Workflow	Evaluate	<input type="checkbox"/>
18		Endif										
19												
20		If	\$LV_Wells=1									
21		Read output sheet	\$VAL_Wells	Row		Column	4	5	Sheet	Workflow	Evaluate	<input type="checkbox"/>
22		Else										
23		Read output sheet	\$VAL_Wells	Row		Column	4	6	Sheet	Workflow	Evaluate	<input type="checkbox"/>
24		Endif										
25												
26		If	\$LV_MO=1									
27		Read output sheet	\$VAL_MO	Row		Column	5	5	Sheet	Workflow	Evaluate	<input type="checkbox"/>
28		Else										
29		Read output sheet	\$VAL_MO	Row		Column	5	6	Sheet	Workflow	Evaluate	<input type="checkbox"/>
30		Endif										
31		If	\$LV_VPC=1									
32		Read output sheet	\$VAL_VPC	Row		Column	6	5	Sheet	Workflow	Evaluate	<input type="checkbox"/>
33		Else										
34		Read output sheet	\$VAL_VPC	Row		Column	6	6	Sheet	Workflow	Evaluate	<input type="checkbox"/>
35		Endif										

Figure 44: The Read Data workflow. Lines 1 to 12 show the prop names for each parameter, what sheet Petrel needs to use (License), and which row and column to use from the experimental design setup from Figure 43. Line 14 starts the process of an if, else, and end statement of loading the assigned set values, which are also given prop names. This process needs to be set up for the 11 tested parameters, but Model 2 does not use VPC hence why it is shaded in this figure.

The modelling workflow structure is a comprehensive procedure that constructs the underlying framework of a model. The workflow involves loading a 3D grid, generating horizons and zones, establishing layering, defining contact points, and conducting geometrical modelling for segments, zones, and the oil-water contact (OWC). Within this workflow, the layering parameter is the initial variable that undergoes testing. Specifically, the \$VAL_Lay parameter is entered into the workflow, as illustrated in Figure 45. The layering values are detailed in Table 10.

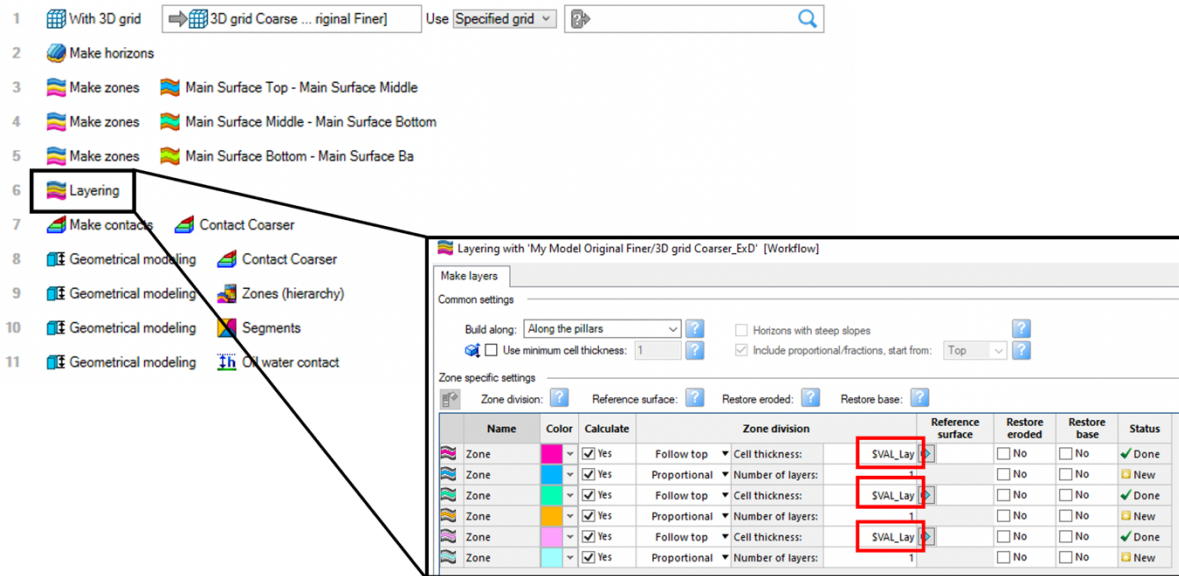


Figure 45: The Structure workflow where the first parameter, layering, is tested. The figure shows where to input the parameter in the “Layering” window. The window is opened by double-clicking on the “Layering” tab in the workflow.

The Facies workflow is responsible for executing the facies modelling procedure, with the majority of its parameters undergoing rigorous testing. These parameters include most of vs. mid-point pick, nr. of wells, and vertical proportion curve (VPC). The workflow is configured to generate either high or low values for these input parameters, depending on the desired outcome. The modelling process employs either one or three wells, the mid-point pick or the most of method, and either turns the VPC on or off (refer to Table 10 for further details). Notably, the VPC is only applicable to the fault model and is not utilized in the turbidite model. For the facies modelling process to function, the facies must be duplicated several times and assigned a new name based on the parameter being tested for those specific facies. In total, there are eight facies for the fault model and four facies for the turbidite model (refer to Figure 46). Specifically, WH denotes a high nr. of wells, WL signifies a low nr. of wells, MH indicates the use of the most of method, ML utilizes the midpoint pick, VH indicates that the VPC is turned on, and VL denotes that the VPC is turned off.

The workflow begins by loading a 3D grid and assigning a unique name to each model via the "Get calculator name" function based on the facies name. The process is then executed using if/end statements, as illustrated in Figure 47. It is within these statements that the parameters are tested, specifically the "Scale up well logs" and "Facies Modelling" parameters (Figure 47). The parameters are inputted by double-clicking on the relevant tabs, which opens the corresponding modelling windows for editing purposes (Figure 48). To ensure that the

appropriate facies are utilized during the process, it is critical to verify that the correct if/end statements are used. For instance, if \$VAL_Wells=1 and \$VAL_MO=1, high values are utilized, and “Facies_MH_WH” needs to be selected. Conversely, if \$VAL_Wells=-1, \$VAL_MO=1, and \$VAL_VH=1 the low value for wells is used, while the high value for the most of vs. mid-point pick is used and VPC is on, the “Facies_MH_WL_VH” needs to be selected, and so forth. In total, there are eight if/end statements for the fault model and four for the turbidite model.

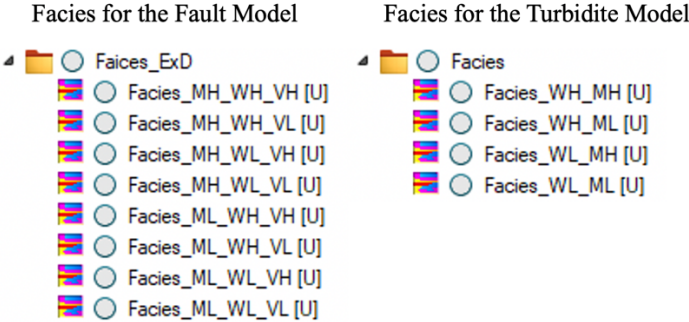


Figure 46: The facies properties for each of the two models. Their names indicate the high (H) or low (L) values used for those particular facies' models.

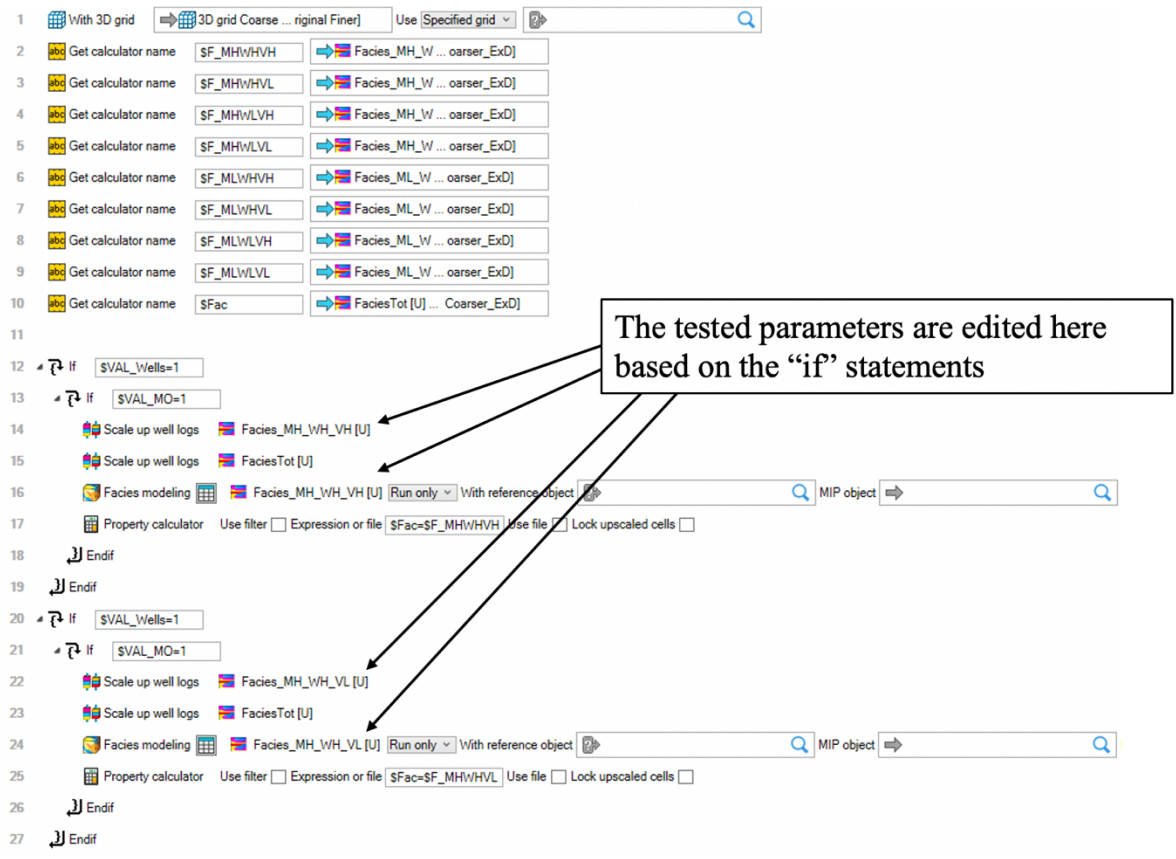


Figure 47: The Facies workflow. Line 1 loads the 3D grid, lines 2 to 10 give the facies calculator names and the facies are inserted, and lines 12 to 19 are if/end statements where the parameters are tested. Lines 12 to 19 contain “Scale up well logs” which upscales the logs, “Facies modelling” which performs the facies modelling process, and a “Property calculator” which inserts the facies that is modelled to the FaciesTot model so that there are not thousands of facies models created. The resulting model will then always be shown in the FaciesTot model.

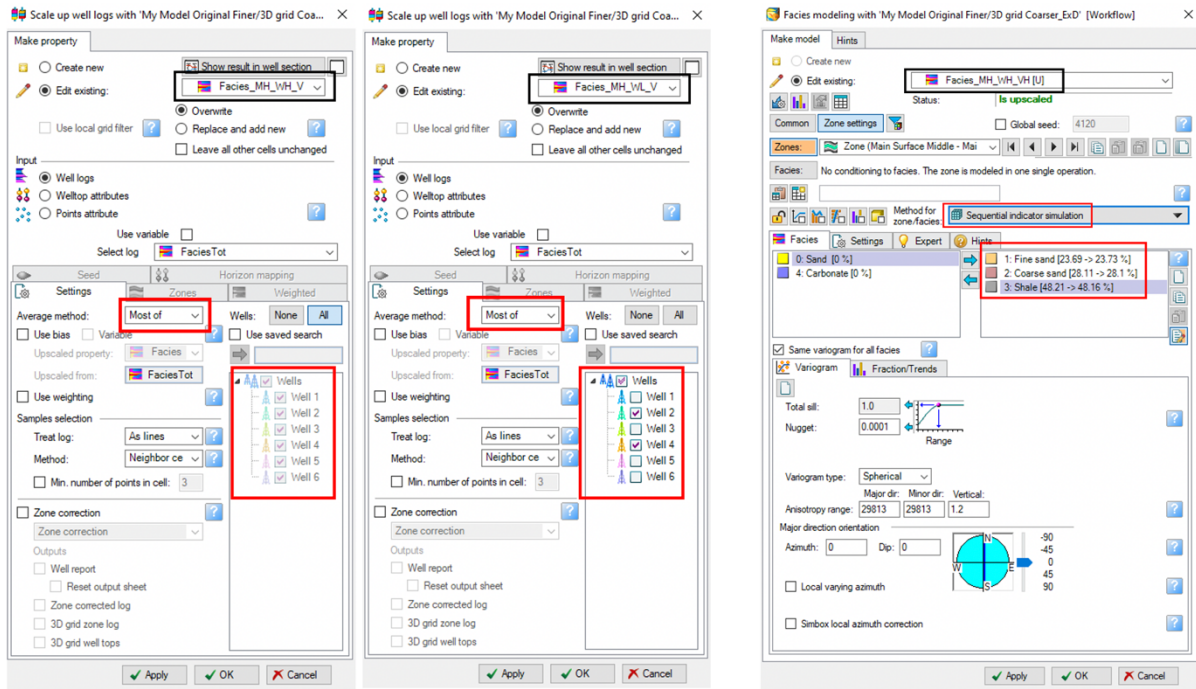


Figure 48: The “Scale up well logs” and “Facies modelling” windows. In the scale-up window nr. of wells is selected in the “Wells” setting as well as either most of or mid-point pick in the “Average method” setting. In the facies window the “Method for zone/facies” is selected and the active lithologies are moved to the right.

The vertical proportion curve (VPC) is executed in the "Data Analysis" section, found under the Property Modelling tab. VPC can either be activated or deactivated by locking or unlocking the relevant setting, as indicated by the red boxes in Figure 49A. If VPC is turned on (unlocked), the "mountain" button must be clicked once, as shown by the red box in Figure 49B. This is done so that the curve better fits the proportions of that facies.

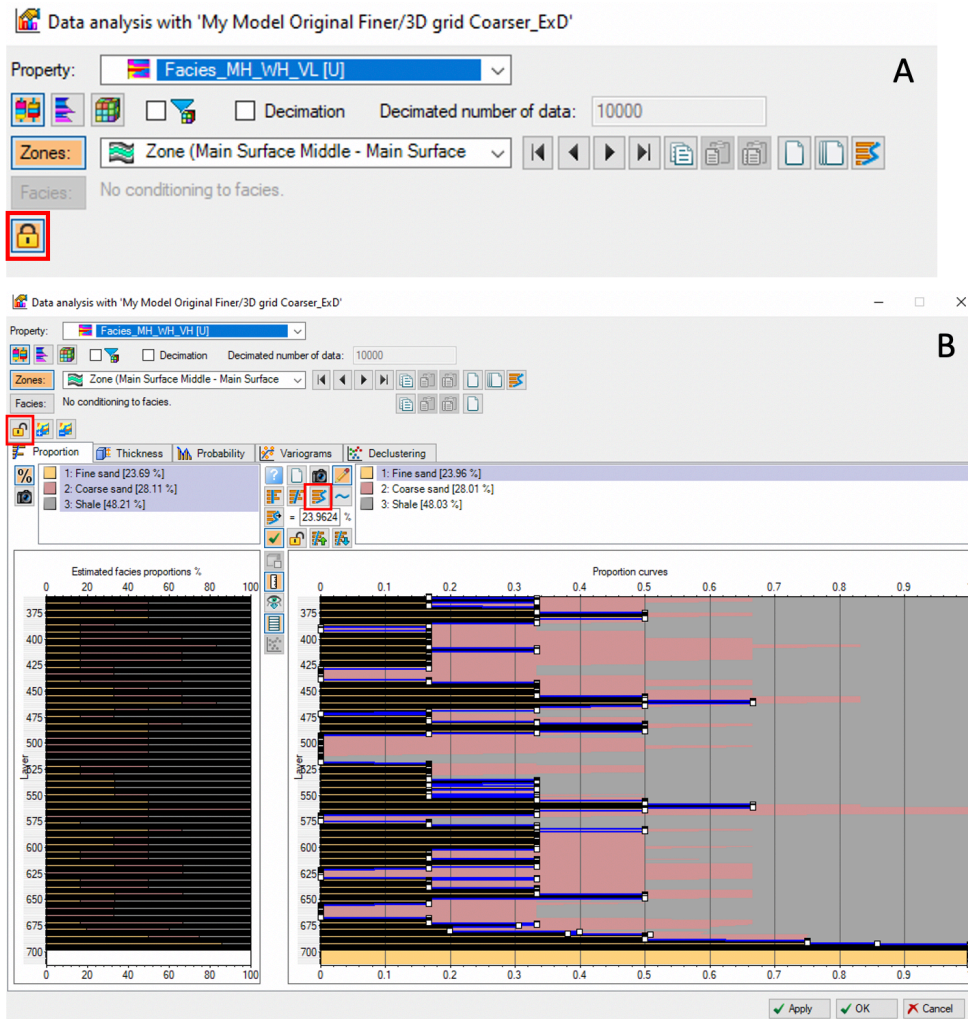


Figure 49: Vertical proportion curve off (A) or on (B) in the "Data Analysis" window.

The Property workflow executes the petrophysical modelling process, as illustrated in Figure 50. This workflow is designed similarly to the Facies workflow, involving the loading of a 3D grid, utilizing "Get calculator name", and if/end statements for all 16 tested variations. The 16 tested variations of the porosity and permeability models are shown in Figure 51. The workflow implements either high or low values for the input parameters. In order to perform porosity and permeability modelling, these models must be duplicated in the same manner as the facies model.

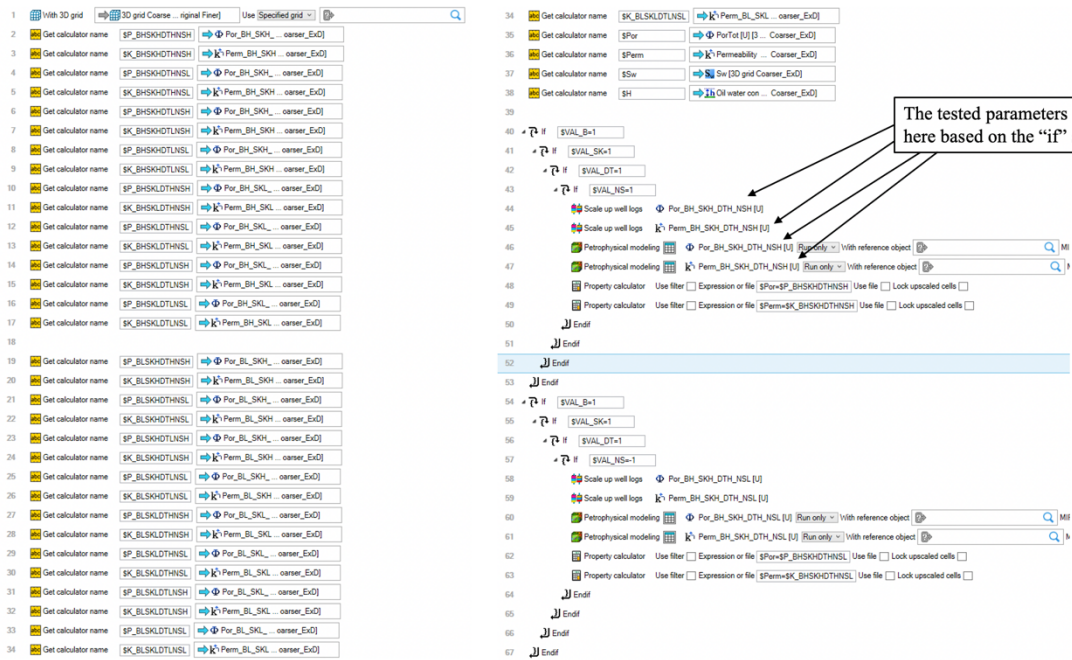


Figure 50: The Petrophysical workflow. Line 1 loads the 3D grid, lines 2 to 34 give calculator names and the porosity and permeability models are inserted using the blue arrows, and line 40 starts the if/end statements where the parameters are tested. Lines 40 to 53 contain “Scale up well logs” which upscales the logs, “Petrophysical modelling” which performs the petrophysical modelling process, and a “Property calculator” which inserts the porosity and permeability that is modelled to the PorTot and PermeabilityTot model so that there are not thousands of por/perme models created. The resulting model will then always be shown in the PorTot and PermeabilityTot model.

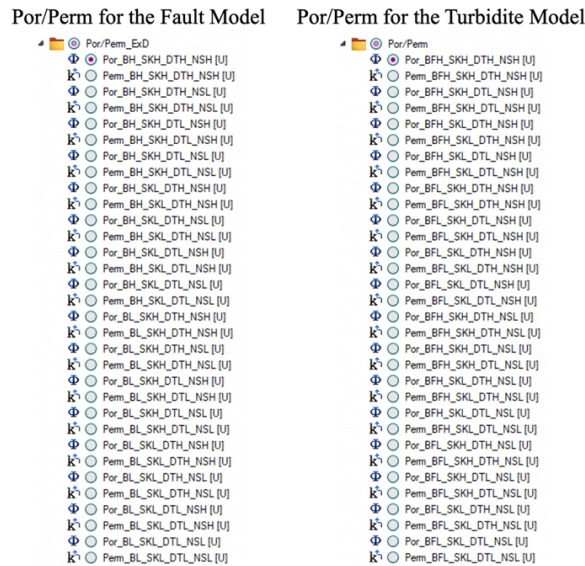


Figure 51: The porosity and permeability models for Model 1 and Model 2. Their names indicate the high (H) or low (L) values used for that particular model.

The petrophysical modelling process can either be executed with or without bias to facies, utilizing either sequential Gaussian simulation (SGS) or Kriging, different variogram range, and with or without depth trend, as well as with a normal or asymmetric distribution. The input parameters can be specified by double-clicking on the "Scale up well logs" and "Petrophysical Modelling" tabs, with details on how and where to input parameters provided in the figure descriptions. Bias to facies can be selected when upscaling the porosity log (Figure 52). SGS vs. Kriging, variogram range, and correlation coefficient can be edited during the petrophysical modelling process (Fig. 53 & 54 & 55), whereas depth trend and normal or asymmetric distribution can be performed in the data analysis phase (Fig. 56 & 57).

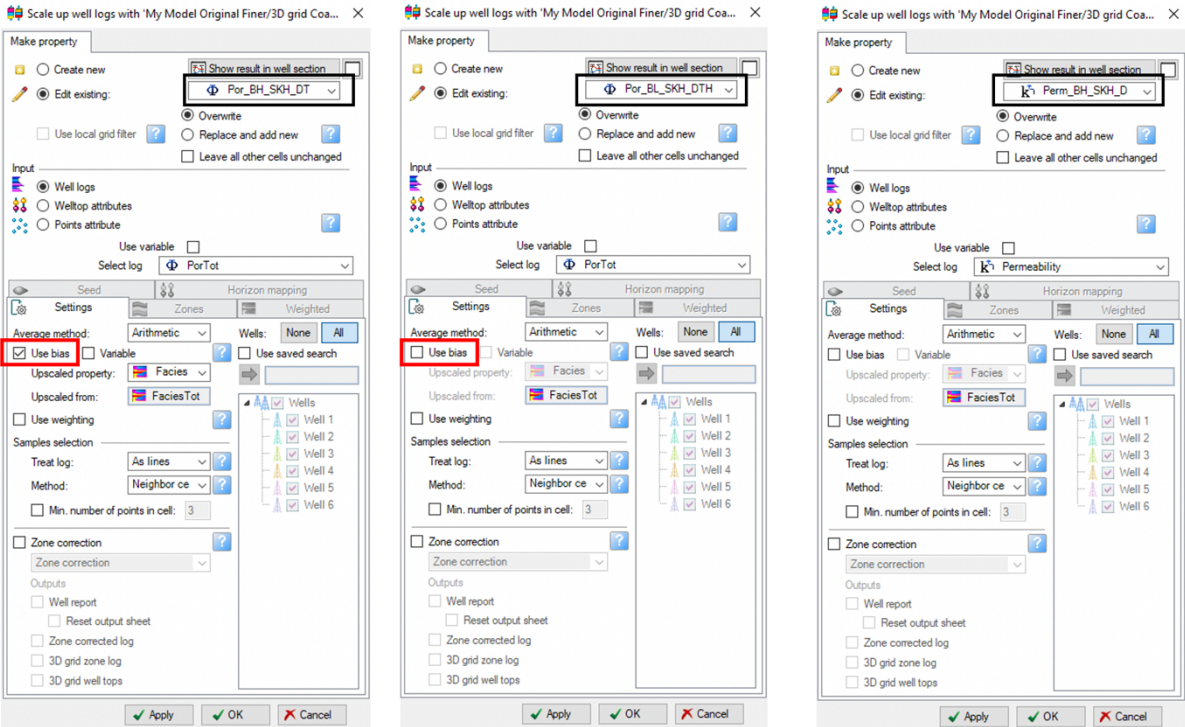


Figure 52: The well log upscaling of porosity and permeability. In the upscaling of porosity, the “Use bias” is either on or off depending on the porosity model name BH (on) or BL (off) as marked with a red box. The upscaling of both porosity and permeability uses Arithmetic as the “Average method”. The permeability upscaling process does not use “Use bias”.

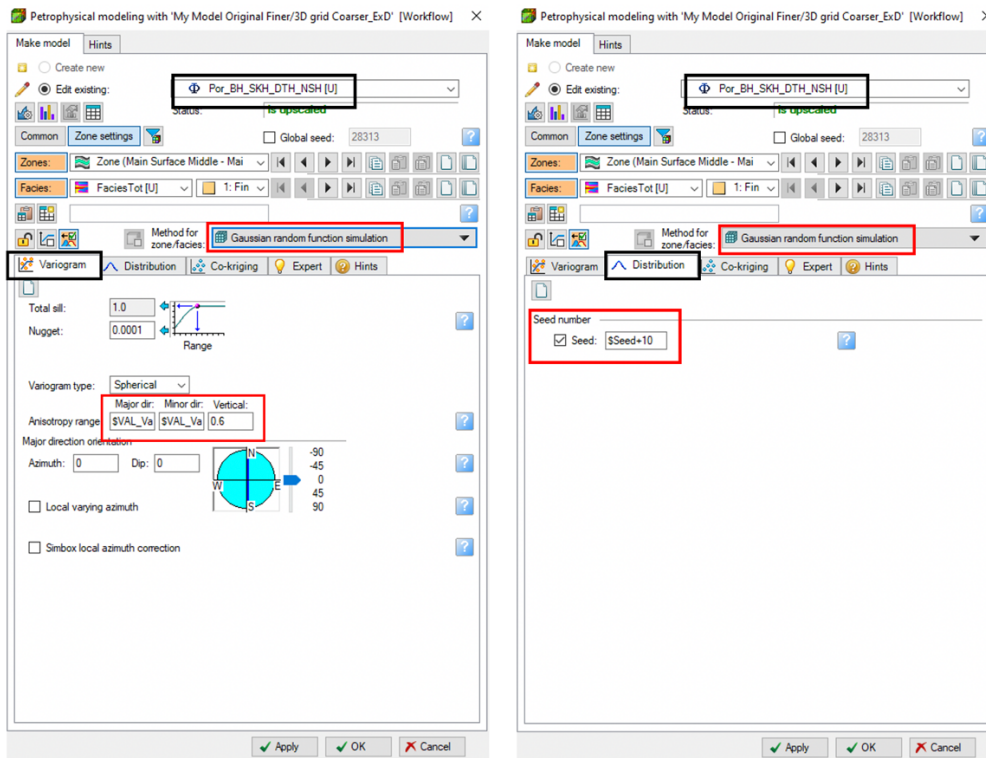


Figure 53: The petrophysical modelling process of the porosity with SGS as “Method for zone/facies”. In the Variogram tab, the variogram range parameter is tested by inserting $SVAL_Var$ to the “Anisotropy range” for Major dir. and Minor dir. Under the “Distribution” tab the “Seed number” is set to $\$Seed+10$ for sand, $\$Seed+20$ for fine sand and $\$Seed+30$ for the sand in the next zone.

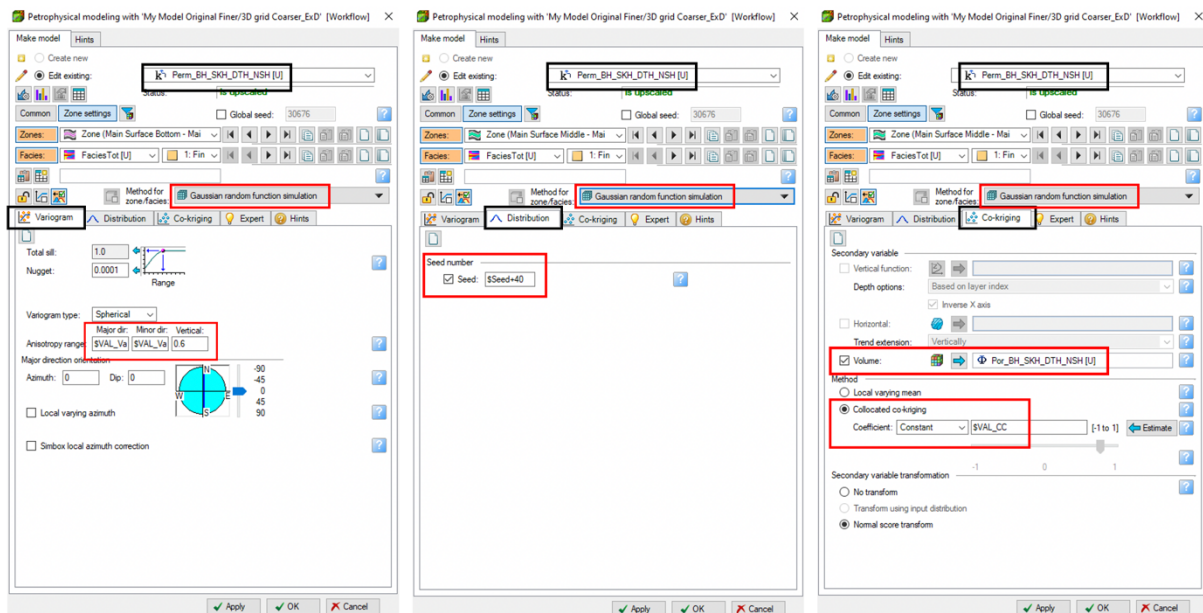


Figure 54: The petrophysical modelling process for permeability with SGS “Method for zone/facies”. In the Variogram tab, the variogram range parameter is tested by inserting $SVAL_Var$ to the “Anisotropy range” for Major dir. and Minor dir. Under the Distribution tab the “Seed number” is set to $\$Seed+40$ for the fine sand, $\$Seed+50$ for sand and $\$Seed+60$ for the sand in the next zone. In the Co-kriging tab, the correlation coefficient is tested by inserting $SVAL_CC$ to the “Collocated co-kriging” setting, and the corresponding porosity model to the permeability is inserted to the “Volumes” setting.

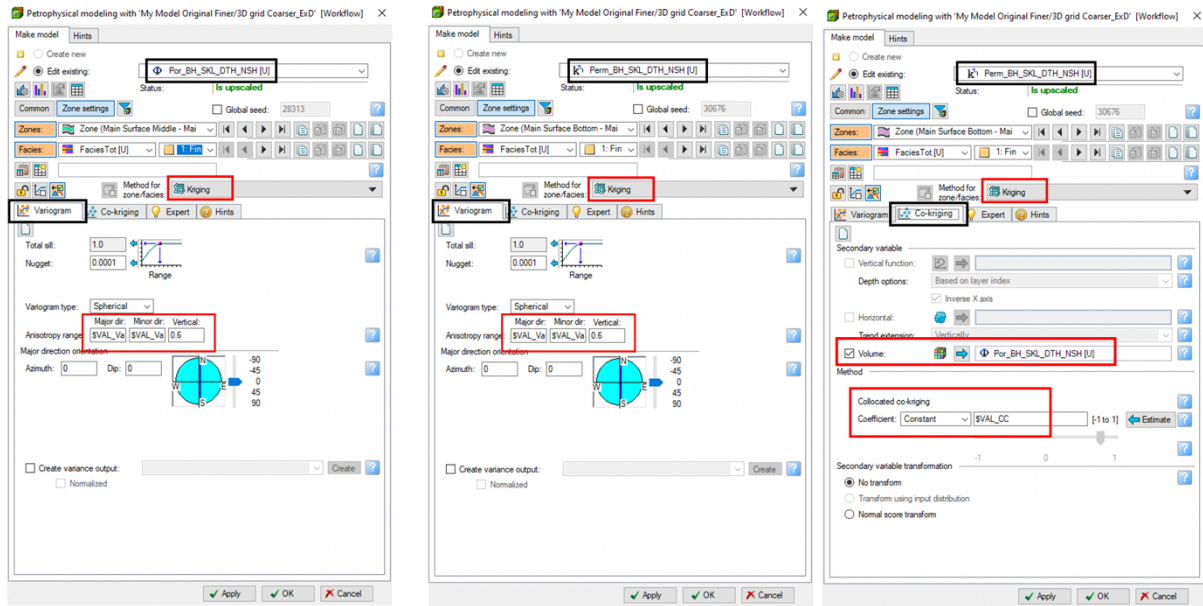


Figure 55: The petrophysical modelling process for porosity and permeability when the “Method for zone/facies” is Kriging and where to insert SV_Var for variogram range and VAL_CC for collocated co-kriging.

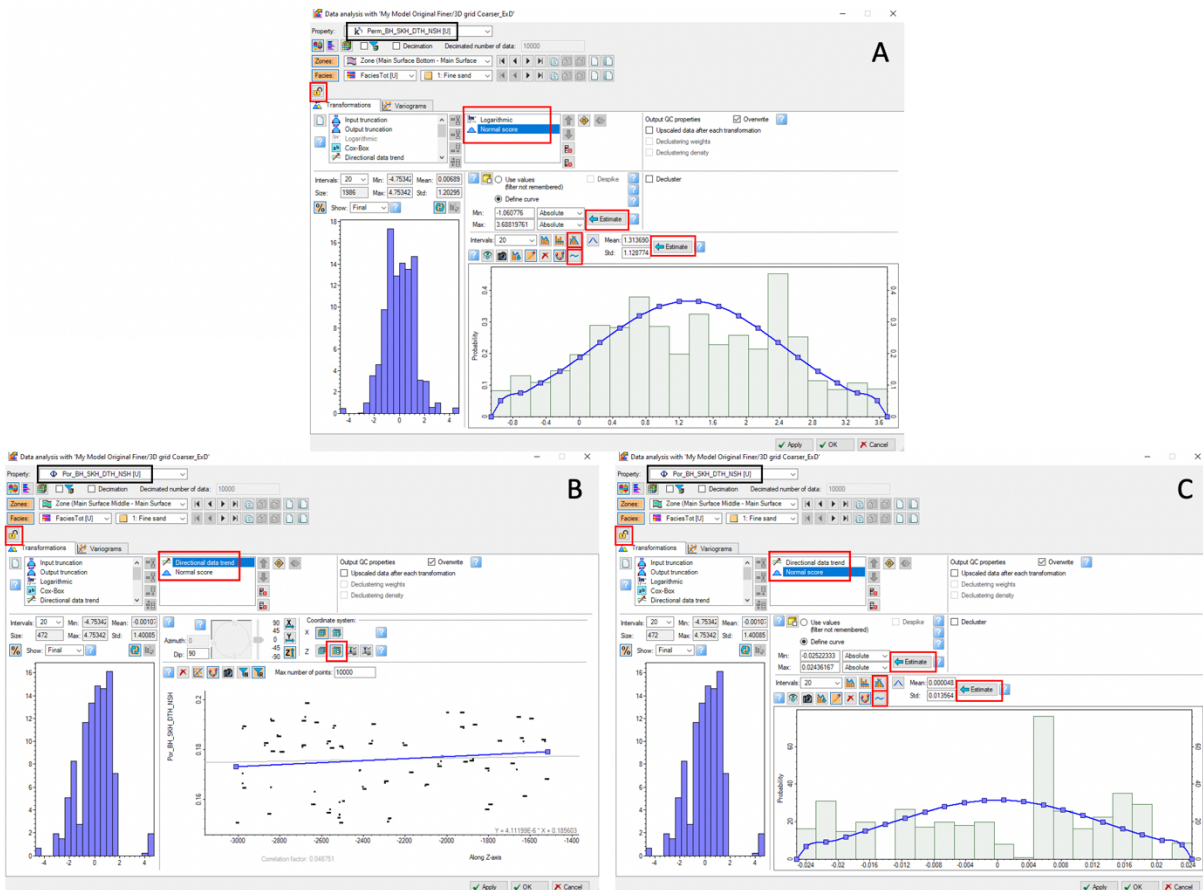


Figure 56: The Data Analysis for porosity and permeability with depth trend and normal distribution. A show the data analysis for permeability, and it uses “Logarithmic” for depth trend and has a normal score. To achieve normal score, one has to select “Estimate” twice and then the settings marked with two small red boxes. B shows the data analysis for porosity with directional data trend (depth trend) and it is important to select the distorted cube in the Z direction in the “Coordinate system”, and C shows the normal score distribution for porosity.

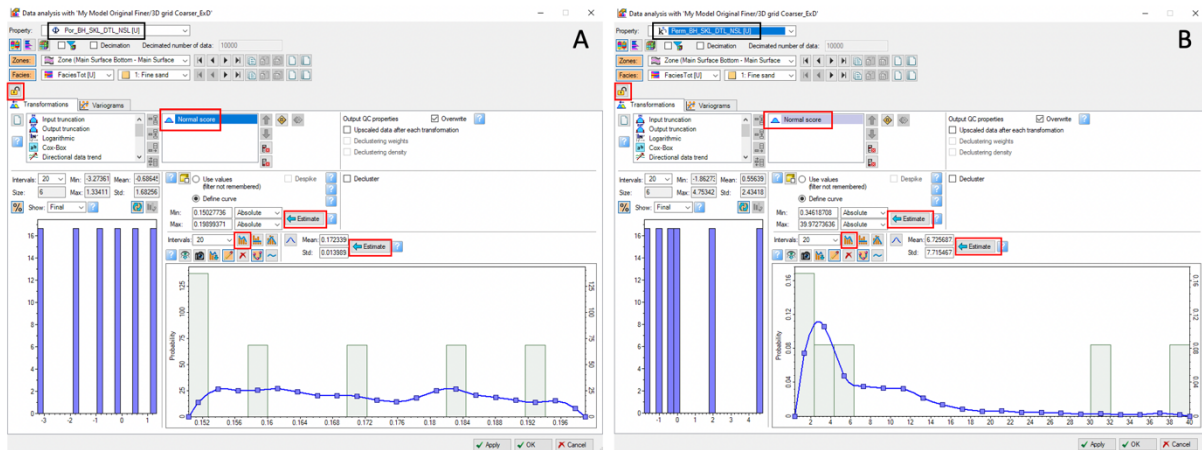


Figure 57: The Data Analysis for porosity (A) and permeability (B) with asymmetric distribution and no depth trend. For asymmetric distribution, the “Estimate” button is selected twice, and then the “mountain” button is used as marked with a little red box.

The Volumes workflow is designed to calculate volumes for each run of the model. There are 2048 runs in the MasterED, so there will be 2048 volumes calculated for this model. The Volumes workflow structure and setup are shown in Figures 58 & 25.

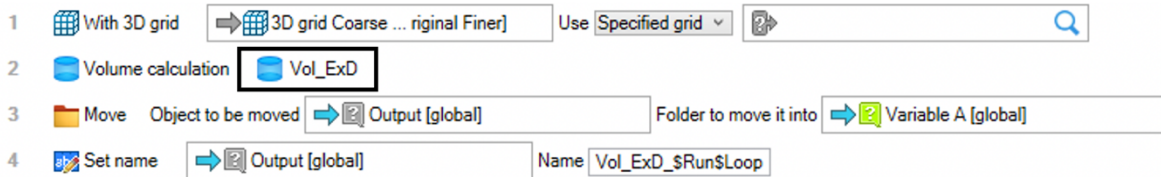


Figure 58: The volume workflow.

After the experiments were conducted on Model 1 (Fluvial) and Model 2 (Turbidite) a third experiment was performed on Model 2 (Turbidite) because a slight mistake was observed. Model 2 was run on a normal distribution but should have been run on an asymmetric distribution for porosity, so a third experiment was performed and is named Model 2B (Turbidite). So, in the results, they will be assigned the names Model 2A and Model 2B as mentioned previously.

5.3 The Parameters

The parameters that are being tested as mentioned are layering, the nr. of wells, most of vs. mid-point pick, vertical proportion curve (VPC), bias to facies on vs. off, Sequential Gaussian simulation (SGS) vs. Kriging, variogram range for porosity and permeability, with vs. without depth trend, the correlation coefficient for permeability, normal vs. asymmetric distribution and the saturation height function. Below is some information about each parameter.

Layering is the internal layering that reflects the geological deposition in a specific zone. The layers sub-divide the grid between the zone-related horizons. There are different settings for layering, the common ones are built along and use minimum cell thickness (Schlumberger 2023b).

The nr. of wells describes how many wells are going to be used in the facies modelling process. It is either 2 or 4 wells in the fault model or 1 or 3 wells in the turbidite model.

Most of selects the value that is represented most in the log for each particular cell and will assign that value to the cell. Mid-point pick will select the log value that is halfway through the cell along the well. This is a random pick and will likely give a property with the same distribution as the input data. It forces the log to be upscaled “as lines” because it needs to calculate the weighted cumulative distribution function from samples from surrounding cells to draw a mid-point value (Schlumberger 2023b).

The vertical proportion curve (VPC) is the curve for each facies code and per layer, and this can be edited. If one edits the curve all other unlocked curves are adjusted to ensure that the sum of all the code proportions is always 1. VPC influences how the proportion of each facies varies vertically in a stratigraphic zone, and it is sensitive to the way the model is layered (Schlumberger 2023b).

Use bias is used to control the upscaling process in a discrete property. With or without bias is tested in the upscaling process of the porosity logs (Schlumberger 2023b).

Sequential Gaussian simulation (SGS) uses the well data, variograms, input distributions, and trends, and these can be used to create local variations. Kriging is a deterministic approach for

kriging discrete properties, and the result depends on the upscaled cells, the defined variogram and the fraction for each individual facies. The results are directly repeatable and avoid overinterpretation of the data (Schlumberger 2023b).

Variogram range is the distance within which the data can be correlated, a large range equals greater continuity, a small range equals less continuity and the larger the range is the smaller the heterogeneity (Schlumberger 2023b).

A directional data trend (depth trend) is a transformation where you can interactively define or generate the trend of a function from the input data used by specifying a vector in space. One should use the trends with care. The vector is defined by using a specific dip and azimuth, and if the trend is valid, the data collect along a straight line in the cross-plot window. Note that if one models the petrophysical trend with different facies, a directional data trend curve needs to be set for each facies (Schlumberger 2023b).

The correlation coefficient determines how strong an impact the second variable should have on the result. The variable should be between 1 and -1, where 1 and -1 mean that there is a 100% correlation and 0 means that there is no correlation. The correlation coefficient will be estimated or set by the user. There are four ways to set the coefficient, using “constant”, “from upscaled”, “property”, and “surface”. The correlation coefficient will be estimated between the transformed primary and secondary data at the upscaled cell’s location. Primary data are normal score transformed; the transformation applied to secondary data is the one specified in the “Secondary data settings” section. If using transformations from data analysis, make sure the normal score is applied (Schlumberger 2023b).

The normal distribution is the most common distribution function for random and independent generated variables. It is also called the Gaussian distribution and is recognized for its bell-shaped curve. The normal distribution graph is characterized by the mean/average and the standard deviation. The mean/average is the maximum of the graph and is always symmetric and the standard deviation decides the dispersion amount away from the mean/average (Britannica 2022). Asymmetric distribution is when the variables are irregular, the mean/average and standard deviation occurs at different points. This type of distribution exhibits skewness, it deviates from the normal distribution. There is no symmetry (Kenton 2022; Chen 2023).

The saturation height function impacts the reserve calculations of oil and gas in a reservoir, it calculates the water content based on the rock properties and the height above contact. The function is used to predict saturations above a set height above the free water level. The function is used by reservoir engineers and geologist (Jamiolahmady, Sohrabi, and Tafat 2007; Esmacili et al. 2022)

6. Results

In this section of the thesis, the results from the three experiments performed in Petrel using the experimental design are presented. Model 1 is a fluvial model with a braided river system and Models 2A and 2B are a turbidite models. The research encompassed three distinct result sets Model 1 (Fluvial), Model 2A (turbidite) with a porosity exhibiting a normal distribution, and Model 2B (turbidite). Model 2B is the same as Model 2A but with the original porosity characterized by a clearly non-normal distribution. The results of this thesis aim to determine the effect changes on several parameters have on volume calculations, to determine which parameters have the highest and lowest impacts, and if these changes could be ubiquitous or are case specific. Several of the parameters have seen to be modelled incorrectly by industry practitioners, these have been tested by varying between correct and incorrect model settings. One of the main aims is to determine the impact of not creating consistent models. In addition, a comparison is made between the known “real cases” volumes with those from a range of “reservoirs” models. If the results are case-specific or universal across different geological situations is also of interest, therefore two fundamentally different models were used in the experiments.

The results for this thesis were extracted from the "volumes" tab within the "output" sheet of Petrel software. Subsequently, the data was transferred to Excel for analysis. Multiple Excel sheets, tables, and diagrams were created to analyse the outcomes obtained from the workflows and the experimental design setup. In total, there were 2048 runs used for each experiment, resulting in 2048 volumes the volumetric measures, including bulk volume, net volume, hydrocarbon pore volume oil (HCPV), hydrocarbon pore volume gas (HCPV), stock tank oil initially in place (STOIP), and gas initially in place (GIIP). For much of the analysis, the average values for each parameter setting is considered in the results section.

6.1 Original Models vs. Experiment Models

Tables 11-13 present a comparison of volumes between the real-case models and the reservoir models used in the experiments. This comparison has been made to check that the range of modelling techniques used and their volume ranges, actually cover the real-case volumes. To facilitate this analysis, the min, max, average, P10, P50 and P90 of the 2048 volumes for each model were computed (Tables 11, 12, and 13).

The real-case volumes exhibit both similarities and differences when compared to the volumes obtained from the modelled experiments. Specifically, the bulk volumes and net volumes demonstrate similarities, with the real-case volumes measuring 3,841,270, while the volumes from the modelled experiments yield 3,788,623 7294 for Model 1. Similarly, for Model 2A and 2B, the real-case volumes for bulk and net volume amount to 7500 and 7294, respectively, in contrast to the modelled experiment results. Model 1 is a large-scale model while Model 2A and 2B are small-scale models, hence the significant volume difference.

For the other volumes measures, pore volume (HCPV gas, HCPV oil, STOIP, and GIIP), Model 1 displays significant differences, while in Model 2A and 2B, the difference is generally acceptable when comparing the real case with the average values for the experiments. For Model 2B, specifically, the reservoir models tend to be on the low side, when comparing to the real case, which tends to lie within the P10-P90 range, but close to the P90.

There is a large difference in the real-case volumes vs. the reservoir volumes in Model 1, specifically pore volume, HCPV oil, HCPV gas, STOIP, and GIIP. This issue will be taken up in the discussion section.

Figures 59, 60 and 61 show a visual representation of the difference in the volumes calculated between the Original and Reservoir case models. The figures display the real-case volumes as a single point, and this is compared to the P10 and P90 for the reservoir model. There is a significant difference in the real-case model vs. the experiment model in Model 1, in all the calculated volumes, where the real-case volumes plot outside the P10 and P90. In Model 2A and 2B nearly all the real-case data plots within the P10 and P90, but in Model 2B some of the real-case volumes plot outside of the P10-P90 range.

The Real-Case data vs Experiment data for Model 1

Model 1 (Fluvial)	Bulk Volume (10 ⁶ m ³)	Net Volume (10 ⁶ m ³)	Pore Volume (10 ⁶ rm ³)	HCPV Oil (10 ⁶ rm ³)	HCPV Gas (10 ⁶ rm ³)	STOIP (10 ⁶ sm ³)	GIIP (10 ⁹ sm ³)	Note
Real-Case data	3841270	3841270	378371	179417	207954	142014	456	Real-Case Model data
Avg	3788623	3788623	118103	97327	320	81106	91	Experiment Model data
Min	3788623	3788623	1009	2310	256	1925	73	Experiment Model data
Max	3788623	3788623	173158	117516	453	97930	130	Experiment Model data
P10	3788623	3788623	109390	85174	286	70978	82	Experiment Model data
P50	3788623	3788623	124850	106661	319	88884	91	Experiment Model data
P90	3788623	3788623	129235	111463	355	92885	101	Experiment Model data

Table 11: The real-case data vs. the experiment data from Model 1.

The Real-Case data vs Experiment data for Model 2A

Model 1 (Fluvial)	Bulk Volume (10 ⁶ m ³)	Net Volume (10 ⁶ m ³)	Pore Volume (10 ⁶ rm ³)	HCPV Oil (10 ⁶ rm ³)	HCPV Gas (10 ⁶ rm ³)	STOIP (10 ⁶ sm ³)	GIIP (10 ⁹ sm ³)	Note
Real-Case data	7500	7500	1497	1057	440	881	126	Real-Case Model data
Avg	7294	7294	1441	856	377	713	108	Experiment Model data
Min	7294	7294	1095	677	225	564	64	Experiment Model data
Max	7294	7294	1895	1093	593	911	169	Experiment Model data
P10	7294	7294	1106	696	231	580	66	Experiment Model data
P50	7294	7294	1549	860	396	717	113	Experiment Model data
P90	7294	7294	1827	1035	556	863	159	Experiment Model data

Table 12: The real-case data vs. the experiment data from Model 2A.

The Real-Case data vs Experiment data for Model 2B

Model 1 (Fluvial)	Bulk Volume (10 ⁶ m ³)	Net Volume (10 ⁶ m ³)	Pore Volume (10 ⁶ rm ³)	HCPV Oil (10 ⁶ rm ³)	HCPV Gas (10 ⁶ rm ³)	STOIP (10 ⁶ sm ³)	GIIP (10 ⁹ sm ³)	Note
Real-Case data	7500	7500	1487	1057	440	881	126	Real-Case Model data
Avg	7294	7294	1192	752	235	627	67	Experiment Model data
Min	7294	7294	949	632	129	527	37	Experiment Model data
Max	7294	7294	1568	938	405	782	116	Experiment Model data
P10	7294	7294	957	655	138	546	39	Experiment Model data
P50	7294	7294	1061	721	184	601	52	Experiment Model data
P90	7294	7294	1457	873	352	727	101	Experiment Model data

Table 13: The real-case data vs. the experiment data from Model 2B.

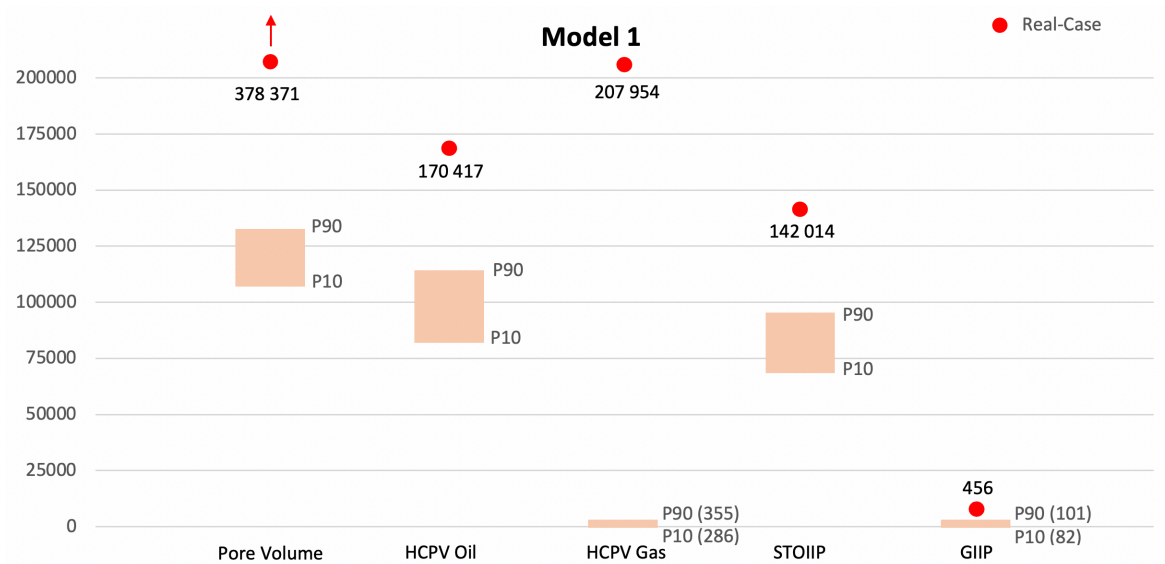


Figure 59: Real-case volumes compared to P10-P90 for Model 1. The real-case values are shown with a red dot.

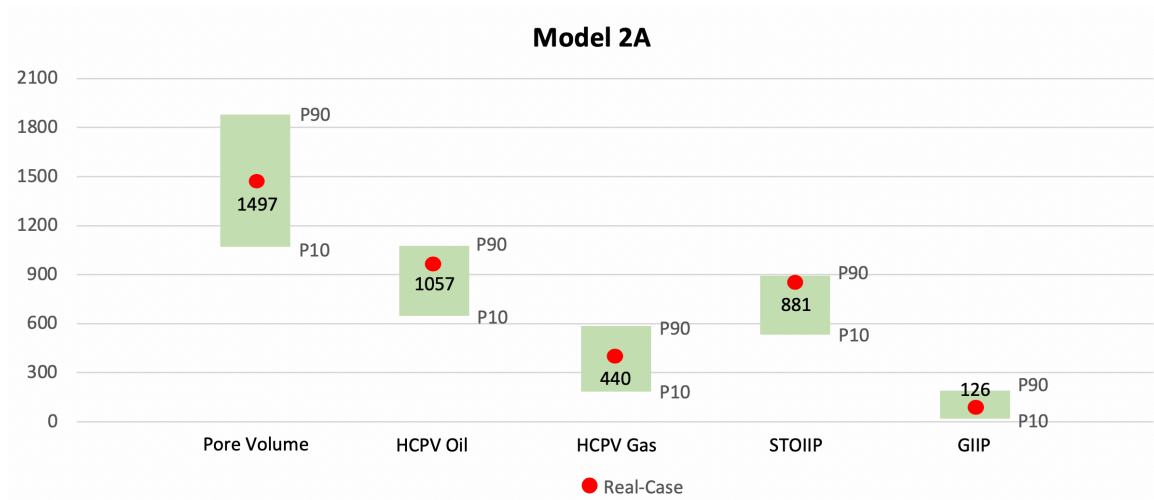


Figure 60: Real-case volumes compared to P10-P90 for Model 2A. The real-case values are shown with a red dot.

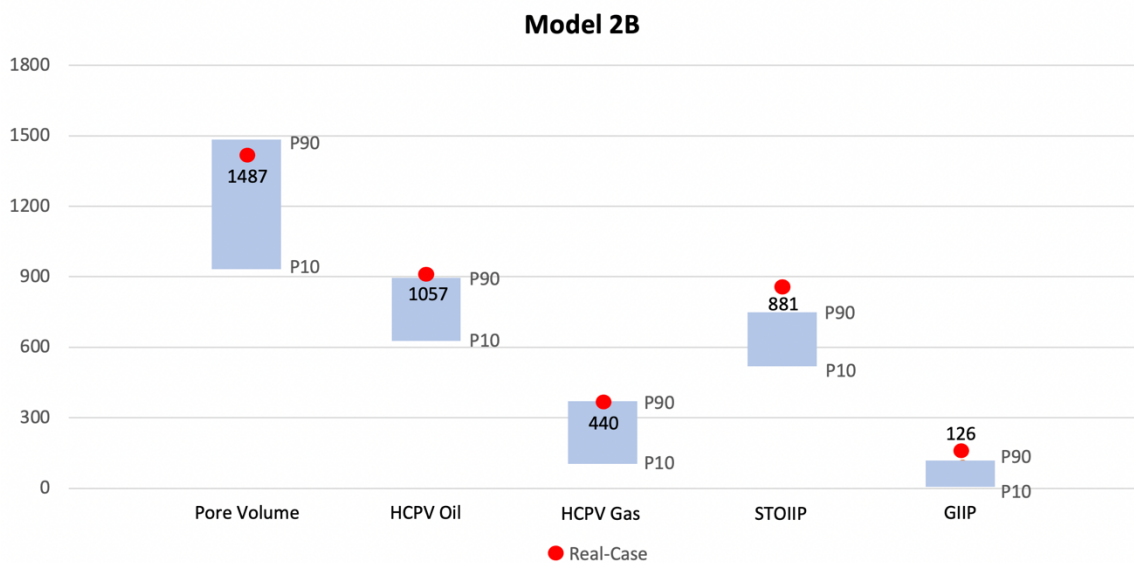


Figure 61: Real-case volumes compared to P10-P90 for Model 2B. The real-case values are shown with a red dot.

6.2 Parameter Analysis

This section provides a summary of the parameter analysis results. For each model a summary table for the differences between the average high volumes and the average low volumes are presented. In the experimental design, the high and low values for each parameter are designated with either 1 or -1 respectively. This allows the results to be analysed to determine the impact of each parameter separately because the high and low values for each parameter vary independently of each other throughout the design matrix. In order to determine the impact of each parameter, the volumes were statistically analysed by computing the minimum, maximum, and average values separately for the high (1's) and low (-1's) runs. The full set of results and analyses for all three models are presented in Appendix A and B. To facilitate analysis within the results section, the average values of the highs (1's) and lows (-1's) are the focus of evaluation. The table is then followed by a set of tornado charts, one for each measure of volume (pore volume, HCPV oil, HCPV gas, STOIP, and GIIP). The summary tables are shown in Tables 14 to 16, while the tornado charts are visualized in Figures 62 to 76.

6.2.1 Model 1

Model 1 (Fluvial)

Parameters	Pore Volume	HCPV Oil	HCPV gas	STOIP	GIIP
Bias to Facies	14,77 %	12,79 %	2,50 %	12,79 %	2,51 %
Correlation Coefficient	0,10 %	0,79 %	0,23 %	0,79 %	0,25 %
Depth Trend	17,21 %	8,37 %	2,19 %	8,37 %	2,19 %
Layering	0,67 %	0,77 %	2,88 %	0,77 %	2,88 %
Most of vs. Mid-point pick	0,01 %	0,01 %	0,15 %	0,01 %	0,14 %
Normal vs. Asymmetric	16,44 %	10,67 %	2,10 %	10,67 %	2,09 %
Saturation Height Func	0,01 %	2,53 %	3,77 %	2,53 %	3,80 %
SGS vs. Kriging	12,52 %	3,46 %	1,32 %	3,46 %	1,36 %
Variogram	0,05 %	0,05 %	0,35 %	0,05 %	0,37 %
Vertical Proportion Curve	0,08 %	0,09 %	0,43 %	0,09 %	0,44 %
Nr. of Wells	3,31 %	4,05 %	1,28 %	4,05 %	1,28 %

Table 14: A summary table of the % difference of average high and average low for each parameter in Model 1 on pore volume, HCPV oil, HCPV gas, STOIP, and GIIP.

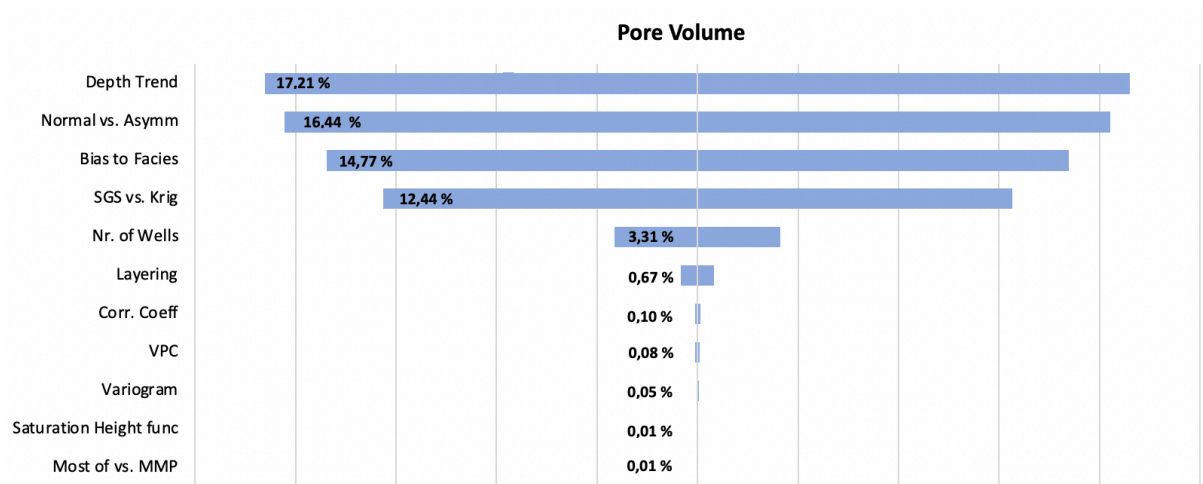


Figure 62: Tornado plot for the % difference in pore volume for Model 1. The % difference values are taken from Table 14.

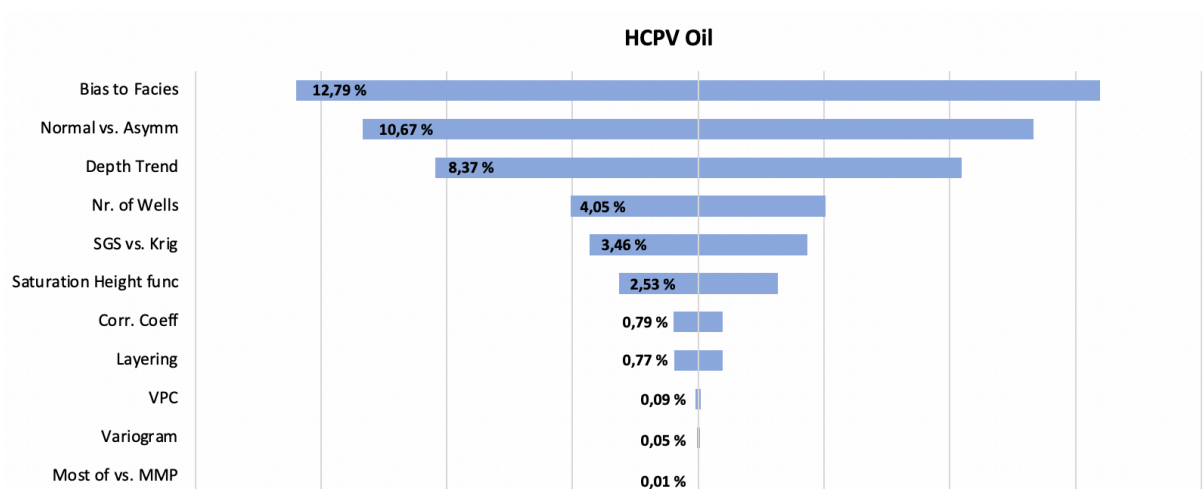


Figure 63: Tornado plot for the % difference in HCPV oil for Model 1. The % difference values are taken from Table 14.

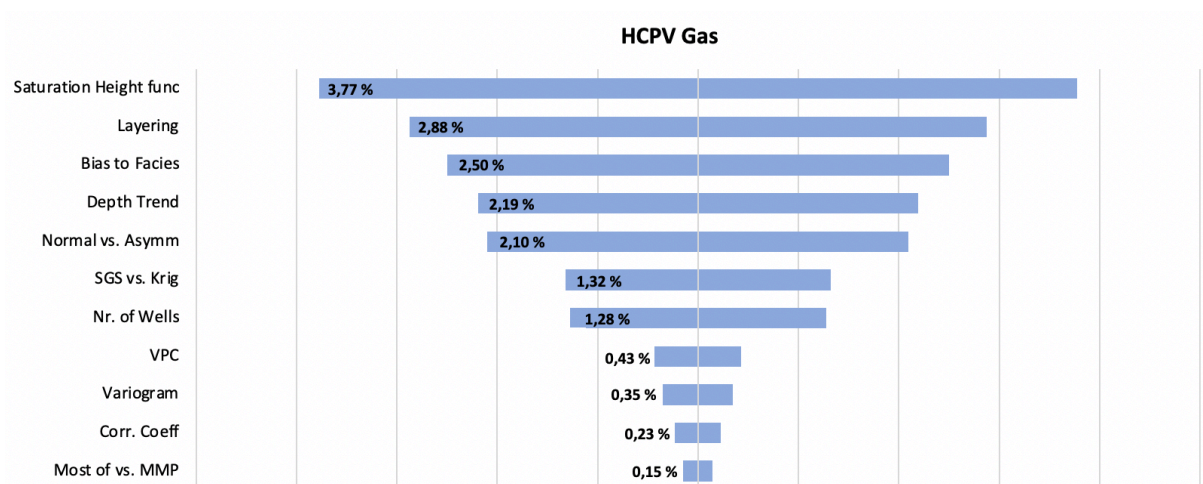


Figure 64: Tornado plot for the % difference in HCPV gas for Model 1. The % difference values are taken from Table 14.

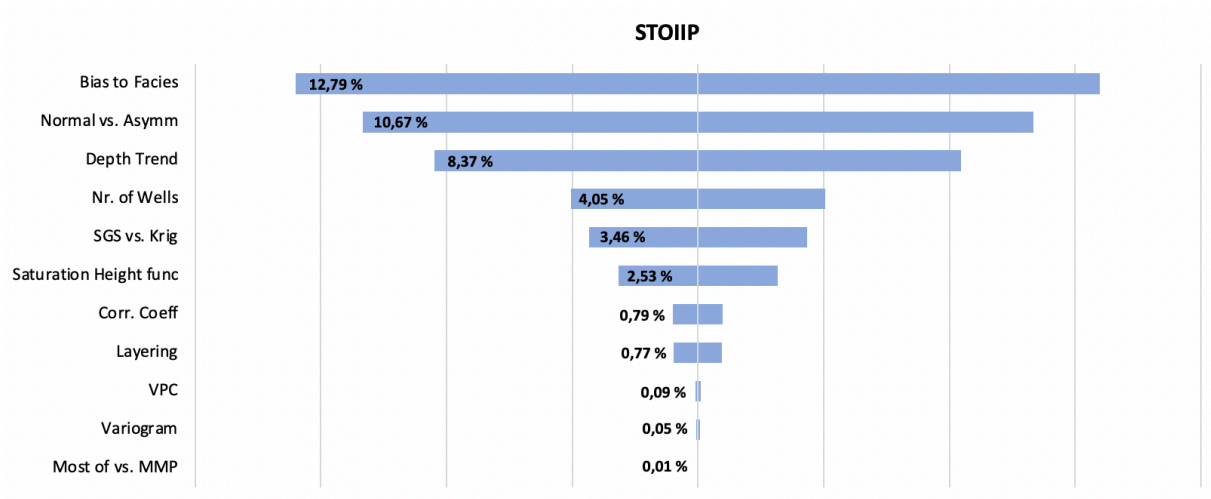


Figure 65: Tornado plot for the % difference in STOIP for Model 1. The % difference values are taken from Table 14.

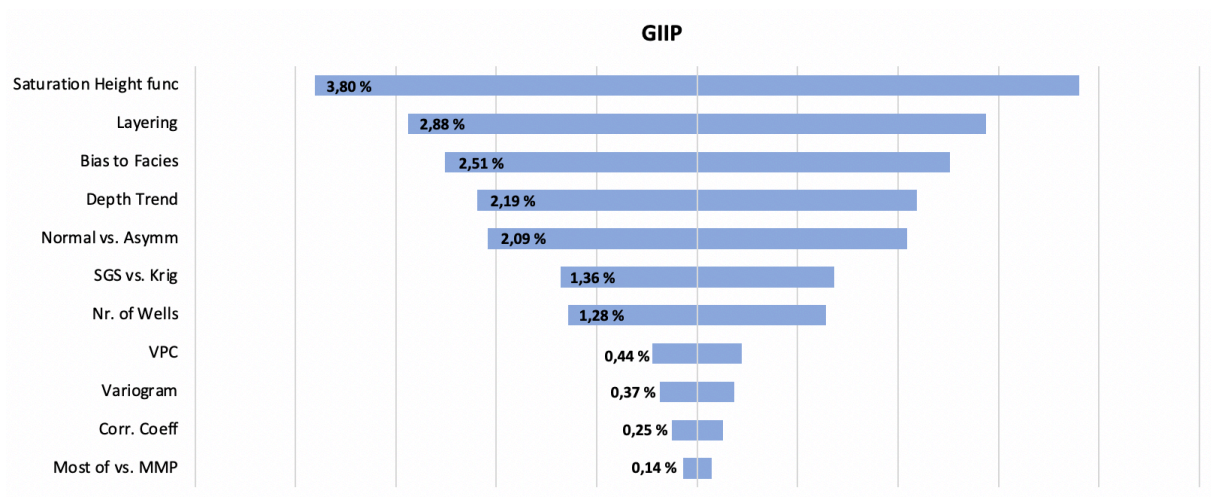


Figure 66: Tornado plot for the % difference in GIIP for Model 1. The % difference values are taken from Table 14.

6.2.2 Model 2A

Model 2A (Turbidite)

Parameter	Pore Volume	HCPV oil	HCPV gas	STOIP	GIIP
Bias to Facies	3,03 %	2,58 %	5,79 %	2,58 %	5,77 %
Correlation Coefficient	0,02 %	0,09 %	0,11 %	0,09 %	0,11 %
Depth Trend	5,47 %	6,12 %	9,68 %	6,12 %	9,66 %
Layering	0,02 %	0,24 %	0,07 %	0,24 %	0,08 %
Most of vs. Mid-point pick	0,02 %	0,03 %	0,12 %	0,03 %	0,10 %
Normal vs. Asymmetric	0,68 %	1,17 %	0,49 %	1,17 %	0,50 %
Saturation Height Func	0,02 %	3,07 %	1,95 %	3,07 %	1,95 %
SGS vs. Kriging	1,69 %	0,74 %	4,42 %	0,74 %	4,41 %
Variogram	0,05 %	0,00 %	0,07 %	0,01 %	0,08 %
Nr. of Wells	34,71 %	26,67 %	52,09 %	26,67 %	52,10 %

Table 15: A summary table of the % difference of average high and low for each parameter in Model 2A on pore volume, HCPV oil, HCPV gas, STOIP, and GIIP.

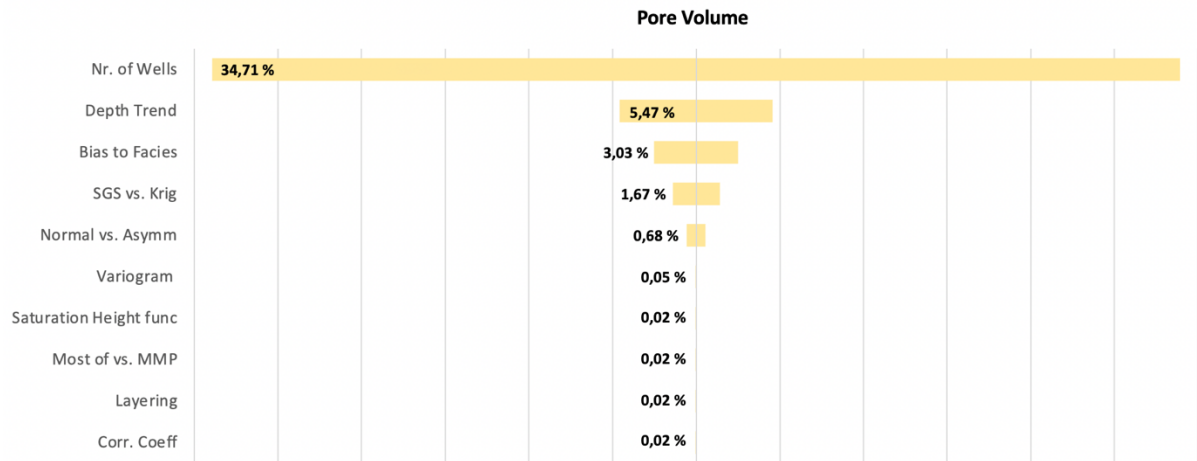


Figure 67: Tornado plot for the % difference in pore volume for Model 2A. The % difference values are taken from Table 15.

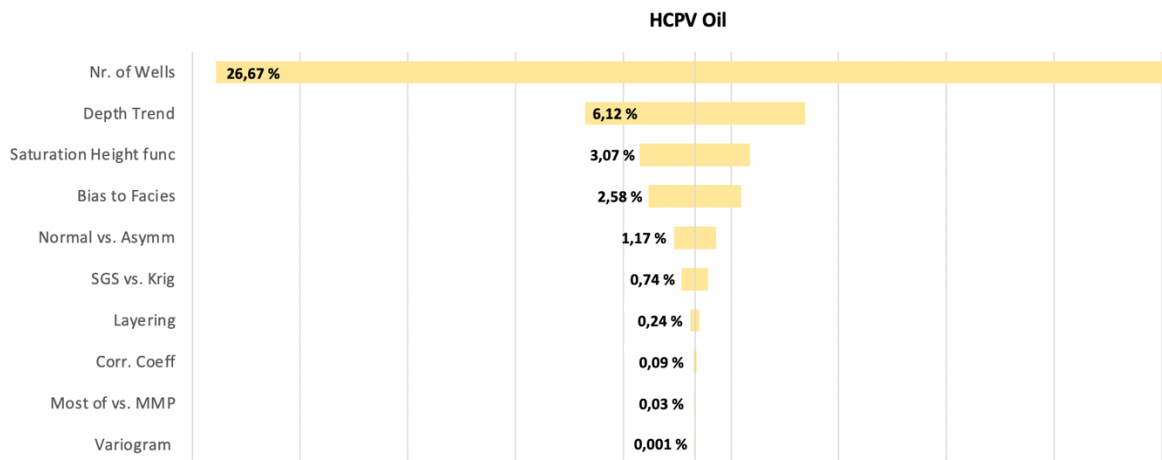


Figure 68: Tornado plot for the % difference in HCPV oil for Model 2A. The % difference values are taken from Table 15.

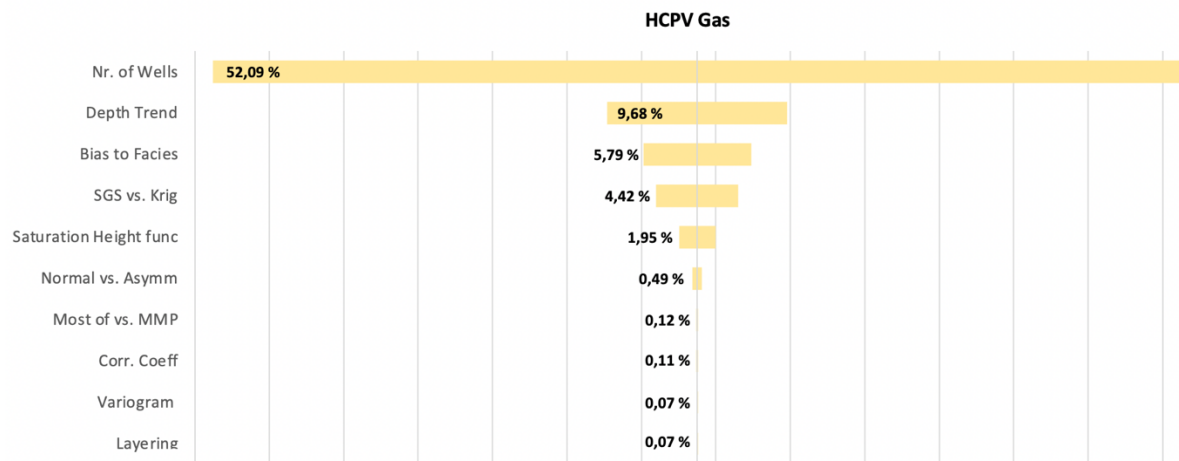


Figure 69: Tornado plot for the % difference in HCPV gas for Model 2A. The % difference values are taken from Table 15.

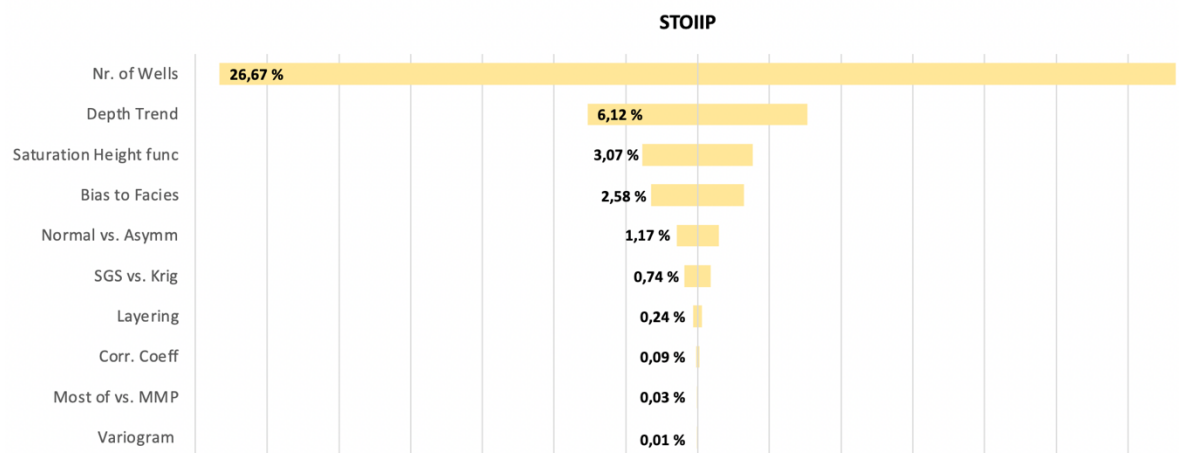


Figure 70: Tornado plot for the % difference in STOIP for Model 2A. The % difference values are taken from Table 15.

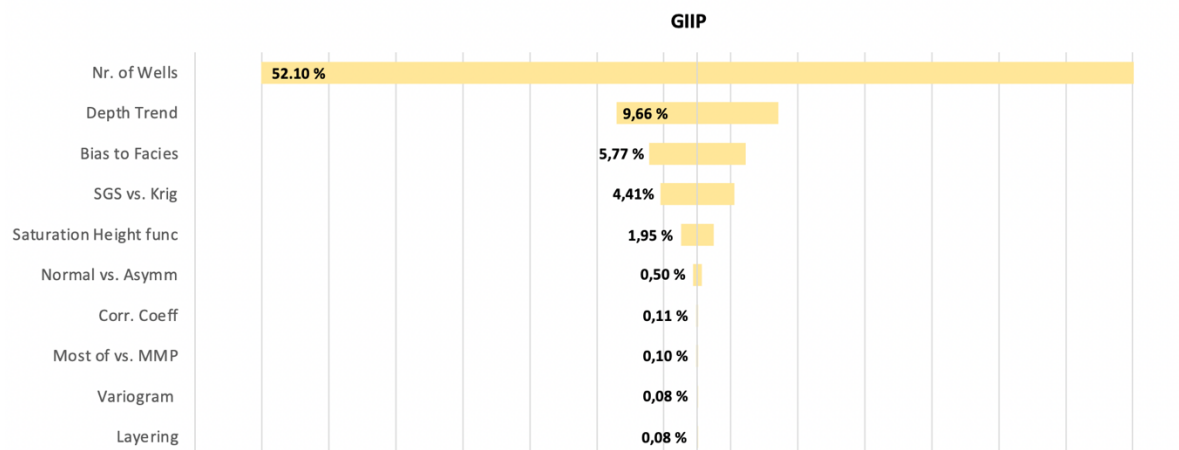


Figure 71: Tornado plot for the % difference in GIIP for Model 2A. The % difference values are taken from Table 15.

6.2.3 Model 2B

Model 2B (Turbidite)

Parameter	Pore Volume	HCPV Oil	HCPV gas	STOIP	GIIP
Bias to Facies	2,04 %	1,64 %	5,63 %	1,64 %	5,65 %
Correlation Coefficient	0,00 %	0,20 %	0,40 %	0,20 %	0,40 %
Depth Trend	6,31 %	4,67 %	11,21 %	4,67 %	11,23 %
Layering	0,06 %	0,29 %	0,21 %	0,29 %	0,20 %
Most of vs. Mid-point pick	0,02 %	0,04 %	0,01 %	0,04 %	0,03 %
Normal vs. Asymmetric	1,54 %	3,08 %	6,48 %	3,08 %	6,49 %
Saturation Height Func	0,05 %	3,32 %	2,78 %	3,32 %	2,79 %
SGS vs. Kriging	1,35 %	2,50 %	3,07 %	2,50 %	3,08 %
Variogram	0,08 %	0,06 %	0,33 %	0,06 %	0,34 %
Nr. of Wells	28,36 %	19,26 %	52,67 %	19,27 %	52,67 %

Table 16: A summary table of the % difference of average high and low for each parameter in Model 2B on pore volume, HCPV oil, HCPV gas, STOIP, and GIIP.

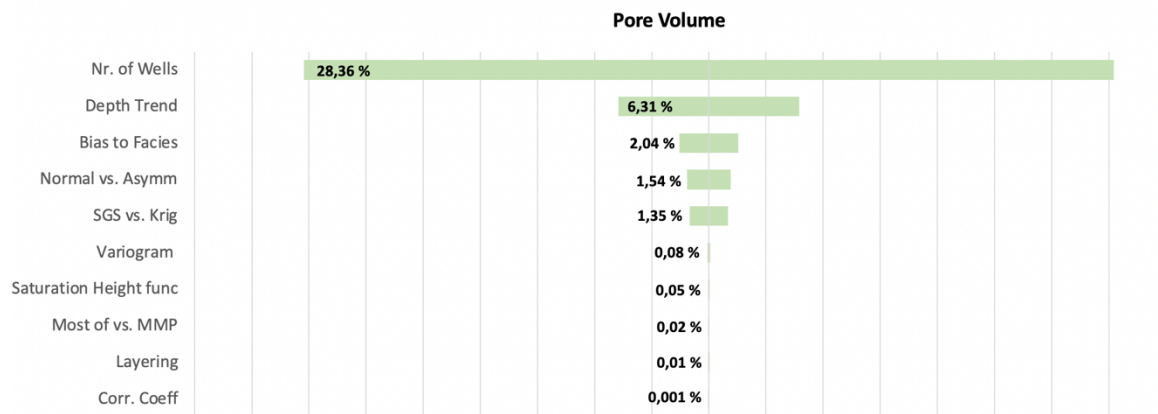


Figure 72: Tornado plot for pore volume Model 2B. The % difference values are taken from Table 16.

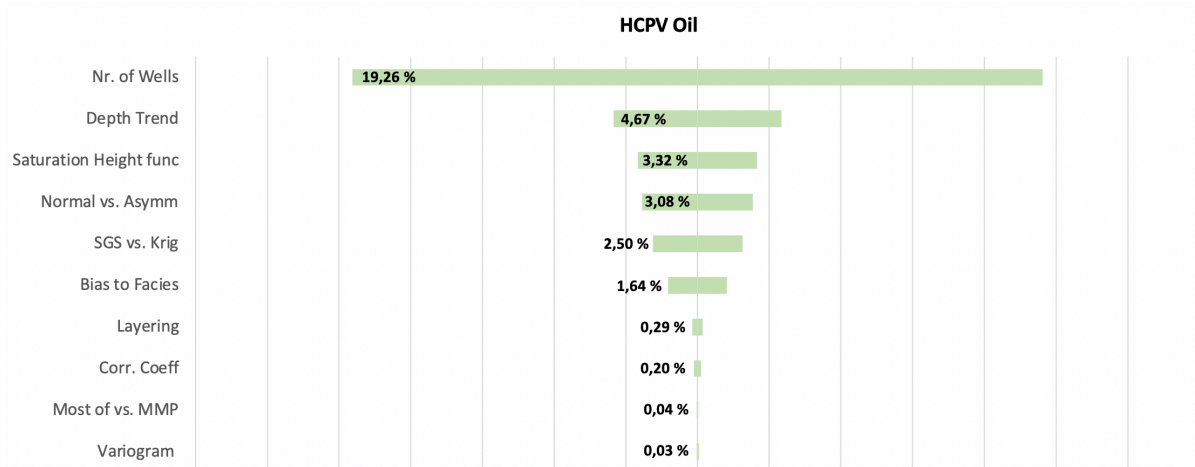


Figure 73: Tornado plot for HCPV oil Model 2B, The % difference values are taken from Table 16.

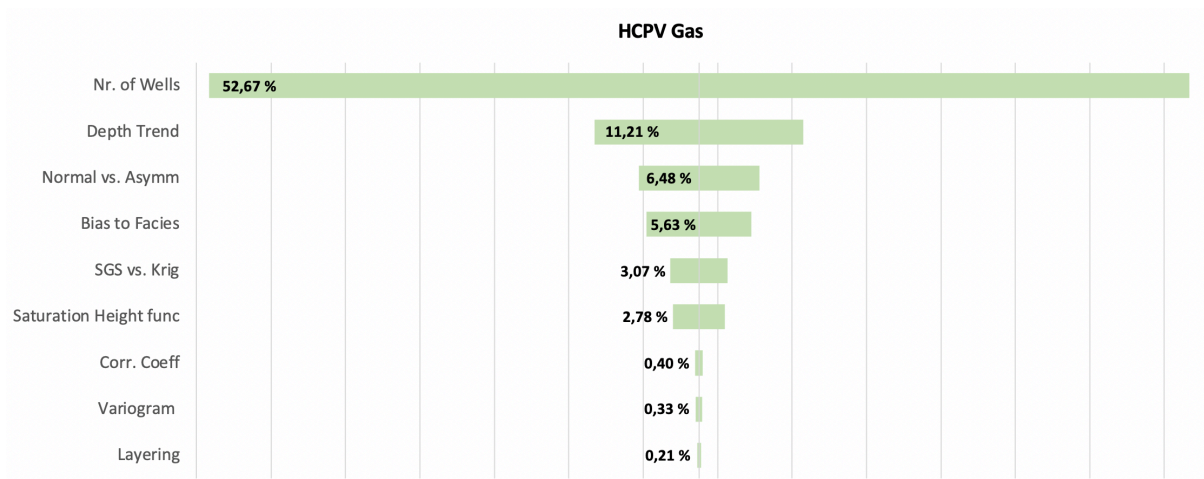


Figure 74: Tornado plot for HCPV gas Model 2B. The % difference values are taken from Table 16

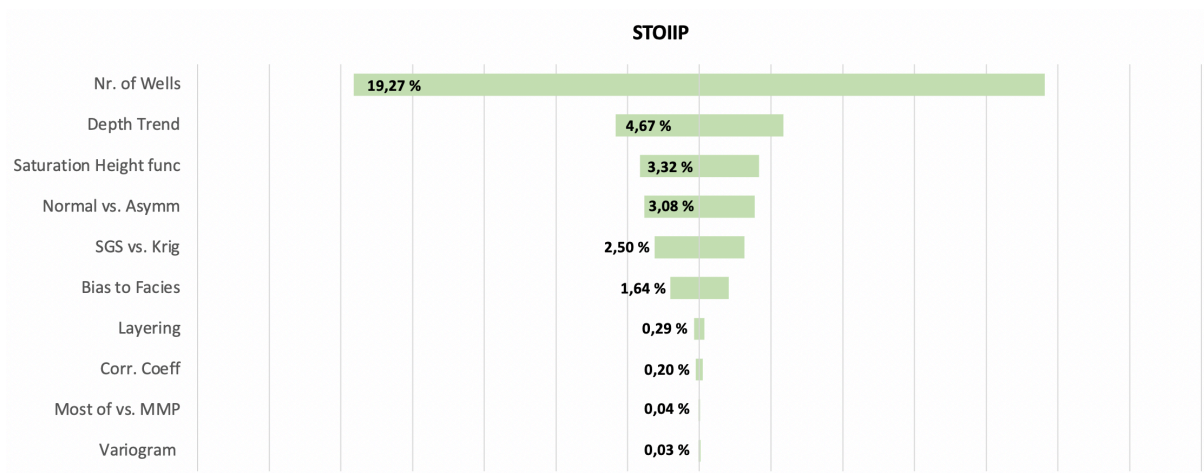


Figure 75: Tornado plot for STOIP Model 2B. The % difference values are taken from Table 16.

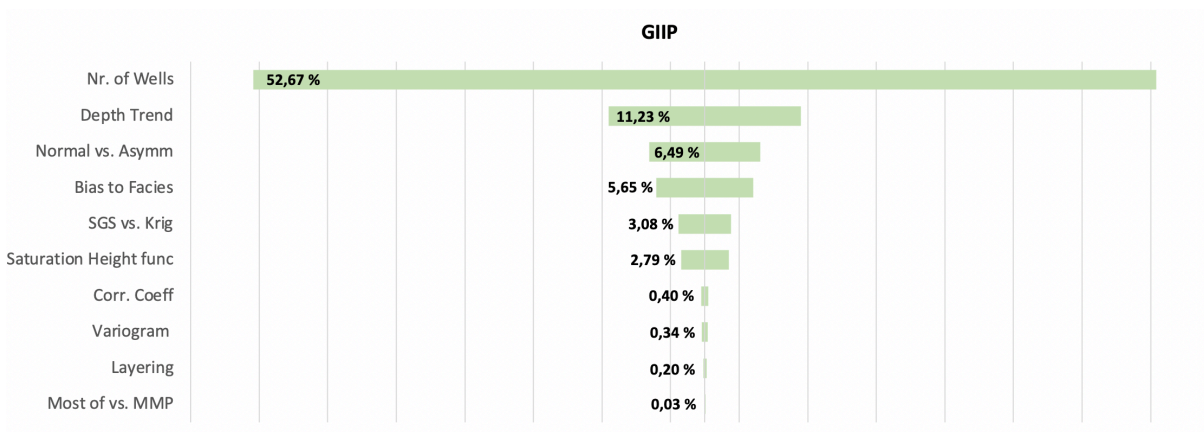


Figure 76: Tornado plot for GIIP Model 2B. The % difference values are taken from Table 16.

6.3 Parameter Impact on STOIP and GIIP

STOIP and GIIP are important volumes to consider since they represent the volume of oil and gas in a reservoir ahead of production. Table 17 provides an overview of the impact of parameters on STOIP and GIIP. The table ranks the parameters from most to least importance. In Model 1 regarding STOIP, the parameter "bias to facies" exhibits the highest impact, while in Models 2A and 2B, the nr. of wells parameter has the greatest influence on STOIP. On the other hand, most of vs. mid-point pick has the least impact on Model 1, while the variogram range has the lowest impact on both Model 2A and Model 2B. The table demonstrates a consistent trend where parameters such as bias to facies, depth trend, normal vs. asymmetric distribution, nr of wells, and SGS vs. Kriging tend to have a greater overall impact on STOIP compared to layering, correlation coefficient, most of vs. mid-point pick, and variogram range. In Model 1 regarding GIIP, the parameter saturation height function demonstrates the greatest impact, while in Models 2A and 2B, the nr. of wells parameter has the highest influence on GIIP. Conversely, most of vs. mid-point pick exhibits the lowest impact in both Model 1 and Model 2B, while in Model 2A, it is layering that has the lowest impact. Notably, the saturation height function and layering parameters have a significantly greater impact in Model 1 compared to Models 2A and 2B, where their overall influence is relatively lower, particularly for layering. Nevertheless, an overall trend persists across all models, with parameters such as bias to facies and depth trend having a larger impact compared to most of vs. mid-point pick, variogram range, and correlation coefficient.

Parameter Impact on STOIP and GIIP						
	Model 1 (Fluvial)		Model 2A (Turbidite)		Model 2B (Turbidite)	
	STOIP	GIIP	STOIP	GIIP	STOIP	GIIP
1	<u>BtF</u>	SHF	W	W	W	W
2	NA	LAY	DT	DT	DT	DT
3	DT	<u>BtF</u>	SHF	<u>BtF</u>	SHF	NA
4	W	DT	<u>BtF</u>	SK	NA	<u>BtF</u>
5	SK	NA	NA	SHF	SK	SK
6	SHF	SK	SK	NA	<u>BtF</u>	SHF
7	CC	W	LAY	CC	LAY	CC
8	LAY	VPC	CC	MM	CC	VR
9	VPC	VR	MM	VR	MM	LAY
10	VR	CC	VR	LAY	VR	MM
11	MM	MM	X*	X*	X*	X*

* VPC was not used on Model 2A and 2B

Table 17: The parameter impact on STOIP and GIIP for all three models, they are ranked from most to least importance. Abbreviations are used in this table; bias to facies (BtF), normal vs. asymmetric distribution (NA), depth trend (DT), nr of wells (W), SGS vs. Kriging (SK), saturation height function (SHF), correlation coefficient (CC), layering (LAY), vertical proportion curve (VPC), variogram range (VR), and most of vs. mid-point pick (MM). X in Model 2A and 2B indicates that there is no VPC in those models.*

6.4 Nr. of Wells for Models 2A and 2B

The nr. of wells' parameter has a significant impact on the calculated volumes for both Model 2A and 2B. In Model 1 although, the impact is probably significant it is very much smaller in comparison (see Tables 14-17).

Since the nr. of wells parameter is so dominant for Models 2A and 2B the results have been re-analysed for both the models. The data for 1 well and 3 wells have been separated for the models and is presented in Tables 18 to 21 with corresponding tornado charts in Figures 77 to 96.

6.4.1 Model 2A – 1 Well

Model 2A (Turbidite) – 1 Well

Parameters	Pore Volume	HCPV Oil	HCPV gas	STOIP	GIIP
Bias to Facies	0,01 %	0,01 %	0,17 %	0,01 %	0,24 %
Correlation Coefficient	0,01 %	0,11 %	0,09 %	0,10 %	0,10 %
Depth Trend	5,30 %	6,30 %	9,48 %	6,30 %	9,40 %
Layering	0,00 %	0,29 %	0,04 %	0,28 %	0,03 %
Most of vs. Mid-point pick	0,00 %	0,00 %	0,04 %	0,00 %	0,04 %
Normal vs. Asymmetric	0,77 %	1,29 %	0,52 %	1,30 %	0,52 %
Saturation Height Func	0,01 %	3,06 %	1,87 %	3,06 %	1,87 %
SGS vs. Kriging	1,28 %	1,85 %	1,48 %	1,85 %	1,49 %
Variogram	0,02 %	0,05 %	0,07 %	0,04 %	0,02 %

Table 18: A summary table of the difference of average high and low for each parameter on pore volume, HCPV oil, HCPV gas, STOIP, and GIIP for 1 well in Model 2A.

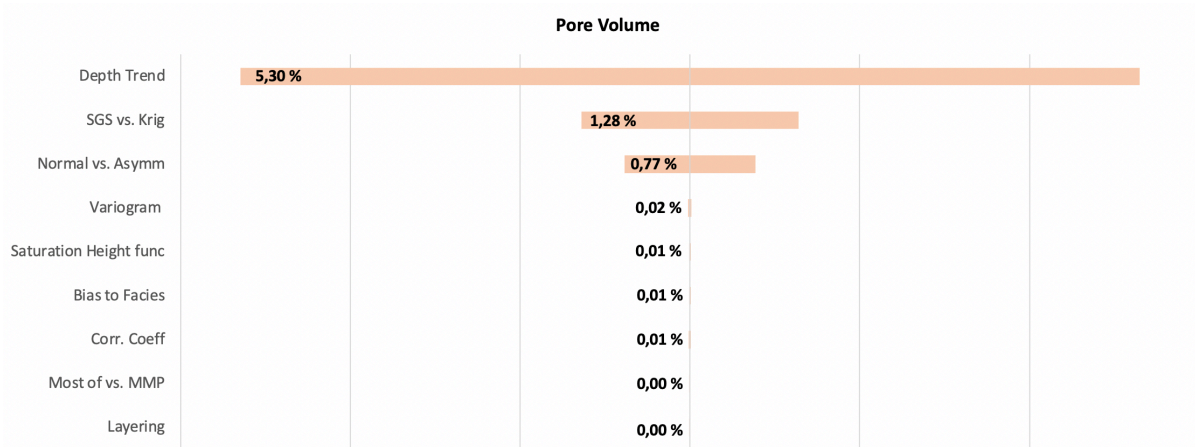


Figure 77: Tornado plot for the % difference in pore volume for Model 2A with 1 well.

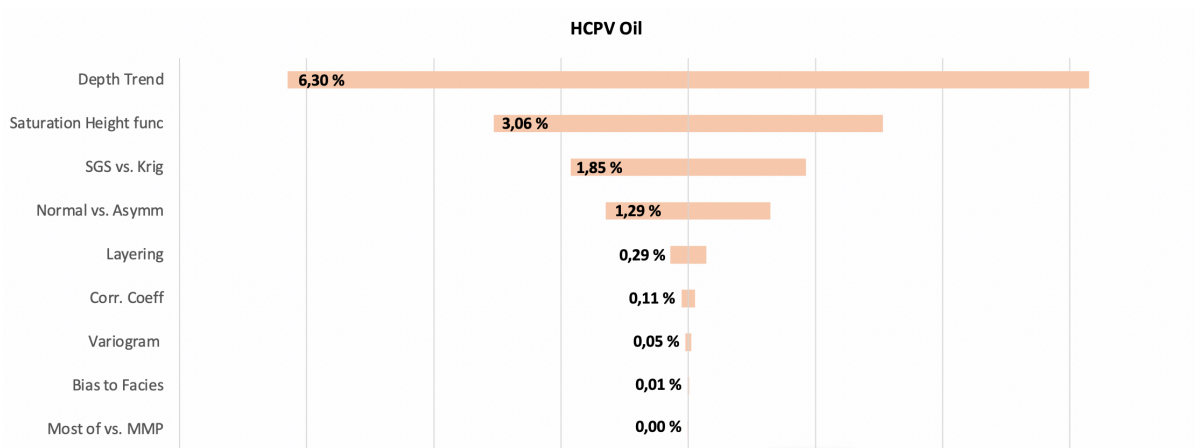


Figure 78: Tornado plot for the % difference in HCPV oil for Model 2A with 1 well.

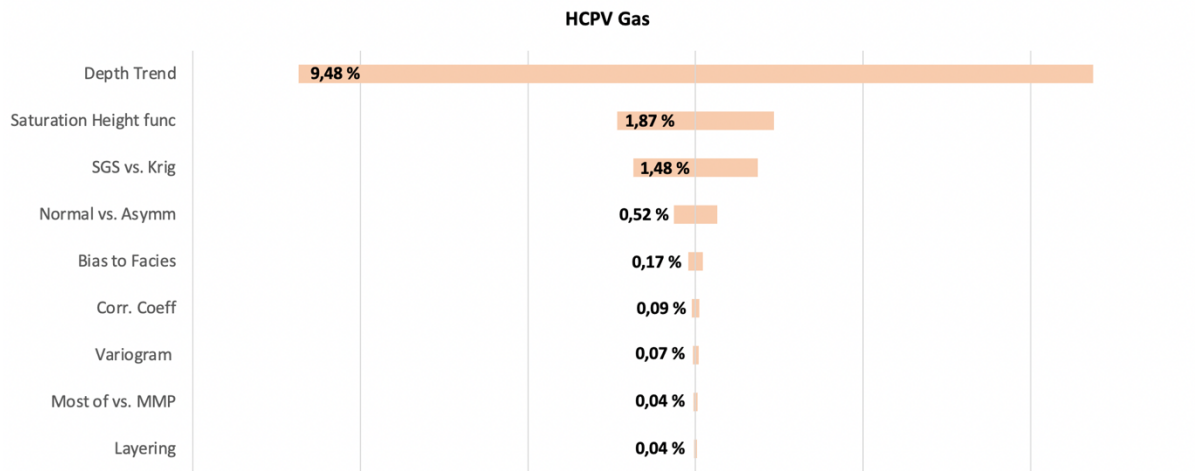


Figure 79: Tornado plot for the % difference in HCPV gas for Model 2A with 1 well.

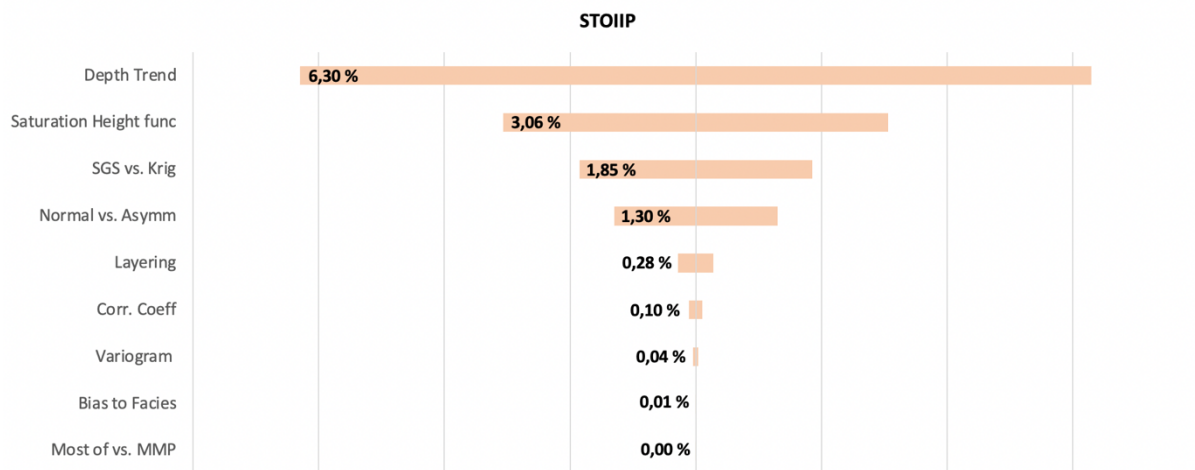


Figure 80: Tornado plot for the % difference in STOIIP for Model 2A with 1 well.

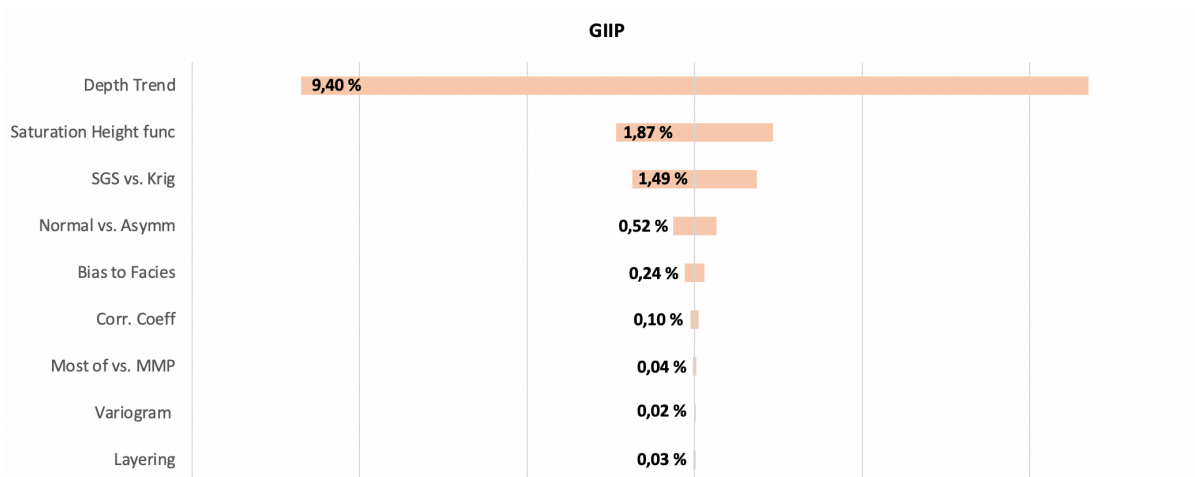


Figure 81: Tornado plot for the % difference in GIIP for Model 2A with 1 well.

6.4.2 Model 2A – 3 Wells

Model 2A (Turbidite) – 3 Wells

Parameters	Pore Volume	HCPV Oil	HCPV gas	STOIP	GIIP
Bias to Facies	4,95 %	4,44 %	8,52 %	4,44 %	8,52 %
Correlation Coefficient	0,02 %	0,08 %	0,13 %	0,08 %	0,11 %
Depth Trend	5,59 %	5,99 %	9,78 %	6,00 %	9,79 %
Layering	0,03 %	0,22 %	0,12 %	0,21 %	0,13 %
Most of vs. Mid-point pick	0,02 %	0,04 %	0,15 %	0,05 %	0,13 %
Normal vs. Asymmetric	0,63 %	1,08 %	0,48 %	1,08 %	0,49 %
Saturation Height Func	0,04 %	3,08 %	1,99 %	3,08 %	1,99 %
SGS vs. Kriging	3,57 %	2,59 %	7,12 %	2,60 %	7,12 %
Variogram	0,09 %	0,04 %	0,14 %	0,04 %	0,13 %

Table 19: A summary table of the difference of average high and low for each parameter on pore volume, HCPV oil, HCPV gas, STOIP, and GIIP for 3 wells in Model 2A.

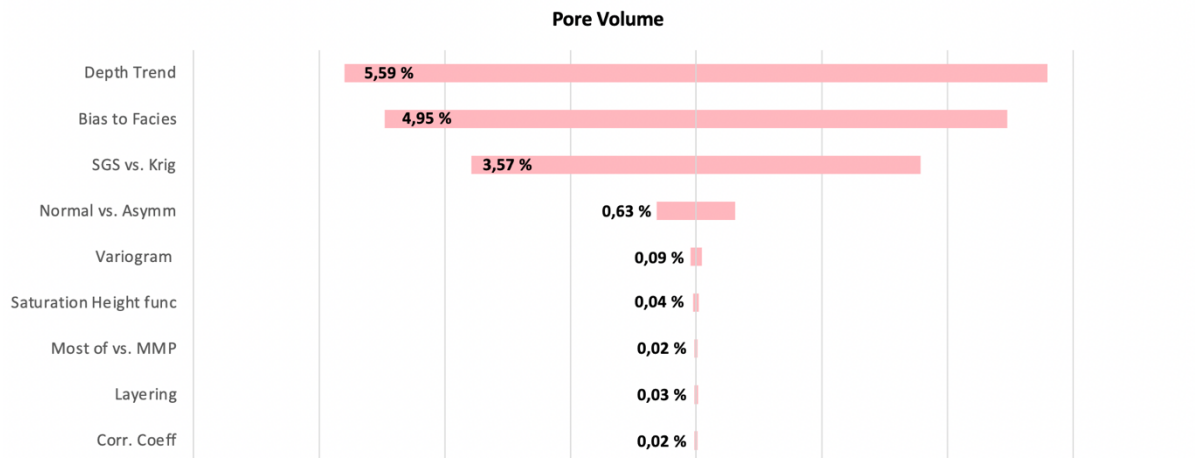


Figure 82: Tornado plot for the % difference in pore volume for Model 2A with 3 wells.

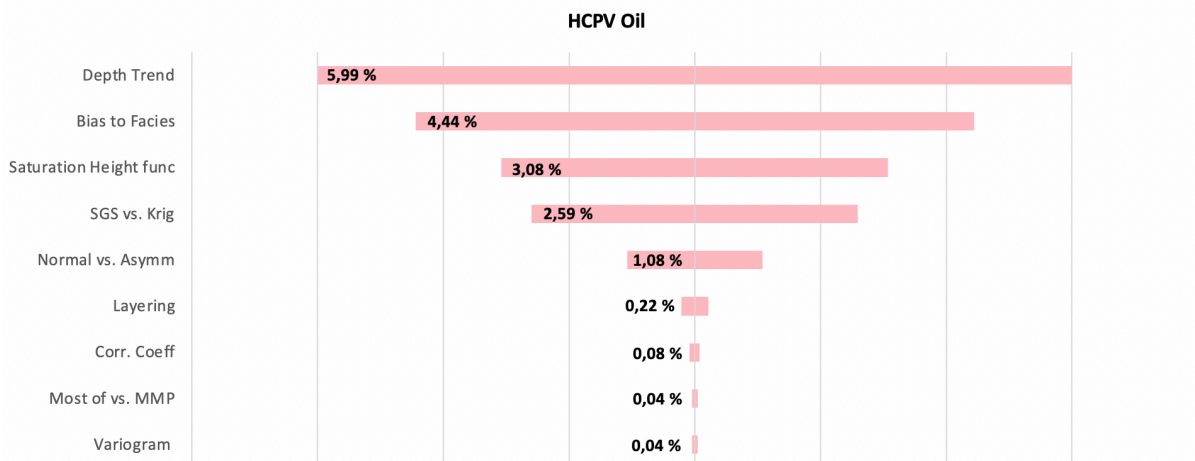


Figure 83: Tornado plot for the % difference in HCPV oil for Model 2A with 3 wells.

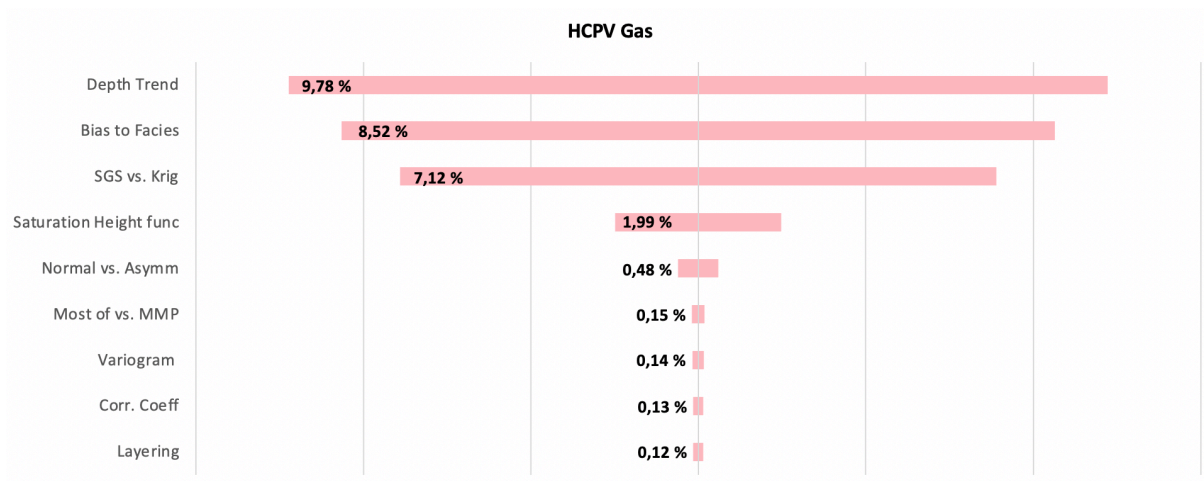


Figure 84: Tornado plot for the % difference in HCPV gas for Model 2A with 3 wells.

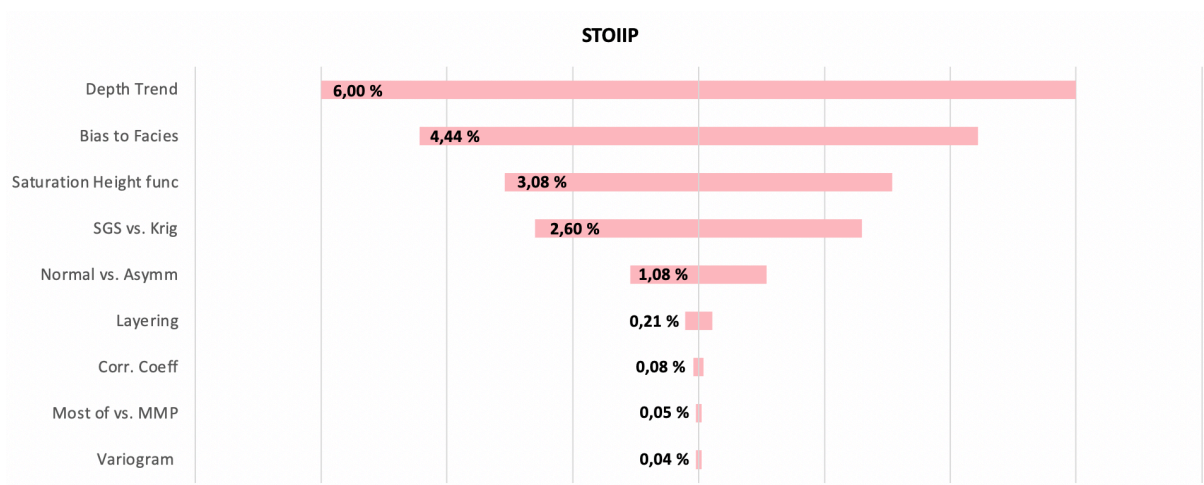


Figure 85: Tornado plot for the % difference in STOIP for Model 2A with 3 wells.

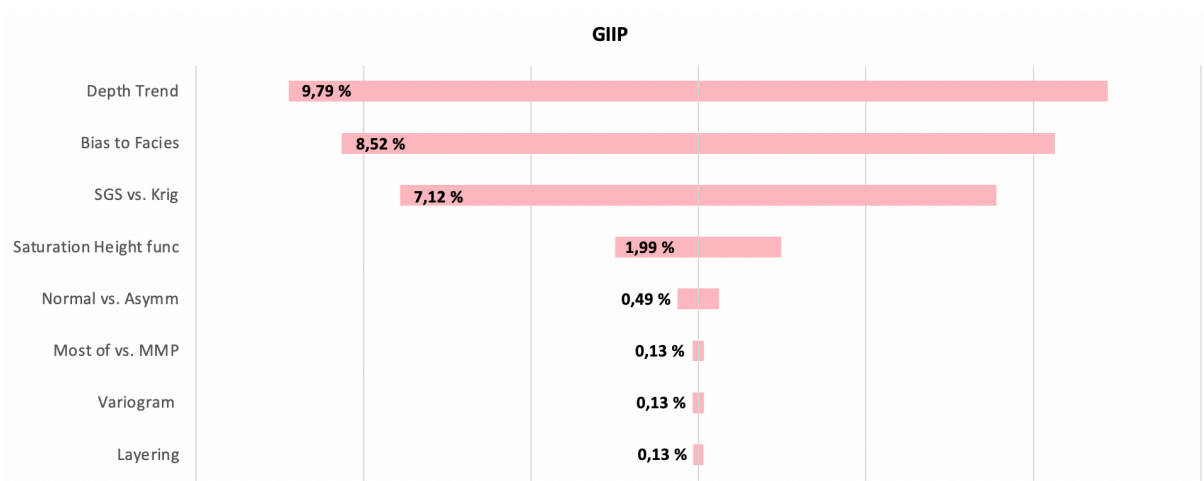


Figure 86: Tornado plot for the % difference in GIIP for Model 2A with 3 wells.

6.4.3 Model 2B – 1 Well

Model 2B (Turbidite) – 1 Well

Parameters	Pore Volume	HCPV Oil	HCPV gas	STOIP	GIIP
Bias to Facies	0,14 %	0,08 %	0,12 %	0,08 %	0,13 %
Correlation Coefficient	0,01 %	0,16 %	0,39 %	0,16 %	0,39 %
Depth Trend	5,72 %	4,88 %	10,71 %	4,88 %	10,73 %
Layering	0,08 %	0,39 %	0,40 %	0,38 %	0,41 %
Most of vs. Mid-point pick	0,02 %	0,01 %	0,06 %	0,02 %	0,03 %
Normal vs. Asymmetric	2,23 %	3,07 %	9,46 %	3,07 %	9,46 %
Saturation Height Func	0,01 %	3,22 %	2,79 %	3,22 %	2,82 %
SGS vs. Kriging	0,82 %	0,71 %	4,02 %	0,71 %	4,07 %
Variogram	0,18 %	0,11 %	0,81 %	0,11 %	0,79 %

Table 20: A summary table of the difference of average high and low for each parameter on pore volume, HCPV oil, HCPV gas, STOIP, and GIIP for 1 well in Model 2B.

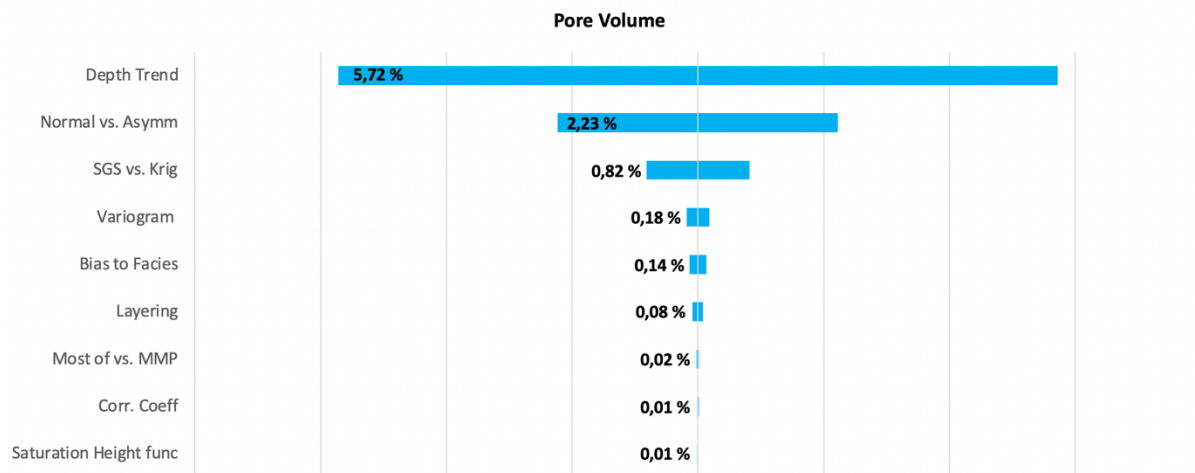


Figure 87: Tornado plot for the % difference in pore volume for Model 2B with 1 well.

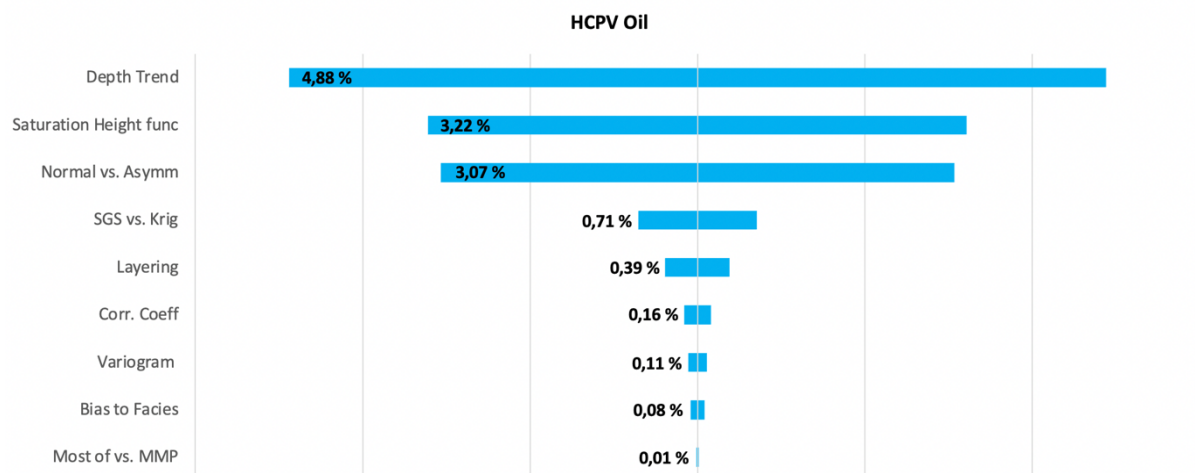


Figure 88: Tornado plot for the % difference in HCPV oil for Model 2B with 1 well.

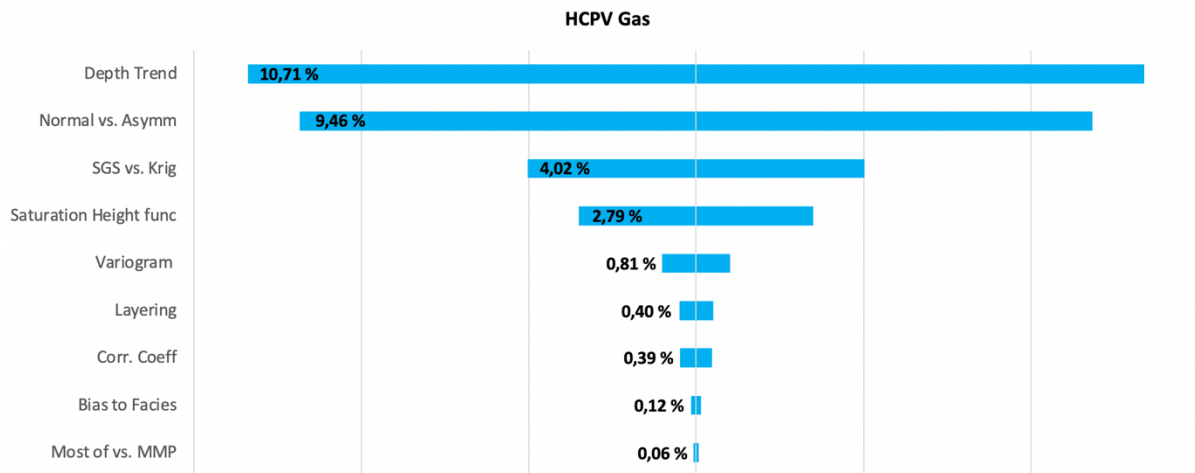


Figure 89: Tornado plot for the % difference in HCPV gas for Model 2B with 1 well.

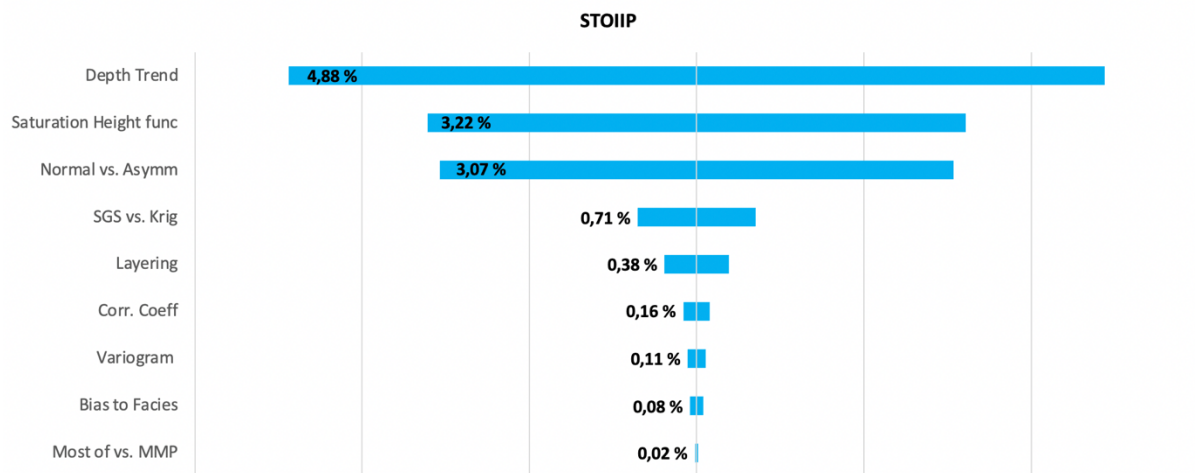


Figure 90: Tornado plot for the % difference in STOIIP for Model 2B with 1 well.

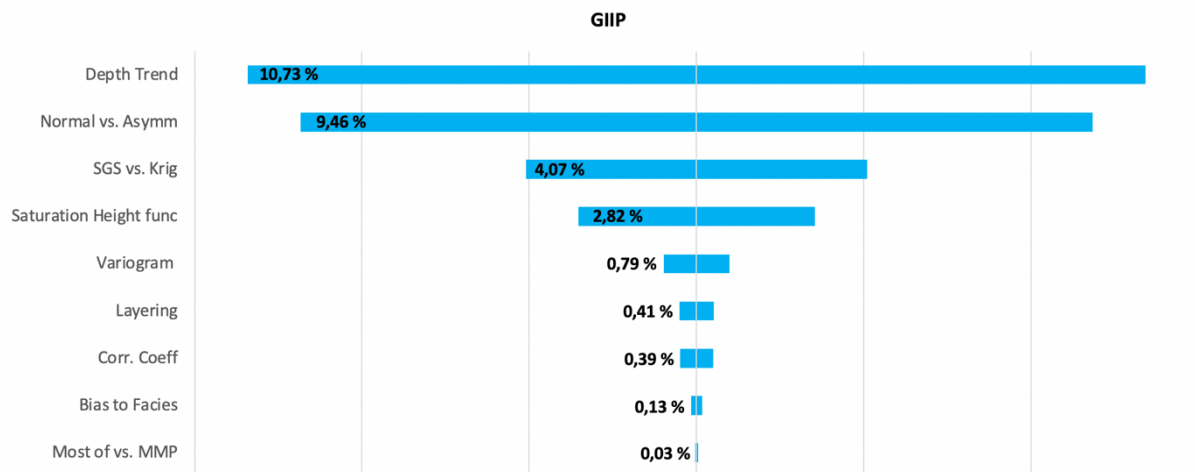


Figure 91: Tornado plot for the % difference in GIIP for Model 2B with 1 well.

6.4.4 Model 2B – 3 Wells

Model 2B (Turbidite) – 3 Wells

Parameters	Pore Volume	HCPV Oil	HCPV gas	STOIP	GIIP
Bias to Facies	3,55 %	2,98 %	8,19 %	2,99 %	8,22 %
Correlation Coefficient	0,03 %	0,22 %	0,36 %	0,21 %	0,35 %
Depth Trend	6,71 %	4,49 %	11,41 %	4,49 %	11,41 %
Layering	0,13 %	0,24 %	0,45 %	0,24 %	0,44 %
Most of vs. Mid-point pick	0,01 %	0,04 %	0,10 %	0,04 %	0,11 %
Normal vs. Asymmetric	1,07 %	3,11 %	5,08 %	3,11 %	5,10 %
Saturation Height Func	0,06 %	3,38 %	2,72 %	3,39 %	2,73 %
SGS vs. Kriging	2,91 %	3,94 %	6,30 %	3,94 %	6,35 %
Variogram	0,02 %	0,01 %	0,05 %	0,01 %	0,08 %

Table 21: A summary table of the difference of average high and low for each parameter on pore volume, HCPV oil, HCPV gas, STOIP, and GIIP for 3 wells in Model 2B.

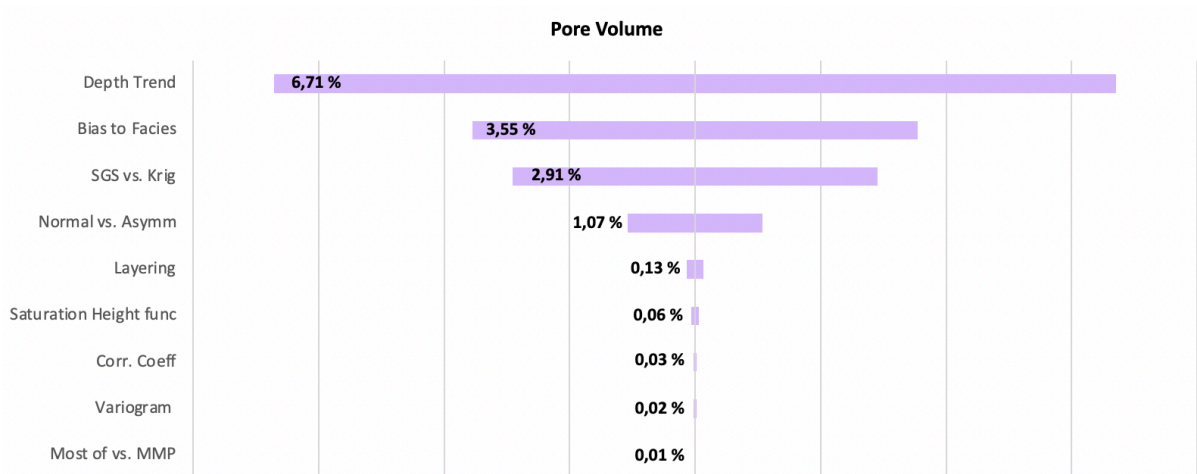


Figure 92: Tornado plot for the % difference in pore volume for Model 2B with 3 wells.

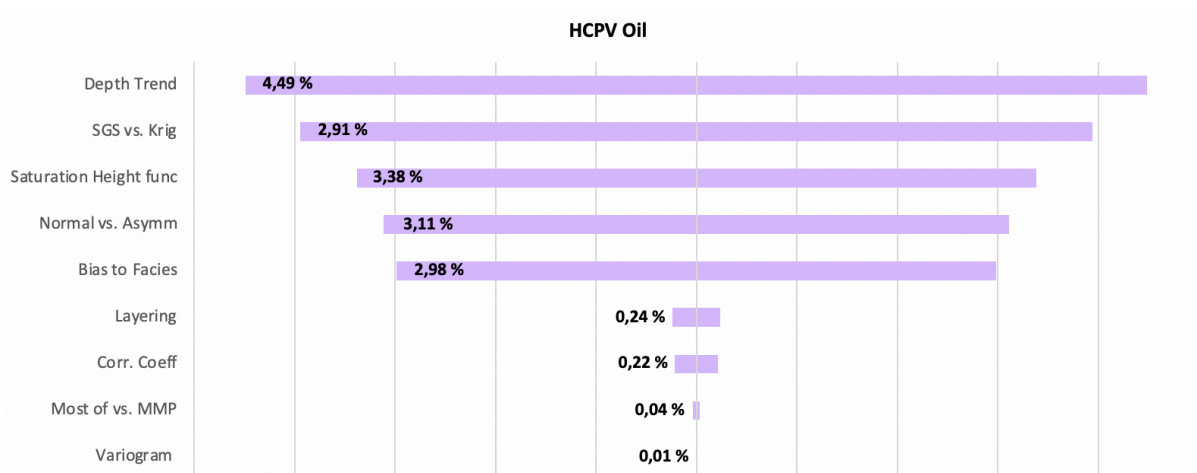


Figure 93: Tornado plot for the % difference in HCPV oil for Model 2B with 3 wells.

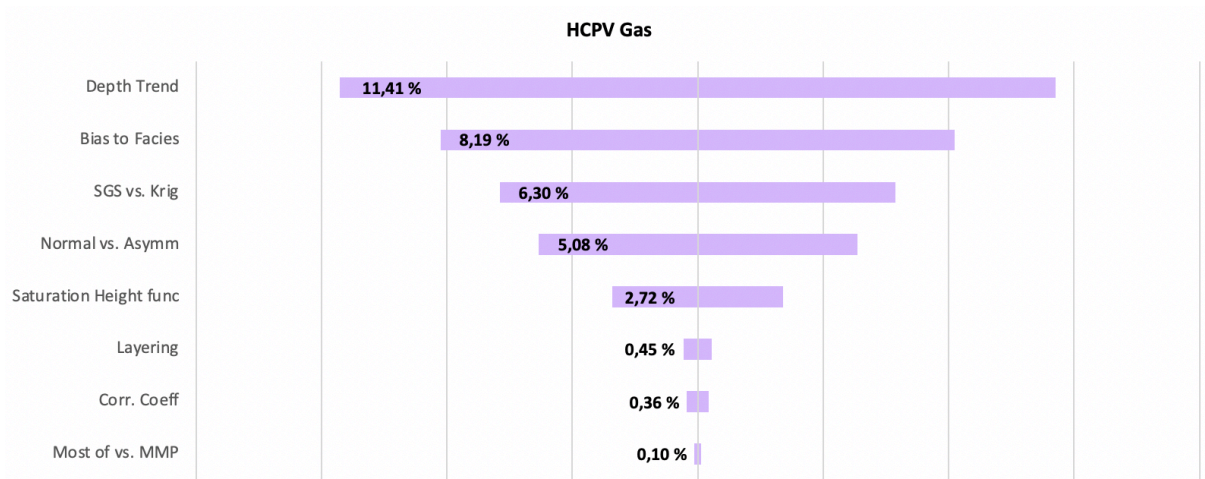


Figure 94: Tornado plot for the % difference in HCPV gas for Model 2B with 3 wells.

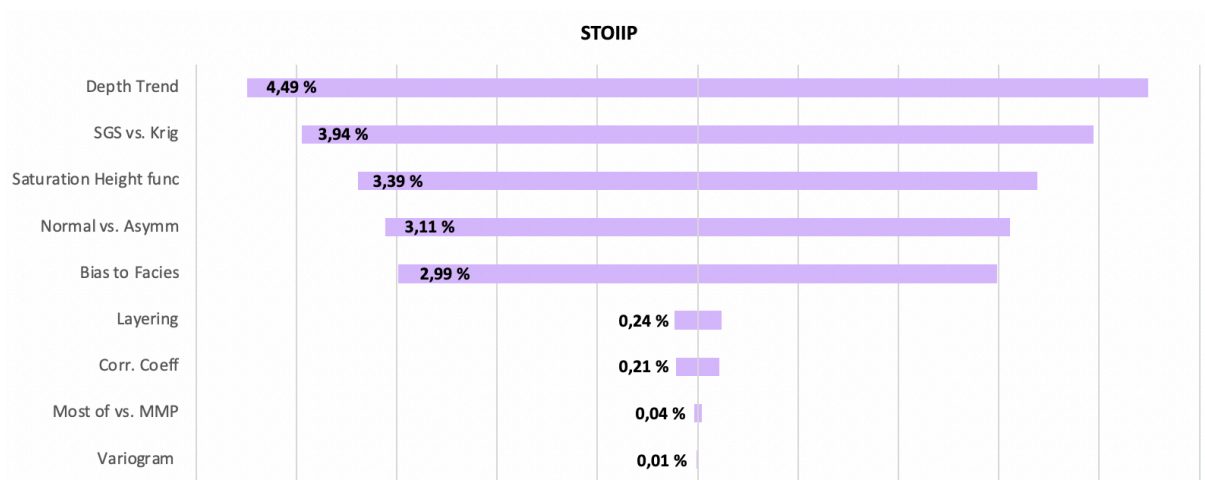


Figure 95: Tornado plot for the % difference in STOIP for Model 2B with 3 wells.

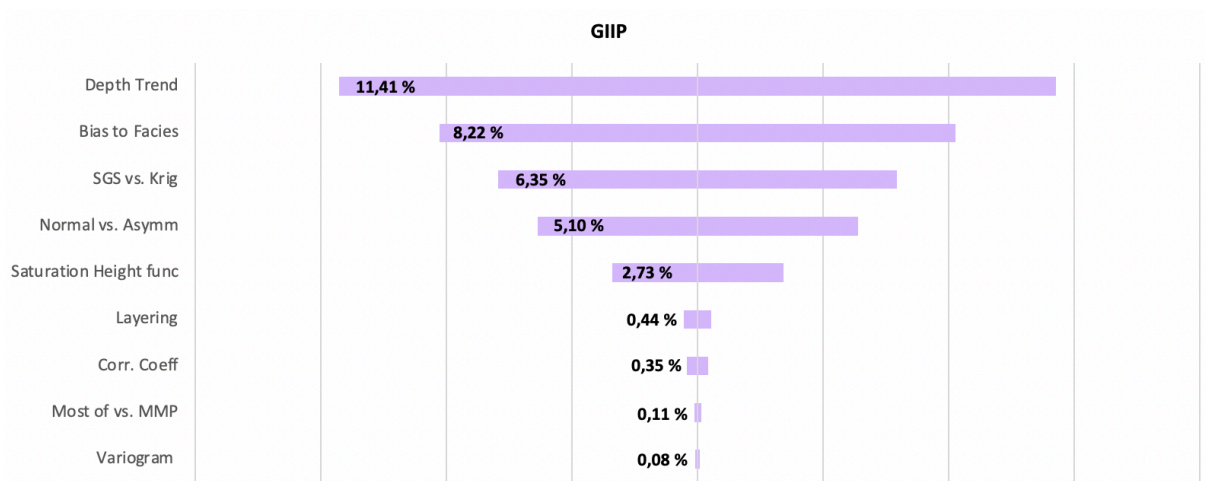


Figure 96: Tornado plot for the % difference in GIIP for Model 2B with 3 wells.

6.4.5 Comparison tables for STOIP and GIIP for 1 Well and 3 Wells

Model 2A	1 Well		3 Wells	
Parameters	STOIP	GIIP	STOIP	GIIP
Bias to Facies	0,01 %	0,24 %	4,44 %	8,52 %
Correlation Coefficient	0,10 %	0,10 %	0,08 %	0,11 %
Depth Trend	6,30 %	9,40 %	6,00 %	9,79 %
Layering	0,28 %	0,03 %	0,21 %	0,13 %
Most of vs. Mid-point pick	0,00 %	0,04 %	0,05 %	0,13 %
Normal vs. Asymmetric	1,30 %	0,52 %	1,08 %	0,49 %
Saturation Height Func	3,06 %	1,87 %	3,08 %	1,99 %
SGS vs. Kriging	1,85 %	1,49 %	2,60 %	7,12 %
Variogram	0,04 %	0,02 %	0,04 %	0,13 %

Table 22: Comparison of STOIP and GIIP for 1 well vs. 3 wells for Model 2A.

Model 2B	1 Well		3 Wells	
Parameters	STOIP	GIIP	STOIP	GIIP
Bias to Facies	0,08 %	0,13 %	2,99 %	8,22 %
Correlation Coefficient	0,16 %	0,39 %	0,21 %	0,35 %
Depth Trend	4,88 %	10,73 %	4,49 %	11,41 %
Layering	0,38 %	0,41 %	0,24 %	0,44 %
Most of vs. Mid-point pick	0,02 %	0,03 %	0,04 %	0,11 %
Normal vs. Asymmetric	3,07 %	9,46 %	3,11 %	5,10 %
Saturation Height Func	3,22 %	2,82 %	3,39 %	2,73 %
SGS vs. Kriging	0,71 %	4,07 %	3,94 %	6,35 %
Variogram	0,11 %	0,79 %	0,01 %	0,08 %

Table 23: Comparison of STOIP and GIIP for 1 well vs. 3 wells for Model 2B.

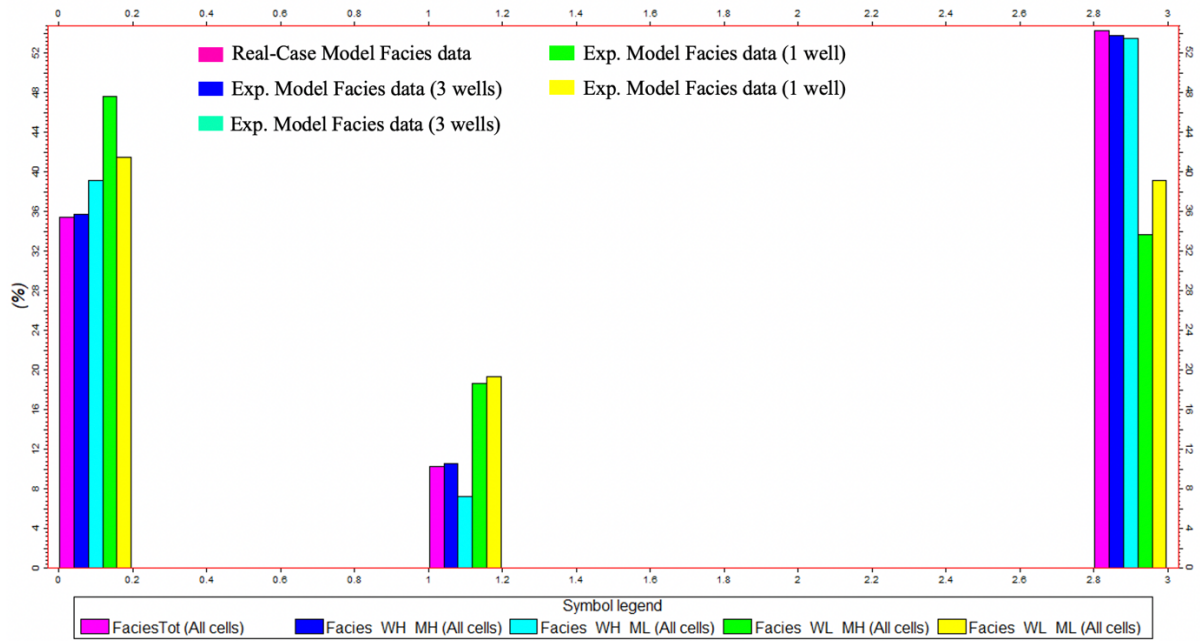


Figure 97: The facies statistics for Model 2A and shows that there is a sampling issue when using only 1 or 3 wells.

6.5 Parameter Interactions

Interactions between parameters can also exist within experiments like the ones carried out in this study. A full evaluation of all parameter interactions would involve a large effort and is beyond the scope of this study. However, interactions for 2 parameters have been analysed from Model 1 to show the impact of 2 interacting parameters. The pair that was analysed was the two parameters with the highest impact on the model, bias to facies and normal vs. asymmetric distribution. Table 24 displays the impact of the parameter interactions. The table is set up to display the interactions (1,1), (1,-1), (-1,1), and (-1,-1) for pore volume, HCPV oil, HCPV gas, STOIP, and GIIP, (1,1) indicates that both parameters are set to high, (1,-1) indicates that the high on bias to facies and the low for normal vs. asymmetric distribution. The parameter interactions with the highest impacts are (1,-1) and (-1,1) for each of the volume measures. The differences for oil volumes appear to be more significant than for gas volumes.

Bias to Facies and Normal vs. Asymmetric Distribution

	(1,1)	(1,-1)	(-1,1)	(-1,-1)
Parameter used	Bias to facies on and normal distribution	Bias to facies on and asymmetric distribution	Bias to facies off and normal distribution	Bias to facies off and asymmetric distribution
Pore Volume	1,06 %	15,54 %	15,68 %	0,90 %
HCPV Oil	1,27 %	11,80 %	11,67 %	1,12 %
HCPV Gas	0,21 %	2,30 %	2,30 %	0,20 %
STOIP	1,27 %	11,80 %	11,67 %	1,12 %
GIIP	0,22 %	2,30 %	2,30 %	0,22 %

Table 24: Parameter interaction impact of bias to facies and normal vs. asymmetric distribution on Model 1.

6.6 Comparing Models Results

A summary table of the impact of each parameter on STOIP and GIIP, comparing Model 1 with Model 2A and 2B, is presented in Table 25. The table is colour coordinated to indicate if the parameter has a high (> 2,0%), medium (1,99-0,30%) or low (< 0,29%) impact on the volumes. The same type of table was set up to compare Model 2A with 1 and 3 wells and Model 2B with 1 and 3 wells (Table 26 & 27).

Parameters	Model 1		Model 2A		Model 2B	
	STOIP	GIIP	STOIP	GIIP	STOIP	GIIP
Bias to Facies	High	High	High	High	Med	High
Correlation Coefficient	Med	Low	Low	Low	Low	Med
Depth Trend	High	High	High	High	High	High
Layering	Med	High	Low	Low	Low	Low
Most of vs. Mid-point pick	Low	Low	Low	Low	Low	Low
Normal vs. Asymmetric	High	High	Med	Med	High	High
Saturation Height Func	High	High	High	Med	High	High
SGS vs. Kriging	High	Med	Med	High	High	High
Variogram	Low	Med	Low	Low	Low	Med
Vertical Proportion Curve	Low	Med	-	-	-	-
Nr. of Wells	High	Med	High	High	High	High

Table 25: The impact of each parameter on STOIP and GIIP ranked in a high, medium and low order for all models.

Parameters	Model 2A		Model 2A – 1 Well		Model 2A – 3 Wells	
	STOIP	GIIP	STOIP	GIIP	STOIP	GIIP
Bias to Facies	High	High	Low	Low	High	High
Correlation Coefficient	Low	Low	Low	Low	Low	Low
Depth Trend	High	High	High	High	High	High
Layering	Low	Low	Low	Low	Low	Low
Most of vs. Mid-point pick	Low	Low	Low	Low	Low	Low
Normal vs. Asymmetric	Med	Med	Med	Med	Med	Med
Saturation Height Func	High	Med	High	Med	High	Med
SGS vs. Kriging	Med	High	Med	Med	High	High
Variogram	Low	Low	Low	Low	Low	Low
Nr of Wells	High	High	-	-	-	-

Table 26: Comparison of Model 2A with 1 well and 3 wells. Where STOIP and GIIP are ranked in a high, medium and low order for all models.

Parameters	Model 2B		Model 2B – 1 Well		Model 2B – 3 Wells	
	STOIP	GIIP	STOIP	GIIP	STOIP	GIIP
Bias to Facies	Med	High	Low	Low	High	High
Correlation Coefficient	Low	Med	Low	Med	Low	Med
Depth Trend	High	High	High	High	High	High
Layering	Low	Low	Med	Med	Low	Med
Most of vs. Mid-point pick	Low	Low	Low	Low	Low	Low
Normal vs. Asymmetric	High	High	High	High	High	High
Saturation Height Func	High	High	High	High	High	High
SGS vs. Kriging	High	High	Med	High	High	High
Variogram	Low	Med	Low	Med	Low	Low
Nr of Wells	High	High	-	-	-	-

Table 27: Comparison of Model 2B with 1 well and 3 wells. Where STOIP and GIIP are ranked in a high, medium and low order for all models.

7. Discussion

The primary goal of this master's thesis was to examine the effects of eleven different parameters on porosity, permeability, water saturation, and volume calculations in two conceptual models: Model 1 (Fluvial) and Model 2 (Turbidite). The results obtained from the experimental design conducted in Petrel were analysed to determine the significance of these parameters and their influence on volumetric calculations. Three sets of results were obtained: Model 1, Model 2A, and Model 2B. The discussion focuses on the key findings, their implications, a comparison with real-case models, the reliability of the outcomes, and the importance of accurately modelling the parameters to determine if they are specific to a particular case or applicable universally across models.

7.1 Real Cases (Original Models) vs. Reservoir Cases (Experiment Models)

By comparing the results from the experimental design with the real-case models, both similarities and differences were discovered. Bulk volume and net volume exhibited similarities in all the models, indicating the reliability of the modelling approach. However, notable differences were observed in pore volume, HCPV oil and gas, STOIP, and GIIP, specially in Model 1.

The most significant disparities found in Model 1 indicate the notable differences between the actual reservoir conditions and the representations used in the experimental models. These differences are so large, they indicate that there is a fundamental problem with either the Original Model or the Reservoir Model. The noticeable difference in the volumes can to some extent be explained by the gross rock volume (GRV). The GRV is 1,4 % smaller in the Experiment Model compared the real-case model. The other reason for the difference can be explained by a modelling issue. The real-case model overcalculated the volumes due to a problem with the facies method used as well as a slightly higher porosity in the real-case model (Fig. 98). The grid cells are also larger in the real-case model. The facies method used for the Original Model was object modelling (stochastic) while for the Reservoir Model sequential indicator simulation was used, and the max real-case porosity was 0,41 while it was 0,39 for the experiments. This only became apparent once the volume results had been produced and analysed. This slightly increased amounts of fine and coarse sand and porosity

in the model increased the pore volume by 4,9 %. This highlights the importance of modelling correctly and carrying out a thorough QC (quality check) to try and eliminate errors before performing an extensive set of experiments.

In Model 2A the real case vs. the experiment yielded acceptable differences where nearly all the real case volumes were within the P10-P90 range. For Model 2B the Reservoir Models tended to be on the low side, when comparing to the real case, lying within the P10-P90 range, but close to the P90. It should be noted that if the modeller uses the parameters inaccurately the volumes can be heavily affected. If the low values of the parameters are used the volumes could be under estimated which could lead to a non-development of a potential economic reservoir.

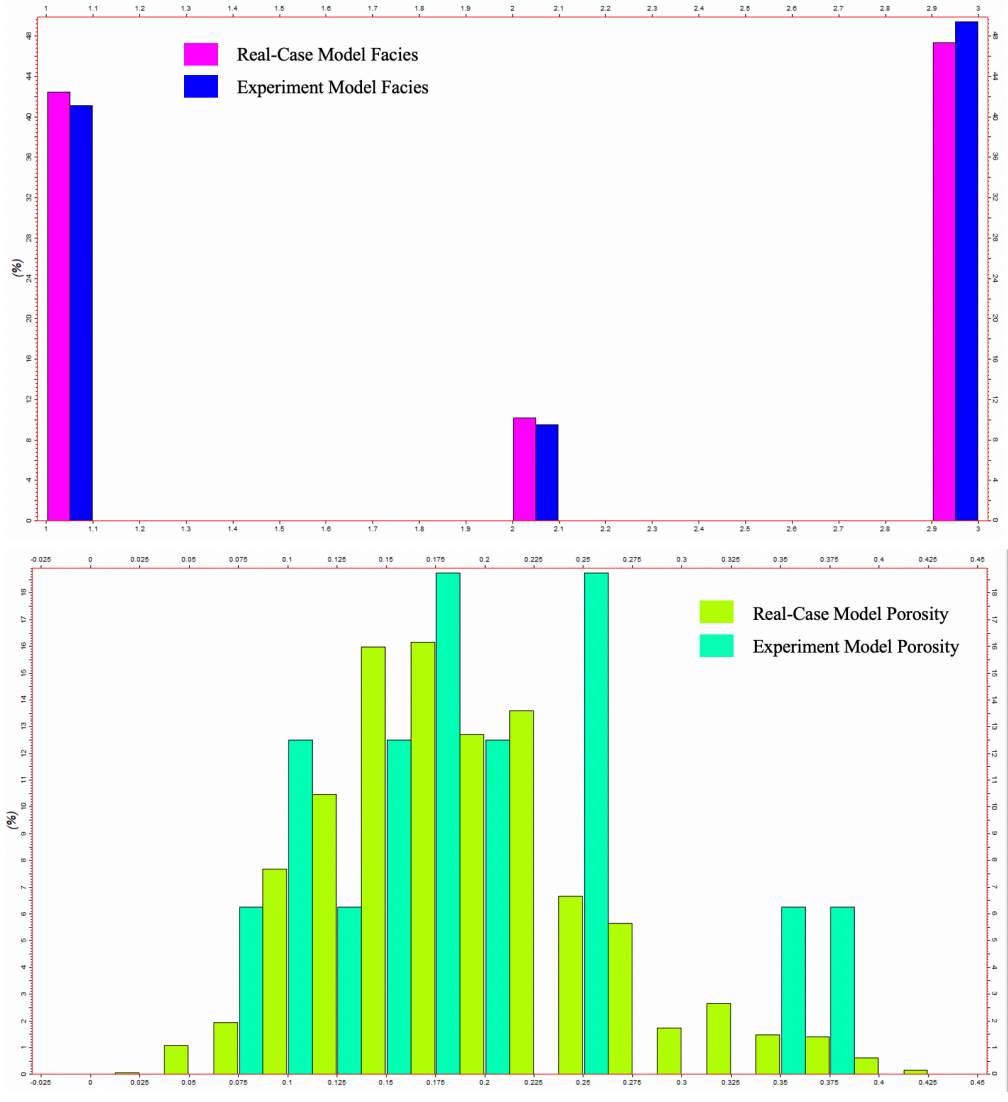


Figure 98: The Real-Case Model Facies and Porosity vs. the Experiment Model Facies and Porosity.

7.2 The Models: Differences and Similarities

The results from each of the models demonstrate that changes in the parameters have an impact on the results, with certain parameters affecting the volumetric outcomes more than others. For instance, in Model 1, the parameter with the greatest impact was bias to facies (Table 11), while in Models 2A (Table 12) and 2B (Table 13) it was nr. of wells that had the most impact. Based on the tables mentioned it is evident that changes in parameters have a notable effect on the calculated volumes.

Other parameters that exhibited a substantial effect on the results included depth trend, bias to facies, normal vs. asymmetric distribution, saturation height function, and SGS vs. Kriging. Parameters with a comparatively lower impact were layering, most of vs. mid-point pick, variogram range, correlation coefficient, and VPC in the case of Model 1. There is a general trend across all three models, with depth trend, bias to facies, normal vs. asymmetric distribution, saturation height function, and SGS vs. Kriging consistently ranking higher in the tables. On the other hand, layering, most of vs. mid-point pick, variogram range, correlation coefficient, and VPC tend to consistently rank lower. This suggests that the low-impact of these parameters might be universal across different geological settings, although further investigation is required. However, there are exceptions. In Model 1, layering has a higher impact compared on the calculated volumes compared to Models 2A and 2B, layering ranks lower. These findings underscore the significance of accurately modelling the parameters to ensure reliable volumetric results. Employing more wells, incorporating bias to facies, using a depth trend, and implementing an asymmetric distribution yield higher volumetric outcomes. The utilization of most of rather than mid-point pick, as well as changes in variogram range and correlation coefficient, have minimal impact on the models. This is likely due to factors such as spatial distribution, the properties of the Reservoir Model, and the connectivity, or the nature of reservoir data and characteristics. However, it is important to note that the limited impact observed in these experiments does not necessarily imply their insignificance in all geomodelling processes.

Table 28 compares the real-case model vs. 2 scenarios, the most “correct” and most “incorrect” model for Models 2A and 2B. The table shows that there is notable difference in the most “incorrect”, where the volumes are significantly lower than the real case and the most “correct” model for both models. The “correct” model is similar to the real case, but some volumes are higher. This could be due to the parameters and the values used in the experiments.

Model 2A	Bulk Volume (10⁶m³)	Net Volume (10⁶m³)	Pore Volume (10⁶rm³)	HCPV Oil (10⁶rm³)	HCPV Gas (10⁶rm³)	STOIP (10⁶sm³)	GIIP (10⁹sm³)	Note
Real-Case	7500	7500	1497	1057	440	881	126	Real-Case Data
Correct	7294	7294	1813	1048	546	874	156	Most correct experiment data
Incorrect	7294	7294	1108	689	230	574	66	Most incorrect experiment data

Model 2B	Bulk Volume (10⁶m³)	Net Volume (10⁶m³)	Pore Volume (10⁶rm³)	HCPV Oil (10⁶rm³)	HCPV Gas (10⁶rm³)	STOIP (10⁶sm³)	GIIP (10⁹sm³)	Note
Real-Case	7500	7500	1487	1057	440	881	126	Real-Case Data
Correct	7294	7294	1455	881	349	734	100	Most correct experiment data
Incorrect	7294	7294	952	638	130	531	37	Most incorrect experiment data

Table 28: Real-Case model data vs. the most “correct” and “incorrect” model data for Models 2A and 2B.

The findings of this thesis have significant implications for reservoir modelling practices, emphasizing the need to accurately model the parameters to ensure reliable volumetric results. Inaccuracies in the important parameters mentioned above can have significant ramifications on the results. Therefore, special attention should be given to bias to facies, depth trend, normal vs. asymmetric distribution, saturation height function, and SGS vs. Kriging in order to mitigate potential errors. The tables and tornado plots presented in this study contribute to the scientific understanding of the impact of each parameter on reservoir properties and volumetric calculations. These visual representations enable a systematic analysis of each parameter's sensitivity to porosity, permeability, water saturation, and volume calculations, aiding reservoir engineers and geoscientists in making informed decisions during the modelling process. For instance, if multiple parameters have been inaccurately modelled, the volumetric results could be significantly affected. In Model 2A, incorrect modelling of bias to facies, depth trend, and the choice between SGS and Kriging could lead to a substantial impact on the volumes. When considering the average difference of these parameters on

STOIP, there could be a 9,44 % difference in the volumetric outcomes when incorporating bias on or off, depth trend inclusion or exclusion, and SGS or Kriging selection.

7.3 Parameter Analysis of STOIP and GIIP

To ascertain the relative significance of different parameters on porosity, permeability, water saturation, and volume calculations, comprehensive tables and tornado plots were generated as part of the result analysis. Specifically, tables were created to evaluate the impact of each individual parameter on STOIP and GIIP (Table 17). These tables were constructed to provide a systematic assessment of the influence exerted by each parameter across various variables of interest.

In the case of Model 1, the table for STOIP and GIIP was derived from tornado plots. These tornado plots, visually represented in Figures 62 & 63, offer a graphical depiction of the magnitude of the impact associated with each parameter, enabling a clearer understanding of their sensitivity and contribution to the volumetric calculations. For Model 2A and Model 2B, the tornado plots STOIP and GIIP can be found in Figures 67, 68, 72 & 73.

Based on Tables 11, 12, 13 & 17, it is evident that changes in the parameters have a notable effect on STOIP and GIIP. For instance, in Model 1 there is a 12,79 % difference in STOIP when using either bias to facies on or off, and there is a 2,88 % difference in GIIP when using either 1,5 or 0,6 in layering. In Model 2A, there is a substantial 6,12 % variation in STOIP and 9,66 % variation in GIIP when comparing the use of with or without depth trend. The same applies to Model 2B where there is a difference of 4,67 % in STOIP and 11,23 % in GIIP. There is also a significant % difference in both models when bias to facies is either turned on or off. The largest impacts in Models 2A and 2B occur when there are either 1 or 3 wells used for the experiment.

These findings highlight the importance of accurately modelling various parameters to mitigate potential discrepancies and ensure reliable volumetric results. Inaccuracies in bias to facies, depth trend, and nr. of wells can have significant ramifications on the calculated volumes and should be carefully addressed during the modelling process. Even small error can give significant consequences.

7.4 Number of Wells Issue in Model 2A and 2B

The impact of either 1 or 3 wells in Models 2A and 2B is over 20% for all calculated volumes and the parameter therefore shows importance as shown in Tables 12 and 13. This implies that the choice of number of wells can significantly impact the calculated volumes, with fewer wells yielding potentially different results compared to more wells. The low number of wells shows a sampling issue and does not represent the reservoir as Figure 97 shows. Figure 97 displays the facies statistics for the real-case model and the experiments model with either 1 or 3 wells. As the figure shows there is a sampling issue, and the low number of wells does not represent the reservoir correctly, especially when using a single well sample.

Using either 1 or 3 wells in the experimental design setup resulted in a difference of over 20% in calculated volumes, such as in STOIP and GIIP. This discrepancy is significant. In comparison, when assessing the impact of the number of wells on Model 1, the difference between 2 or 4 wells was less than 4%. The difference observed could be attributed to the fact that Model 1 utilizes more wells, or it could be that the other model has a big lateral variation, that the random well sample taken is highly variable or that the location of the well does not represent an average for the reservoir. There is an uncertainty and therefore employing more wells can lead to more reliable volumetric calculations with reduced variations and with less sampling issues that result in poor reservoir representations.

7.5 Interaction Between Two Parameters

The examination of the analysed pair of parameters has revealed that the combined utilization of low and high values, represented by (1,-1) and (-1,1) respectively, has a more pronounced effect on volumetrics when compared to the utilization of solely high and low values, represented by (1,1) and (-1,-1). This observation suggests that when an asymmetric distribution exists in the presence of bias to facies on, or vice versa, the volumetrics are significantly impacted. These findings also underscore the crucial significance of accurately modelling the parameters.

7.6 Other Remarks

The reliability of the experimental outcomes should also be considered. The use of Petrel software, known for its robustness, enhances the credibility of the findings. However, errors in the building and modelling process should be acknowledged, even with thorough double-checking. The large number of runs and comprehensive analysis of high and low parameter settings provide a solid foundation for drawing conclusions. Nevertheless, it is important to recognize that there may be limitations in the experimental design and potential sources of uncertainties in the modelling process that could have influenced the outcomes.

It is important to note that the findings of this thesis may be specific to the experimental design setup and models used. The values chosen for the high and low settings of the parameters may be relatively high or low. While these results offer valuable insights into the impact of each parameter on volumetric calculations in different models, further exploration is needed to generalize these findings to other geological situations. Conducting similar experiments on real-life reservoir models and different geological settings would help confirm the results and determine whether the impacts are universal, as somewhat observed in this study, or case-specific.

8. Conclusion

This thesis has studied and analysed the impact of layering, the nr. of wells, most of vs. mid-point pick, vertical proportion curve (VPC), bias to facies on vs. off, Sequential Gaussian simulation (SGS) vs. Kriging, variogram range for porosity and permeability, with vs. without depth trend, the correlation coefficient for permeability, normal vs. asymmetric distribution and the saturation height function on porosity, permeability, water saturation and volume calculations.

The main findings are:

- Comparing the experiment volumetric to the real-case volumetric there are both similarities and differences. Bulk volume and net volume exhibited similarities in all the models, but there are notable differences observed in some of the parameters on pore volume, HCPV oil, HCPV gas, STOIP, and GIIP, specially in Model 1. This was due to modelling issues in the real-case volumes. The volumes from the experiments on Model 2A and 2B tends to compare to the real-case volumes and somewhat plots in the P10-P90 range.
- The changes in the mentioned parameters have an impact on porosity, permeability, water saturation, and consequently volume calculation. The degree of impact varies from parameter to parameter and slightly from model to model.
- The parameters that impact the models most are nr. of wells, bias to facies, depth trend, SGS vs. Kriging, saturation height function, and normal vs. asymmetric distribution, and the parameters that have the least impact are most of vs. mid-point pick, variogram range, layering, correlation coefficient, and VPC (only on Model 1).
- The greatest impact on the results occurs when bias to facies is either on or off for Model 1, and when the nr. of wells is either 1 or 3 for Models 2A and 2B.
- If several parameters have not been modelled correctly the impact on the volume calculations can be significant, especially considering bias to facies, depth trend, normal vs. asymmetric distribution, saturation height function, and SGS vs. Kriging.
- There is a general similarity in all the models; depth trend, bias to facies, normal vs. asymmetric distribution, saturation height function, and SGS vs. Kriging consistently tend to rank higher than layering, most of vs. mid-point pick, variogram range,

correlation coefficient, and VPC. So, there is an indication that the impacts are universal, but it should be noted that there are exceptions.

Future work

- Test the experimental design setup on more conceptual models as well as real-life reservoirs to definitely determine if the impacts are universal or could be case-specific.
- Perform and explore more experiments with more wells since few wells displayed a sampling issue.

9. References

- Allen, Paul. 2020. *Design of Experiments for 21st Century Engineers*: Lulu.com.
- Bell, S. 2009. "Experimental Design." In *International Encyclopedia of Human Geography*, edited by Rob Kitchin and Nigel Thrift, 672-675. Oxford: Elsevier.
- Box, George E. P., J. Stuart Hunter, and William G. Hunter. 2005. *Statistics for experimenters : design, innovation, and discovery*. 2nd ed, *Wiley series in probability and statistics*. Hoboken. N.J: Wiley-Interscience.
- Britannica, T. Editors of Encyclopaedia. 2022. "Normal Distribution." Encyclopedia Britannica. <https://www.britannica.com/topic/normal-distribution>.
- Cao, Anye, Yaoqi Liu, Siqi Jiang, Qi Hao, Yujie Peng, Xianxi Bai, and Xu Yang. 2021. "Numerical Investigation on Influence of Two Combined Faults and Its Structure Features on Rock Burst Mechanism." *Minerals (Basel)* 11 (12):1438. doi: 10.3390/min11121438.
- Chen, James. 2023. "Skewness: Positively and Negatively Skewed Defined with Formula." Investopedia, accessed 28.03.23. <https://www.investopedia.com/terms/s/skewness.asp>.
- Esmacili, Behnam, Hossein Rahimpour-Bonab, Ali Kadkhodaie, Amir Ahmadi, and Sirous Hosseinzadeh. 2022. "Developing a saturation-height function for reservoir rock types and comparing the results with the well log-derived water saturation, a case study from the Fahliyan formation, Dorood oilfield, Southwest of Iran." *Journal of petroleum science & engineering* 212:110268. doi: 10.1016/j.petrol.2022.110268.
- Frank, Tobias, Anne-Laure Tertois, and Jean-Laurent Mallet. 2007. "3D-reconstruction of complex geological interfaces from irregularly distributed and noisy point data." *Computers & geosciences* 33 (7):932-943. doi: 10.1016/j.cageo.2006.11.014.
- Hanrahan, G., J. Zhu, S. Gibani, and D. G. Patil. 2005. "CHEMOMETRICS AND STATISTICS | Experimental Design." In *Encyclopedia of Analytical Science (Second Edition)*, edited by Paul Worsfold, Alan Townshend and Colin Poole, 8-13. Oxford: Elsevier.
- Huang, Yanqing. 2018. "Sedimentary characteristics of turbidite fan and its implication for hydrocarbon exploration in Lower Congo Basin." *Petroleum Research* 3 (2):189-196. doi: 10.1016/j.ptlrs.2018.02.001.
- Jamiolahmady, Mahmoud, Mehran Sohrabi, and Mohammed Tafat. 2007. "Estimation of Saturation Height Function Using Capillary Pressure by Different Approaches." EUROPEC/EAGE Conference and Exhibition.

- Kenton, Will. 2022. "Asymmetric Distribution: Definition and Examples in Statistics." Investopedia, Last Modified 18.12.22, accessed 28.03.23.
<https://www.investopedia.com/terms/a/asymmetrical-distribution.asp>.
- Li, Hong, Bo Wan, Deping Chu, Run Wang, Guoxi Ma, Jinming Fu, and Zhuocheng Xiao. 2023. "Progressive Geological Modeling and Uncertainty Analysis Using Machine Learning." *ISPRS International Journal of Geo-Information* 12 (3):97.
- Mallet, Jean-Laurent. 2002. *Geomodeling*. Cary: Cary: Oxford University Press, Incorporated.
- Mukhopadhyay, Ananya, Priyanka Mazumdar, and A. J. van Loon. 2016. "A new superassemblage model explaining proximal-to-distal and lateral facies changes in fluvial environments, based on the Proterozoic Sanjauli Formation (Lesser Himalaya, India)." *Journal of Palaeogeography* 5 (4):391-408. doi: 10.1016/j.jop.2016.08.001.
- Nemes, István. 2022. "Applications of automated Petrel workflows in 3D reservoir geologic modelling – A case study." *Central European Geology*. doi: <https://doi.org/10.1556/24.2022.00129>.
- Ortiz, Julien M. 2013. "Jef Caers: Modeling Uncertainty in the Earth Sciences." *Mathematical geosciences* 45 (1):127. doi: 10.1007/s11004-012-9432-3.
- Petrofaq.org. 2019. "Common Workflow for Geological Modeling." Petrofaq.org, accessed 15.03.2023. http://petrofaq.org/wiki/Common_Workflow_for_Geological_Modeling
- ProcessStreet. 2023. "What is a Workflow? A Beginner's Guide to Workflow Management." Process Street, accessed 14.03.23. <https://www.process.st/what-is-a-workflow/>.
- Pyrzcz, Michael J., and Clayton V. Deutsch. 2014. "Geostatistical reservoir modeling." In. New York: Oxford University Press.
- Ringrose, Philip, and Mark Bentley. 2021. "Reservoir model design : a practitioner's guide." In. Cham, Switzerland: Springer.
- Schlumberger. 2023a. "Petrel Geology and Modeling." Schlumberger, accessed 15.03.23. <https://www.software.slb.com/products/petrel/petrel-geology-and-modeling>.
- Petrel Guru. Schlumberger, software.slb.com.
- Thornton, James M., Gregoire Mariethoz, and Philip Brunner. 2018. "A 3D geological model of a structurally complex Alpine region as a basis for interdisciplinary research." *Sci Data* 5 (1):180238-20. doi: 10.1038/sdata.2018.238.
- Vargas Grajales, Viviana, Tamires Pereira Pinto da Silva, Abelardo Borges Barreto, and Sinesio Pesco. 2020. "A New Object-Based Algorithm To Simulate Geometrical and Petrophysical Turbidite Channel Properties." *SPE journal (Society of Petroleum Engineers (U.S.) : 1996)* 25 (5):2433-2449. doi: 10.2118/199086-PA.

Wellmann, Florian, and Guillaume Caumon. 2018. "3-D Structural geological models: Concepts, methods, and uncertainties." In, 1-121. Elsevier.

Wellmann, Florian, Alexander Schaaf, Miguel de la Varga, and Christoph von Hagke. 2019. "From Google Earth to 3D Geology Problem 2: Seeing Below the Surface of the Digital Earth." In *Developments in Structural Geology and Tectonics*, 189-204. Elsevier.

Appendix

Appendix A

A.1 - Model 1 (Fluvial) parameter tables with sum, min, max, and avg

Bias to Facies

	Bulk Volume	Net Volume	Pore Volume	HCPV oil	HCPV gas	STOIP	GIIP
Sum (x=1)	3879549952	3879549952	111294679	92856313	323226	77380247	92338
Sum (x=-1)	3879549952	3879549952	130581181	106469772	331509	88724798	94720
Difference %	0	0	0,147697	0,127862	0,024986	0,127862	0,025148
Min (x=1)	3788623	3788623	1009	2310	256	1925	73
Min (x=-1)	3788623	3788623	101532	76972	266	64143	76
Difference %	0	0	0,990062	0,969989	0,037594	0,969989	0,039474
Max (x=1)	3788623	3788623	133566	117516	453	97930	130
Max (x=-1)	3788623	3788623	173158	115441	431	96201	123
Difference %	0	0	0,228647	0,017657	0,048565	0,017655	0,053846
Average (x=1)	3788623	3788623	108686,2100	90679,9932	315,6504	75566,6475	90,1738
Average (x=-1)	3788623	3788623	127520,6846	103974,3867	323,7393	86645,3105	92,5000
Difference %	0	0	0,147697	0,127862	0,024986	0,127862	0,025148

Correlation Coefficient

	Bulk Volume	Net Volume	Pore Volume	HCPV oil	HCPV gas	STOIP	GIIP
Sum (x=1)	3879549952	3879549952	120999855	99269631	327745	82724689	93648
Sum (x=-1)	3879549952	3879549952	120876005	100056454	326990	83380356	93410
Difference %	0	0	0,001024	0,007864	0,002304	0,007864	0,002541
Min (x=1)	3788623	3788623	1018	2310	256	1925	73
Min (x=-1)	3788623	3788623	1009	2314	256	1928	73
Difference %	0	0	0,008841	0,001729	0,000000	0,001556	0
Max (x=1)	3788623	3788623	173158	116896	453	97413	130
Max (x=-1)	3788623	3788623	172472	117516	446	97930	127
Difference %	0	0	0,003962	0,005276	0,015453	0,005279	0,023077
Average (x=1)	3788623	3788623	118163,9209	96942,99902	320,06348	80785,8291	91,453125
Average (x=-1)	3788623	3788623	118042,9736	97711,38086	319,32617	81426,1289	91,2207031
Difference %	0	0	0,001024	0,007864	0,002304	0,007864	0,002541

Depth Trend

	Bulk Volume	Net Volume	Pore Volume	HCPV oil	HCPV gas	STOIIIP	GIIP
Sum (x=1)	3879549952	3879549952	132321224	104016819	330993	86680666	94563
Sum (x=-1)	3879549952	3879549952	109554636	95309266	323742	79424379	92495
Difference %	0	0	0,172055452	0,083712933	0,0219068	0,08371287	0,02186902
Min (x=1)	3788623	3788623	105865	76972	266	64143	76
Min (x=-1)	3788623	3788623	1009	2310	256	1925	73
Difference %	0	0	0,990468994	0,969989087	0,037594	0,96998893	0,03947368
Max (x=1)	3788623	3788623	173158	116896	453	97413	130
Max (x=-1)	3788623	3788623	133221	117516	446	97930	127
Difference %	0	0	0,23063907	0,005275877	0,0154525	0,00527928	0,02307692
Average (x=1)	3788623	3788623	129219,9453	101578,9248	323,23535	84649,0879	92,3466797
Average (x=-1)	3788623	3788623	106986,9492	93075,45508	316,1543	77562,8701	90,3271484
Difference %	0	0	0,172055452	0,083712933	0,0219068	0,08371287	0,02186902

Layering

	Bulk Volume	Net Volume	Pore Volume	HCPV oil	HCPV gas	STOIIIP	GIIP
Sum (x=1)	3879549952	3879549952	120533359	99276415	332143	82730345	94894
Sum (x=-1)	3879549952	3879549952	121342501	100049670	322592	83374700	92164
Difference %	0	0	0,006668249	0,007728711	0,0287557	0,00772842	0,02876894
Min (x=1)	3788623	3788623	1009	2314	256	1928	73
Min (x=-1)	3788623	3788623	1018	2310	256	1925	73
Difference %	0	0	0,008840864	0,001728608	0	0,00155602	0
Max (x=1)	3788623	3788623	172660	116896	453	97413	130
Max (x=-1)	3788623	3788623	173158	117516	382	97930	109
Difference %	0	0	0,002875986	0,005275877	0,1567329	0,00527928	0,16153846
Average (x=1)	3788623	3788623	117708,3584	96949,62402	324,3584	80791,3525	92,6699219
Average (x=-1)	3788623	3788623	118498,5361	97704,75586	315,03125	81420,6055	90,0039063
Difference %	0	0	0,006668249	0,007728711	0,0287557	0,00772842	0,02876894

Most of vs. Mid Point Pick

	Bulk Volume	Net Volume	Pore Volume	HCPV oil	HCPV gas	STOIP	GIIP
Sum (x=1)	3879549952	3879549952	120946937	99668057	327127	83056694	93462
Sum (x=-1)	3879549952	3879549952	120928923	99658028	327608	83048351	93596
Difference %	0	0	0,000148941	0,000100624	0,0014682	0,00010045	0,00143169
Min (x=1)	3788623	3788623	1018	2310	256	1925	73
Min (x=-1)	3788623	3788623	1009	2321	256	1934	73
Difference %	0	0	0,008840864	0,004739336	0	0,00465357	0
Max (x=1)	3788623	3788623	172472	116896	453	97413	130
Max (x=-1)	3788623	3788623	173158	117516	424	97930	121
Difference %	0	0	0,0039617	0,005275877	0,0640177	0,00527928	0,06923077
Average (x=1)	3788623	3788623	118112,2432	97332,08691	319,45996	81110,0527	91,2714844
Average (x=-1)	3788623	3788623	118094,6514	97322,29297	319,92969	81101,9053	91,4023438
Difference %	0	0	0,000148941	0,000100624	0,0014682	0,00010045	0,00143169

Normal vs. Asymmetric Distribution

	Bulk Volume	Net Volume	Pore Volume	HCPV oil	HCPV gas	STOIP	GIIP
Sum (x=1)	3879549952	3879549952	110109611	94047156	323899	78372615	92543
Sum (x=-1)	3879549952	3879549952	131766249	105278929	330836	87732430	94515
Difference %	0	0	0,164356489	0,10668586	0,020968093	0,10668592	0,020864413
Min (x=1)	3788623	3788623	1009	2310	256	1925	73
Min (x=-1)	3788623	3788623	101532	76972	266	64143	76
Difference %	0	0	0,990062246	0,96998909	0,037593985	0,96998893	0,039473684
Max (x=1)	3788623	3788623	132795	116431	431	97026	123
Max (x=-1)	3788623	3788623	173158	117516	453	97930	130
Difference %	0	0	0,23309925	0,00923279	0,048565121	0,00923108	0,053846154
Average (x=1)	3788623	3788623	107528,917	91842,9258	316,3076172	76535,7568	90,37402344
Average (x=-1)	3788623	3788623	128677,9775	102811,454	323,0820313	85676,2012	92,29980469
Difference %	0	0	0,164356489	0,10668586	0,020968093	0,10668592	0,020864413

Saturation Heigh Function

	Bulk Volume	Net Volume	Pore Volume	HCPV oil	HCPV gas	STOIP	GIIP
Sum (x=1)	3879549952	3879549952	120944845	100939666	333663	84116355	95342
Sum (x=-1)	3879549952	3879549952	120931015	98386419	321072	81988690	91716
Difference %	0	0	0,00011435	0,02529478	0,037735679	0,02529431	0,038031508
Min (x=1)	3788623	3788623	1009	2385	267	1988	76
Min (x=-1)	3788623	3788623	1018	2310	256	1925	73
Difference %	0	0	0,008840864	0,03144654	0,041198502	0,03169014	0,039473684
Max (x=1)	3788623	3788623	172627	117516	453	97930	130
Max (x=-1)	3788623	3788623	173158	113547	431	94623	123
Difference %	0	0	0,003066563	0,03377412	0,048565121	0,03376902	0,053846154
Average (x=1)	3788623	3788623	118110,2002	98573,8926	325,8427734	82144,8779	93,10742188
Average (x=-1)	3788623	3788623	118096,6943	96080,4873	313,546875	80067,0801	89,56640625
Difference %	0	0	0,00011435	0,02529478	0,037735679	0,02529431	0,038031508

SGS vs. Kriging

	Bulk Volume	Net Volume	Pore Volume	HCPV oil	HCPV gas	STOIP	GIIP
Sum (x=1)	3879549952	3879549952	112859751	97905993	325190	81588311	92888
Sum (x=-1)	3879549952	3879549952	129016109	101420092	329545	84516734	94170
Difference %	0	0	0,125227447	0,03464894	0,013215191	0,03464903	0,013613677
Min (x=1)	3788623	3788623	1009	2310	256	1925	73
Min (x=-1)	3788623	3788623	101532	76972	266	64143	76
Difference %	0	0	0,990062246	0,96998909	0,037593985	0,96998893	0,039473684
Max (x=1)	3788623	3788623	133566	117516	453	97930	130
Max (x=-1)	3788623	3788623	173158	115441	417	96201	119
Difference %	0	0	0,22864667	0,01765717	0,079470199	0,01765547	0,084615385
Average (x=1)	3788623	3788623	110214,6006	95611,3213	317,5683594	79676,085	90,7109375
Average (x=-1)	3788623	3788623	125992,2939	99043,0586	321,8212891	82535,873	91,96289063
Difference %	0	0	0,125227447	0,03464894	0,013215191	0,03464903	0,013613677

Variogram Range

	Bulk Volume	Net Volume	Pore Volume	HCPV oil	HCPV gas	STOIP	GIIP
Sum (x=1)	3879549952	3879549952	120909906	99636046	327939	83030013	93703
Sum (x=-1)	3879549952	3879549952	120965954	99690039	326796	83075032	93355
Difference %	0	0	0,000463337	0,00054161	0,003485404	0,00054191	0,003713862
Min (x=1)	3788623	3788623	1023	2314	256	1928	73
Min (x=-1)	3788623	3788623	1009	2310	256	1925	73
Difference %	0	0	0,013685239	0,00172861	0	0,00155602	0
Max (x=1)	3788623	3788623	173158	117516	453	97930	130
Max (x=-1)	3788623	3788623	172627	115870	431	96559	123
Difference %	0	0	0,003066563	0,0140066	0,048565121	0,0139998	0,053846154
Average (x=1)	3788623	3788623	118076,0801	97300,8262	320,2529297	81083,9971	91,50683594
Average (x=-1)	3788623	3788623	118130,8145	97353,5537	319,1367188	81127,9609	91,16699219
Difference %	0	0	0,000463337	0,00054161	0,003485404	0,00054191	0,003713862

Vertical Proportion Curve

	Bulk Volume	Net Volume	Pore Volume	HCPV oil	HCPV gas	STOIP	GIIP
Sum (x=1)	3879549952	3879549952	120887130	99620641	326660	83017197	93321
Sum (x=-1)	3879549952	3879549952	120988730	99705444	328075	83087848	93737
Difference %	0	0	0,000839748	0,00085054	0,004313038	0,00085032	0,004437949
Min (x=1)	3788623	3788623	1009	2310	256	1925	73
Min (x=-1)	3788623	3788623	1017	2314	256	1928	73
Difference %	0	0	0,007866273	0,00172861	0	0,00155602	0
Max (x=1)	3788623	3788623	172627	117516	446	97930	127
Max (x=-1)	3788623	3788623	173158	116896	453	97413	130
Difference %	0	0	0,003066563	0,00527588	0,015452539	0,00527928	0,023076923
Average (x=1)	3788623	3788623	118053,8379	97285,7822	319,0039063	81071,4814	91,13378906
Average (x=-1)	3788623	3788623	118153,0566	97368,5977	320,3857422	81140,4766	91,54003906
Difference %	0	0	0,000839748	0,00085054	0,004313038	0,00085032	0,004437949

Nr of Wells

	Bulk Volume	Net Volume	Pore Volume	HCPV oil	HCPV gas	STOIP	GIIP
Sum (x=1)	3879549952	3879549952	122971431	101721786	329468	84768133	94133
Sum (x=-1)	3879549952	3879549952	118904429	97604299	325267	81336912	92925
Difference %	0	0	0,033072739	0,04047793	0,012750859	0,04047772	0,012832907
Min (x=1)	3788623	3788623	1017	2314	256	1928	73
Min (x=-1)	3788623	3788623	1009	2310	256	1925	73
Difference %	0	0	0,007866273	0,00172861	0	0,00155602	0
Max (x=1)	3788623	3788623	164939	115441	431	96201	123
Max (x=-1)	3788623	3788623	173158	117516	453	97930	130
Difference %	0	0	0,047465321	0,01765717	0,048565121	0,01765547	0,053846154
Average (x=1)	3788623	3788623	120089,2881	99337,6816	321,7460938	82781,3799	91,92675781
Average (x=-1)	3788623	3788623	116117,6064	95316,6982	317,6435547	79430,5781	90,74707031
Difference %	0	0	0,033072739	0,04047793	0,012750859	0,04047772	0,012832907

A.2 - Model 2A (Turbidite) parameter tables with sum, min, max, and avg

Bias to Facies

	Bulk Volume	Net Volume	Pore Volume	HCPV oil	HCPV gas	STOIP	GIIP
Sum (x=1)	7469056	7469056	1498118	887874	397369	739894	113517
Sum (x=-1)	7469056	7469056	1452724	864961	374366	720795	106964
Difference %	0	0	0,030301	0,025807	0,057888	0,025813	0,057727
Min (x=1)	7294	7294	1096	677	226	564	64
Min (x=-1)	7294	7294	1095	679	225	566	64
Difference %	0	0	0,000912	0,002946	0,004425	0,003534	0
Max (x=1)	7294	7294	1895	1093	593	911	169
Max (x=-1)	7294	7294	1850	1057	578	881	165
Difference %	0	0	0,023747	0,032937	0,025295	0,032931	0,023669
Average (x=1)	7294	7294	1463,0059	867,0645	388,0557	722,5527	110,8564
Average (x=-1)	7294	7294	1418,6758	844,6885	365,5918	703,9014	104,4570
Difference %	0	0	0,030301	0,025807	0,057888	0,025813	0,057727

Correlation Coefficient

	Bulk Volume	Net Volume	Pore Volume	HCPV oil	HCPV gas	STOIIP	GIIP
Sum (x=1)	7469056	7469056	1475274	876819	386089	730671	110299
Sum (x=-1)	7469056	7469056	1475568	876016	385646	730018	110182
Difference %	0	0	0,999023	0,000916	0,001147	0,000894	0,001061
Min (x=1)	7294	7294	1095	677	225	564	64
Min (x=-1)	7294	7294	1096	679	226	566	64
Difference %	0	0	0,000912	0,002946	0,004425	0,003534	0
Max (x=1)	7294	7294	1895	1093	593	911	169
Max (x=-1)	7294	7294	1892	1089	584	908	167
Difference %	0	0	0,001583	0,003660	0,015177	0,003293	0,011834
Average (x=1)	7294	7294	1440,6973	856,2686	377,0400	713,5459	107,7139
Average (x=-1)	7294	7294	1440,9844	855,4844	376,6074	712,9082	107,5996
Difference %	0	0	0,000199	0,000916	0,001147	0,000894	0,001061

Depth Trend

	Bulk Volume	Net Volume	Pore Volume	HCPV oil	HCPV gas	STOIIP	GIIP
Sum (x=1)	7469056	7469056	1516945	904097	405499	753413	115835
Sum (x=-1)	7469056	7469056	1433897	848738	366236	707276	104646
Difference %	0	0	0,05474688	0,06123126	0,09682638	0,06123733	0,09659429
Min (x=1)	7294	7294	1152	721	247	601	70
Min (x=-1)	7294	7294	1095	677	225	564	64
Difference %	0	0	0,04947917	0,06102635	0,08906883	0,06156406	0,08571429
Max (x=1)	7294	7294	1895	1093	593	911	169
Max (x=-1)	7294	7294	1782	1023	535	853	153
Difference %	0	0	0,05963061	0,06404392	0,09780776	0,0636663	0,09467456
Average (x=1)	7294	7294	1481,3916	882,9072	395,9951	735,7549	113,1201
Average (x=-1)	7294	7294	1400,2900	828,8457	357,6523	690,6992	102,1934
Difference %	0	0	0,05474688	0,06123126	0,09682638	0,06123733	0,09659429

Layering

	Bulk Volume	Net Volume	Pore Volume	HCPV oil	HCPV gas	STOIIP	GIIP
Sum (x=1)	7469056	7469056	1475561	875343	385996	729454	110283
Sum (x=-1)	7469056	7469056	1475281	877492	385739	731235	110198
Difference %	0	0	0,00018976	0,00244903	0,00066581	0,00243561	0,00077074
Min (x=1)	7294	7294	1095	677	226	564	64
Min (x=-1)	7294	7294	1095	679	225	566	64
Difference %	0	0	0	0,00294551	0,00442478	0,00353357	0
Max (x=1)	7294	7294	1895	1088	593	907	169
Max (x=-1)	7294	7294	1892	1093	589	911	168
Difference %	0	0	0,00158311	0,00457457	0,00674536	0,00439078	0,00591716
Average (x=1)	7294	7294	1440,9775	854,8271	376,9492	712,3574	107,6982
Average (x=-1)	7294	7294	1440,7041	856,9258	376,6982	714,0967	107,6152
Difference %	0	0	0,00018976	0,00244903	0,00066581	0,00243561	0,00077074

Most of vs. Mid Point Pick

	Bulk Volume	Net Volume	Pore Volume	HCPV oil	HCPV gas	STOIIP	GIIP
Sum (x=1)	7469056	7469056	1475306	876532	385641	730448	110184
Sum (x=-1)	7469056	7469056	1475536	876303	386094	730241	110297
Difference %	0	0	0,00015588	0,00026126	0,00117329	0,00028339	0,00102451
Min (x=1)	7294	7294	1095	677	226	564	64
Min (x=-1)	7294	7294	1095	679	225	566	64
Difference %	0	0	0	0,00294551	0,00442478	0,00353357	0
Max (x=1)	7294	7294	1895	1093	593	911	169
Max (x=-1)	7294	7294	1894	1088	584	907	167
Difference %	0	0	0,0005277	0,00457457	0,01517707	0,00439078	0,01183432
Average (x=1)	7294	7294	1440,7285	855,9883	376,6025	713,3281	107,6016
Average (x=-1)	7294	7294	1440,9531	855,7646	377,0449	713,1260	107,7119
Difference %	0	0	0,00015588	0,00026126	0,00117329	0,00028339	0,00102451

Normal vs. Asymmetric Distribution

	Bulk Volume	Net Volume	Pore Volume	HCPV oil	HCPV gas	STOIP	GIIP
Sum (x=1)	7469056	7469056	1470369	871261	384911	726035	109963
Sum (x=-1)	7469056	7469056	1480473	881574	386824	734654	110518
Difference %	0	0	0,00682485	0,01169839	0,0049454	0,01173205	0,00502181
Min (x=1)	7294	7294	1095	677	225	564	64
Min (x=-1)	7294	7294	1101	684	226	570	65
Difference %	0	0	0,00544959	0,01023392	0,00442478	0,01052632	0,01538462
Max (x=1)	7294	7294	1878	1083	584	902	167
Max (x=-1)	7294	7294	1895	1093	593	911	169
Difference %	0	0	0,00897098	0,00914913	0,01517707	0,00987925	0,01183432
Average (x=1)	7294	7294	1435,9072	850,8408	375,8896	709,0186	107,3857
Average (x=-1)	7294	7294	1445,7744	860,9121	377,7578	717,4355	107,9277
Difference %	0	0	0,00682485	0,01169839	0,0049454	0,01173205	0,00502181

Saturation Height Function

	Bulk Volume	Net Volume	Pore Volume	HCPV oil	HCPV gas	STOIP	GIIP
Sum (x=1)	7469056	7469056	1475594	890079	389665	741733	111326
Sum (x=-1)	7469056	7469056	1475248	862756	382070	718956	109155
Difference %	0	0	0,00023448	0,03069728	0,0194911	0,03070782	0,01950128
Min (x=1)	7294	7294	1095	700	230	583	66
Min (x=-1)	7294	7294	1095	677	225	564	64
Difference %	0	0	0	0,03285714	0,02173913	0,03259005	0,03030303
Max (x=1)	7294	7294	1895	1093	593	911	169
Max (x=-1)	7294	7294	1894	1061	581	884	166
Difference %	0	0	0,0005277	0,02927722	0,02023609	0,02963776	0,01775148
Average (x=1)	7294	7294	1441,0098	869,2178	380,5322	724,3486	108,7168
Average (x=-1)	7294	7294	1440,6719	842,5352	373,1152	702,1055	106,5967
Difference %	0	0	0,00023448	0,03069728	0,0194911	0,03070782	0,01950128

SGS vs. Kriging

	Bulk Volume	Net Volume	Pore Volume	HCPV oil	HCPV gas	STOIP	GIIP
Sum (x=1)	7469056	7469056	1487962	879661	394579	733054	112728
Sum (x=-1)	7469056	7469056	1462880	873174	377156	727635	107753
Difference %	0	0	0,01685661	0,00737443	0,04415592	0,00739236	0,04413278
Min (x=1)	7294	7294	1095	677	225	564	64
Min (x=-1)	7294	7294	1105	684	226	570	65
Difference %	0	0	0,00904977	0,01023392	0,00442478	0,01052632	0,01538462
Max (x=1)	7294	7294	1860	1069	578	891	165
Max (x=-1)	7294	7294	1895	1093	593	911	169
Difference %	0	0	0,01846966	0,02195791	0,02529511	0,0219539	0,02366864
Average (x=1)	7294	7294	1453,0879	859,0439	385,3311	715,8730	110,0859
Average (x=-1)	7294	7294	1428,5938	852,7090	368,3164	710,5811	105,2275
Difference %	0	0	0,01685661	0,00737443	0,04415592	0,00739236	0,04413278

Variogram Range

	Bulk Volume	Net Volume	Pore Volume	HCPV oil	HCPV gas	STOIP	GIIP
Sum (x=1)	7469056	7469056	1475083	876396	385728	730321	110195
Sum (x=-1)	7469056	7469056	1475759	876439	386007	730368	110286
Difference %	0	0	0,00045807	4,9062E-05	0,00072278	6,4351E-05	0,00082513
Min (x=1)	7294	7294	1095	679	226	566	64
Min (x=-1)	7294	7294	1095	677	225	564	64
Difference %	0	0	0	0,00294551	0,00442478	0,00353357	0
Max (x=1)	7294	7294	1895	1090	593	908	169
Max (x=-1)	7294	7294	1892	1093	589	911	168
Difference %	0	0	0,00158311	0,00274474	0,00674536	0,00329308	0,00591716
Average (x=1)	7294	7294	1440,51074	855,855469	376,6875	713,204102	107,612305
Average (x=-1)	7294	7294	1441,1709	855,897461	376,959961	713,25	107,701172
Difference %	0	0	0,00045807	4,9062E-05	0,00072278	6,4351E-05	0,00082513

Nr of Wells

	Bulk Volume	Net Volume	Pore Volume	HCPV oil	HCPV gas	STOIIP	GIIP
Sum (x=1)	7469056	7469056	1165587	741563	249976	617955	71404
Sum (x=-1)	7469056	7469056	1785255	1011272	521759	842734	149077
Difference %	0	0	0,34710335	0,26670273	0,52089758	0,26672592	0,52102605
Min (x=1)	7294	7294	1095	677	225	564	64
Min (x=-1)	7294	7294	1549	860	396	717	113
Difference %	0	0	0,29309232	0,2127907	0,43181818	0,21338912	0,43362832
Max (x=1)	7294	7294	1190	779	266	649	76
Max (x=-1)	7294	7294	1895	1093	593	911	169
Difference %	0	0	0,37203166	0,28728271	0,55143339	0,28759605	0,55029586
Average (x=1)	7294	7294	1138,26855	724,182617	244,117188	603,47168	69,7304688
Average (x=-1)	7294	7294	1743,41309	987,570313	509,530273	822,982422	145,583008
Difference %	0	0	0,34710335	0,26670273	0,52089758	0,26672592	0,52102605

A.3 - Model 2B (Turbidite) parameter tables with sum, min, max, and avg

Bias to Facies

	Bulk Volume	Net Volume	Pore Volume	HCPV oil	HCPV gas	STOIIP	GIIP
Sum (x=1)	7469056	7469056	1232763	776726	247950	647279	70841
Sum (x=-1)	7461762	7461762	1206410	763271	233763	636055	66775
Difference %	0	0	0,021377	0,017323	0,057217	0,017340	0,057396
Min (x=1)	7294	7294	949	633	129	527	37
Min (x=-1)	7294	7294	949	632	129	527	37
Difference %	0	0	0,000000	0,001580	0,000000	0,000000	0
Max (x=1)	7294	7294	1568	938	405	782	116
Max (x=-1)	7294	7294	1485	904	374	754	107
Difference %	0	0	0,052934	0,036247	0,076543	0,035806	0,077586
Average (x=1)	7294	7294	1203,8701	758,5215	242,1387	632,1084	69,1807
Average (x=-1)	7294	7294	1179,2864	746,1105	228,5073	621,7546	65,2737
Difference %	0	0	0,020421	0,016362	0,056296	0,016380	0,056475

Correlation Coefficient

	Bulk Volume	Net Volume	Pore Volume	HCPV oil	HCPV gas	STOIIP	GIIP
Sum (x=1)	7469056	7469056	1220154	771155	241458	642620	68978
Sum (x=-1)	7461762	7461762	1219019	768842	240255	640714	68638
Difference %	0	0	0,999022	0,002999	0,004982	0,002966	0,004929
Min (x=1)	7294	7294	949	633	129	527	37
Min (x=-1)	7294	7294	949	632	130	527	37
Difference %	0	0	0,000000	0,001580	0,007692	0,000000	0
Max (x=1)	7294	7294	1568	938	405	782	116
Max (x=-1)	7294	7294	1549	919	395	766	113
Difference %	0	0	0,012117	0,020256	0,024691	0,020460	0,025862
Average (x=1)	7294	7294	1191,5566	753,0811	235,7988	627,5586	67,3613
Average (x=-1)	7294	7294	1191,6119	751,5562	234,8534	626,3089	67,0948
Difference %	0	0	0,000046	0,002025	0,004010	0,001991	0,003956

Depth Trend

	Bulk Volume	Net Volume	Pore Volume	HCPV oil	HCPV gas	STOIIP	GIIP
Sum (x=1)	7469056	7469056	1259932	788796	255278	657332	72933
Sum (x=-1)	7461762	7461762	1179241	751201	226435	626002	64683
Difference %	0	0	0,06404393	0,0476612	0,11298663	0,04766237	0,1131175
Min (x=1)	7294	7294	981	653	131	544	37
Min (x=-1)	7294	7294	949	632	129	527	37
Difference %	0	0	0,03261978	0,0321593	0,01526718	0,03125	0
Max (x=1)	7294	7294	1568	938	405	782	116
Max (x=-1)	7294	7294	1494	898	379	749	108
Difference %	0	0	0,04719388	0,0426439	0,06419753	0,04219949	0,0689655
Average (x=1)	7294	7294	1230,4023	770,3086	249,2949	641,9258	71,2236
Average (x=-1)	7294	7294	1152,7283	734,3118	221,3441	611,9277	63,2287
Difference %	0	0	0,06312902	0,0467303	0,11211956	0,04673144	0,1122506

Layering

	Bulk Volume	Net Volume	Pore Volume	HCPV oil	HCPV gas	STOIIP	GIIP
Sum (x=1)	7469056	7469056	1220528	769239	241228	641043	68910
Sum (x=-1)	7461762	7461762	1218645	770758	240485	642291	68706
Difference %	0	0	0,00154277	0,0019708	0,00308007	0,00194304	0,0029604
Min (x=1)	7294	7294	949	632	129	527	37
Min (x=-1)	7294	7294	950	635	129	529	37
Difference %	0	0	0,00105263	0,0047244	0	0,00378072	0
Max (x=1)	7294	7294	1568	938	405	782	116
Max (x=-1)	7294	7294	1549	927	395	772	113
Difference %	0	0	0,01211735	0,0117271	0,02469136	0,01278772	0,0258621
Average (x=1)	7294	7294	1191,9219	751,2100	235,5742	626,0186	67,2949
Average (x=-1)	7294	7294	1191,2463	753,4291	235,0782	627,8504	67,1613
Difference %	0	0	0,00056677	0,0029454	0,00210557	0,00291771	0,0019858

Most of vs. Mid Point Pick

	Bulk Volume	Net Volume	Pore Volume	HCPV oil	HCPV gas	STOIIP	GIIP
Sum (x=1)	7469056	7469056	1220305	770514	240957	642108	68831
Sum (x=-1)	7461762	7461762	1218868	769483	240756	641226	68785
Difference %	0	0	0,00117757	0,0013381	0,00083417	0,0013736	0,0006683
Min (x=1)	7294	7294	949	632	129	527	37
Min (x=-1)	7294	7294	949	633	129	527	37
Difference %	0	0	0	0,0015798	0	0	0
Max (x=1)	7294	7294	1568	938	405	782	116
Max (x=-1)	7294	7294	1559	930	398	775	114
Difference %	0	0	0,0057398	0,0085288	0,01728395	0,00895141	0,0172414
Average (x=1)	7294	7294	1191,7041	752,4551	235,3096	627,0586	67,2178
Average (x=-1)	7294	7294	1191,4643	752,1828	235,3431	626,8094	67,2385
Difference %	0	0	0,00020121	0,0003619	0,00014251	0,00039743	0,0003085

Normal vs. Asymmetric Distribution

	Bulk Volume	Net Volume	Pore Volume	HCPV oil	HCPV gas	STOIP	GIIP
Sum (x=1)	7469056	7469056	1210705	758320	232908	631931	66534
Sum (x=-1)	7461762	7461762	1228468	781677	248805	651403	71082
Difference %	0	0	0,01445947	0,02988063	0,06389341	0,0298924	0,06398244
Min (x=1)	7294	7294	949	632	129	527	37
Min (x=-1)	7294	7294	952	637	136	531	39
Difference %	0	0	0,00315126	0,00784929	0,05147059	0,00753296	0,05128205
Max (x=1)	7294	7294	1568	938	405	782	116
Max (x=-1)	7294	7294	1525	927	397	772	113
Difference %	0	0	0,02742347	0,01172708	0,01975309	0,01278772	0,02586207
Average (x=1)	7294	7294	1182,3291	740,5469	227,4492	617,1201	64,9746
Average (x=-1)	7294	7294	1200,8485	764,1026	243,2111	636,7576	69,4839
Difference %	0	0	0,01542192	0,03082801	0,06480758	0,03083977	0,06489652

Saturation Height Function

	Bulk Volume	Net Volume	Pore Volume	HCPV oil	HCPV gas	STOIP	GIIP
Sum (x=1)	7469056	7469056	1220475	783369	244365	652815	69816
Sum (x=-1)	7461762	7461762	1218698	756628	237348	630519	67800
Difference %	0	0	0,00145599	0,03413589	0,02871524	0,03415363	0,0288759
Min (x=1)	7294	7294	949	654	132	545	38
Min (x=-1)	7294	7294	949	632	129	527	37
Difference %	0	0	0	0,03363914	0,02272727	0,03302752	0,02631579
Max (x=1)	7294	7294	1568	938	405	782	116
Max (x=-1)	7294	7294	1545	902	394	752	113
Difference %	0	0	0,01466837	0,03837953	0,02716049	0,03836317	0,02586207
Average (x=1)	7294	7294	1191,8701	765,0088	238,6377	637,5146	68,1797
Average (x=-1)	7294	7294	1191,2981	739,6168	232,0117	616,3431	66,2757
Difference %	0	0	0,0004799	0,03319174	0,02776579	0,0332095	0,02792661

SGS. Vs Kriging

	Bulk Volume	Net Volume	Pore Volume	HCPV oil	HCPV gas	STOIIP	GIIP
Sum (x=1)	7469056	7469056	1211876	760628	237223	633857	67765
Sum (x=-1)	7461762	7461762	1227297	779369	244490	649477	69851
Difference %	0	0	0,01256501	0,02404638	0,0297231	0,02405012	0,02986357
Min (x=1)	7294	7294	952	632	136	527	39
Min (x=-1)	7294	7294	949	633	129	527	37
Difference %	0	0	0,00315126	0,00157978	0,05147059	0	0,05128205
Max (x=1)	7294	7294	1485	890	374	741	107
Max (x=-1)	7294	7294	1568	938	405	782	116
Difference %	0	0	0,05293367	0,05117271	0,07654321	0,05242967	0,07758621
Average (x=1)	7294	7294	1183,4727	742,8008	231,6631	619,0010	66,1768
Average (x=-1)	7294	7294	1199,7038	761,8465	238,9932	634,8749	68,2805
Difference %	0	0	0,0135293	0,02499946	0,03067063	0,0250032	0,03081097

Variogram Range

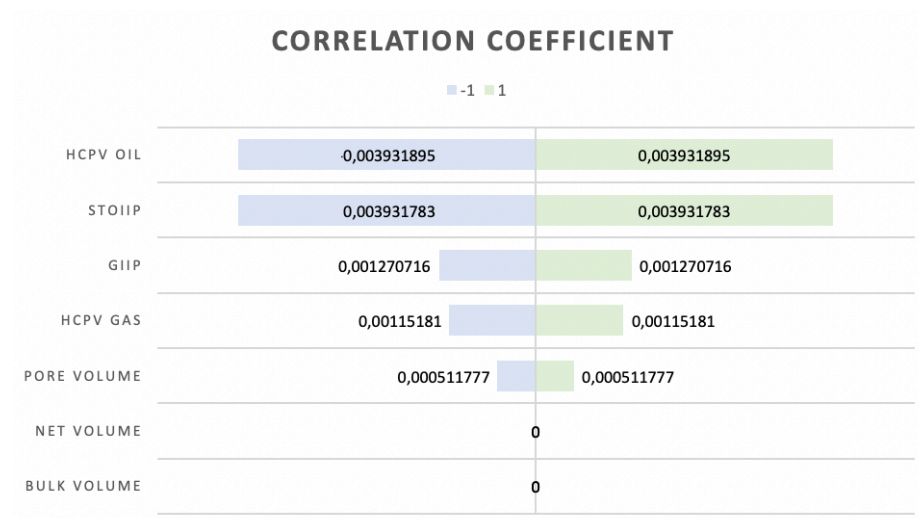
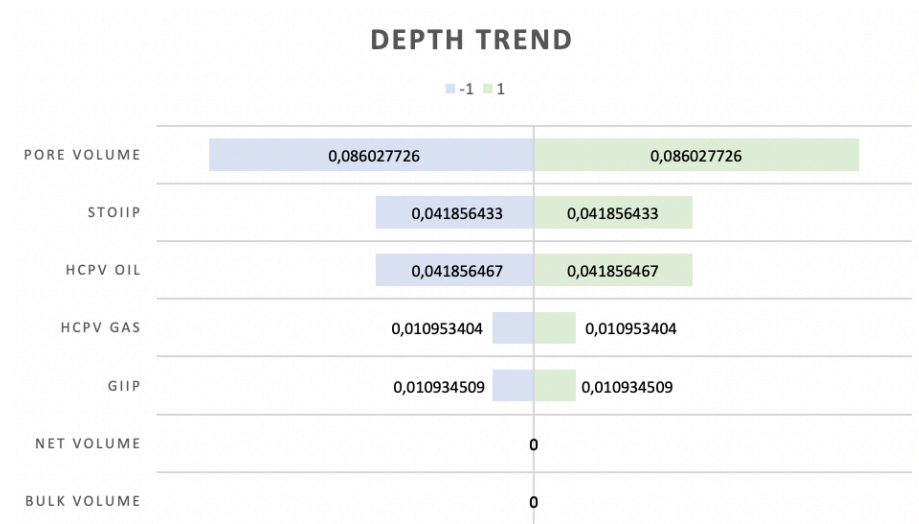
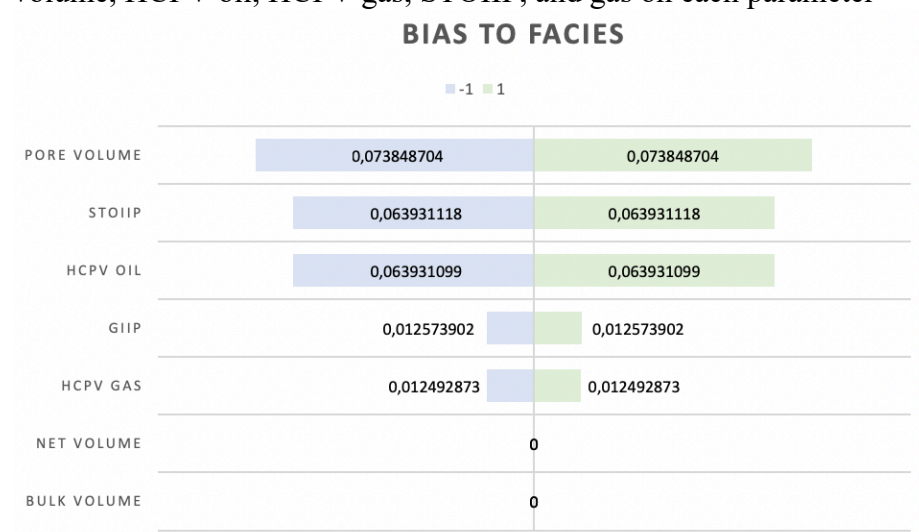
	Bulk Volume	Net Volume	Pore Volume	HCPV oil	HCPV gas	STOIIP	GIIP
Sum (x=1)	7469056	7469056	1220647	770619	241374	642185	68959
Sum (x=-1)	7461762	7461762	1218526	769378	240339	641149	68657
Difference %	0	0	0,0017376	0,00161039	0,00428795	0,00161324	0,00437941
Min (x=1)	7294	7294	952	634	130	528	37
Min (x=-1)	7294	7294	949	632	129	527	37
Difference %	0	0	0,00315126	0,00315457	0,00769231	0,00189394	0
Max (x=1)	7294	7294	1545	924	402	770	115
Max (x=-1)	7294	7294	1568	938	405	782	116
Difference %	0	0	0,01466837	0,01492537	0,00740741	0,01534527	0,00862069
Average (x=1)	7294	7294	1192,03809	752,557617	235,716797	627,133789	67,3427734
Average (x=-1)	7294	7294	1191,13001	752,080156	234,935484	626,734115	67,113392
Difference %	0	0	0,00076178	0,00063445	0,00331463	0,0006373	0,00340618

Nr of Wells

	Bulk Volume	Net Volume	Pore Volume	HCPV oil	HCPV gas	STOIP	GIIP
Sum (x=1)	7469056	7469056	1018654	688302	154845	573574	44237
Sum (x=-1)	7461762	7461762	1420519	851695	326868	709760	93379
Difference %	0	0	0,28290012	0,1918445	0,52627666	0,19187613	0,52626394
Min (x=1)	7294	7294	949	632	129	527	37
Min (x=-1)	7294	7294	1257	746	247	621	71
Difference %	0	0	0,24502784	0,15281501	0,47773279	0,15136876	0,47887324
Max (x=1)	7294	7294	1061	721	184	601	52
Max (x=-1)	7294	7294	1568	938	405	782	116
Difference %	0	0	0,32334184	0,23134328	0,54567901	0,2314578	0,55172414
Average (x=1)	7294	7294	994,779297	672,169922	151,21582	560,130859	43,2001953
Average (x=-1)	7294	7294	1388,58162	832,546432	319,519062	693,802542	91,2795699
Difference %	0	0	0,28360042	0,19263371	0,52673928	0,19266531	0,52672657

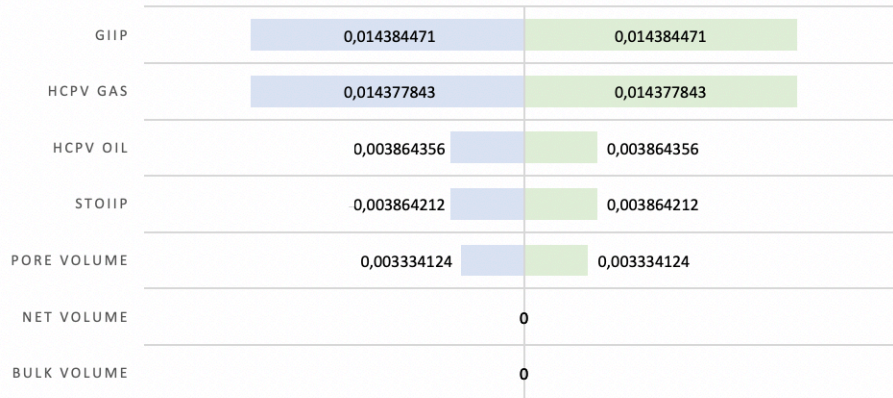
Appendix B

B.1 - Model 1 (Fluvial) Tornado plots of the impact of bulk volume, net volume, pore volume, HCPV oil, HCPV gas, STOIP, and gas on each parameter



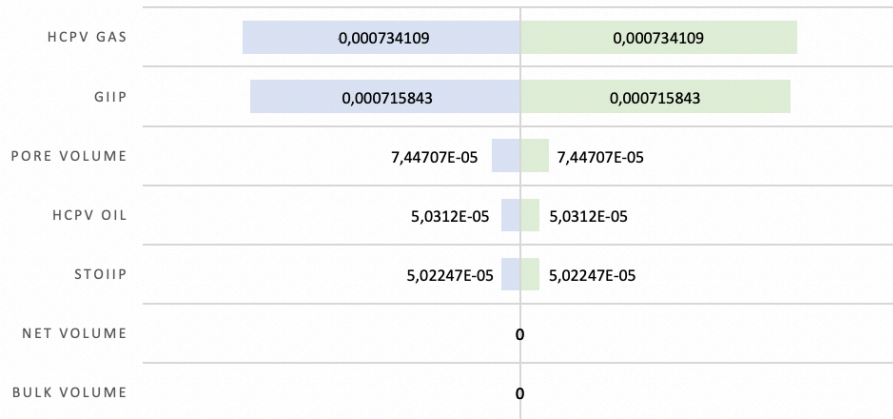
LAYERING

-1 1



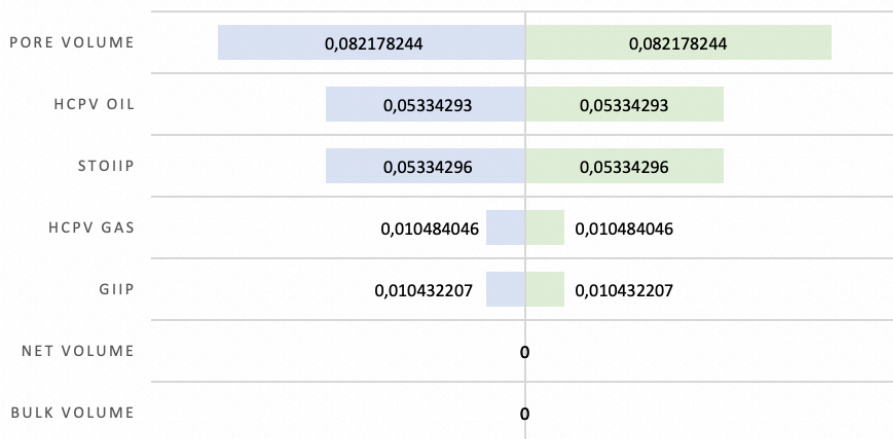
MOST OF VS MID POINT PICK

-1 1

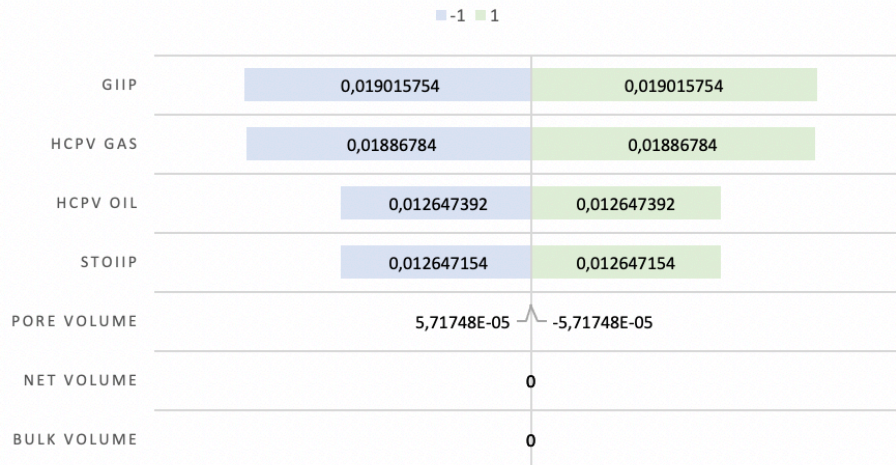


NORMAL VS ASYMMERTRIC DISTRIBUTION

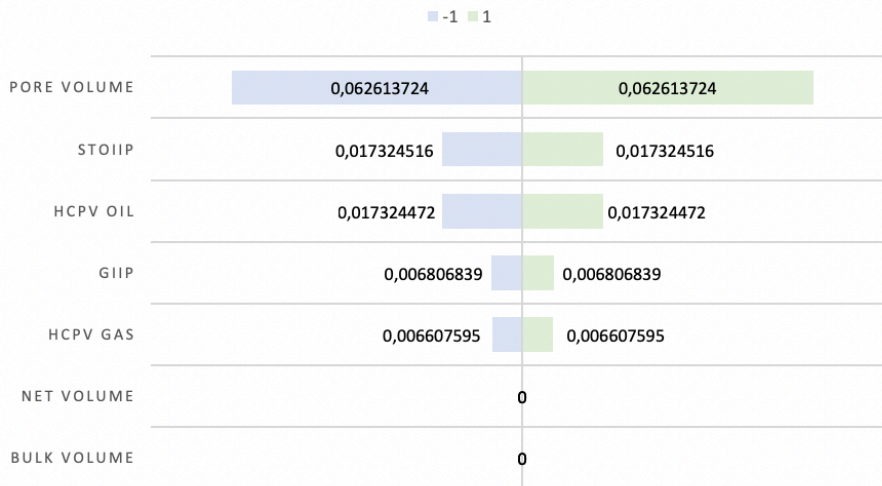
-1 1



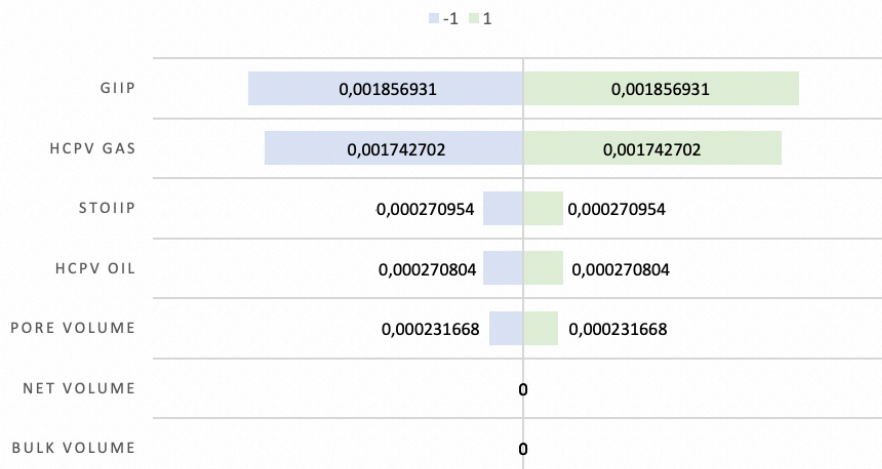
SATURATION HEIGHT FUNCTION



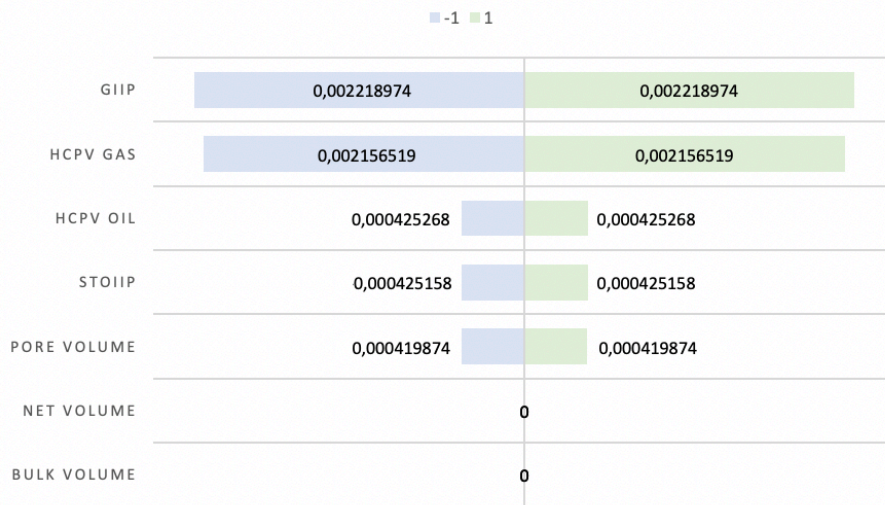
SGS VS KRIGING



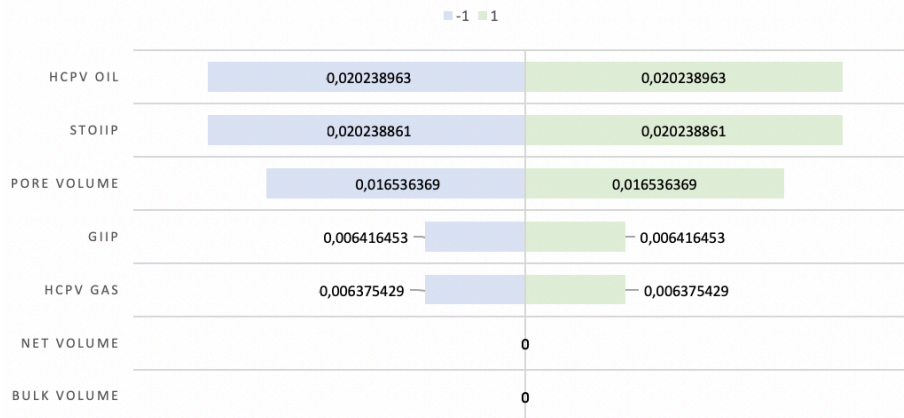
VARIOGRAM RANGE FOR POR AND PERM



VERTICAL PROPORTION CURVE (VPC)

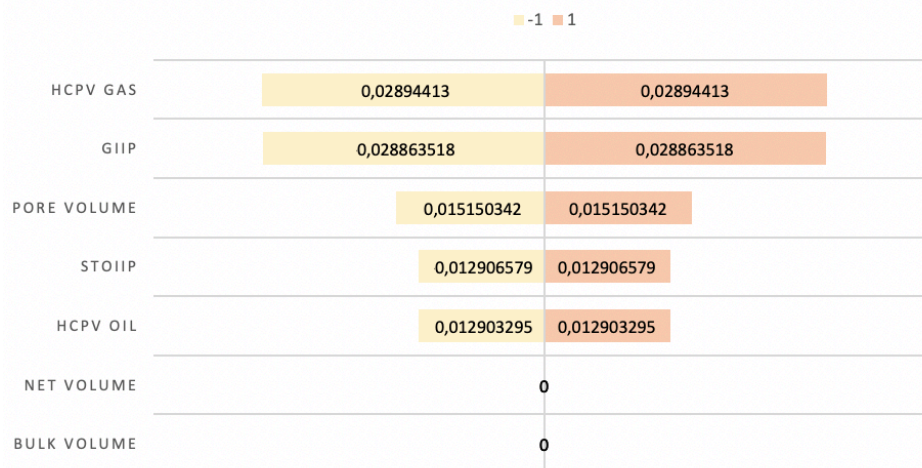


NR OF WELLS

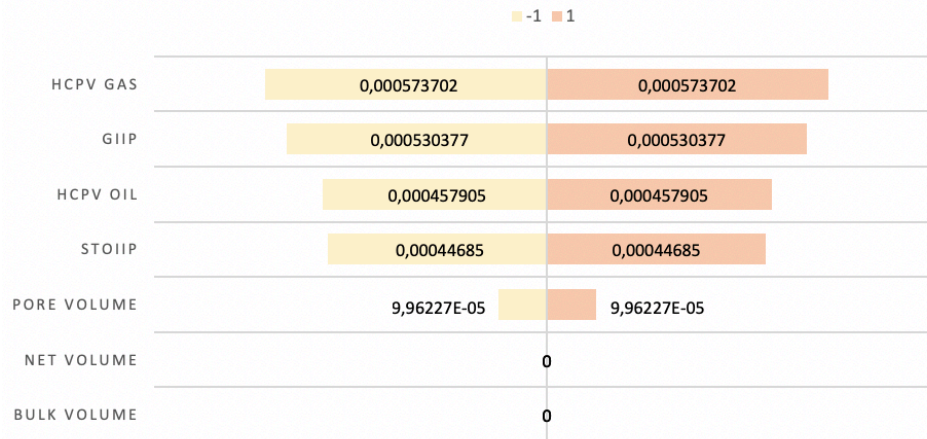


B.2 - Model 2A (Turbidite) Tornado plots of the impact of bulk volume, net volume, pore volume, HCPV oil, HCPV gas, STOIIP, and gas on each parameter

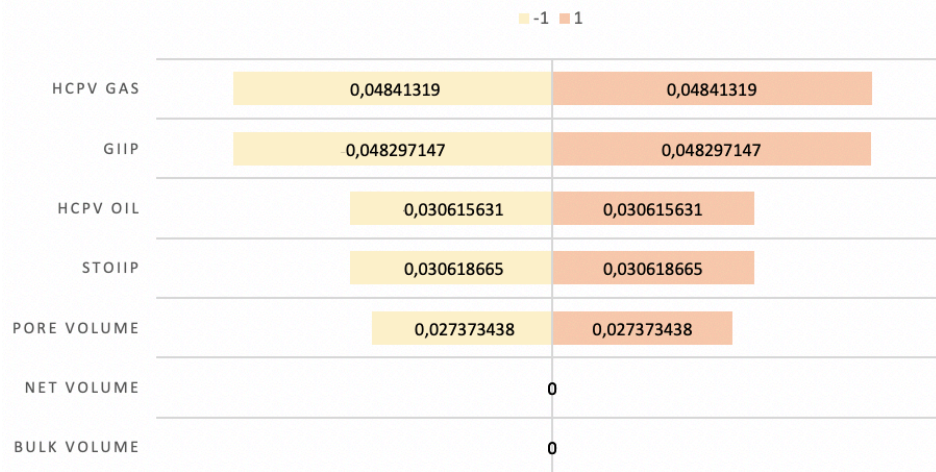
BIAS TO FACIES



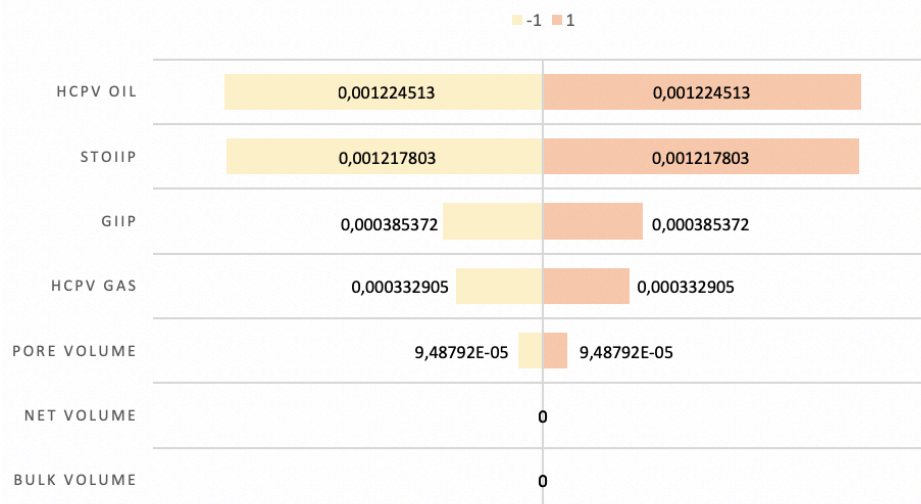
CORRELATION COEFFICIENT



DEPTH TREND



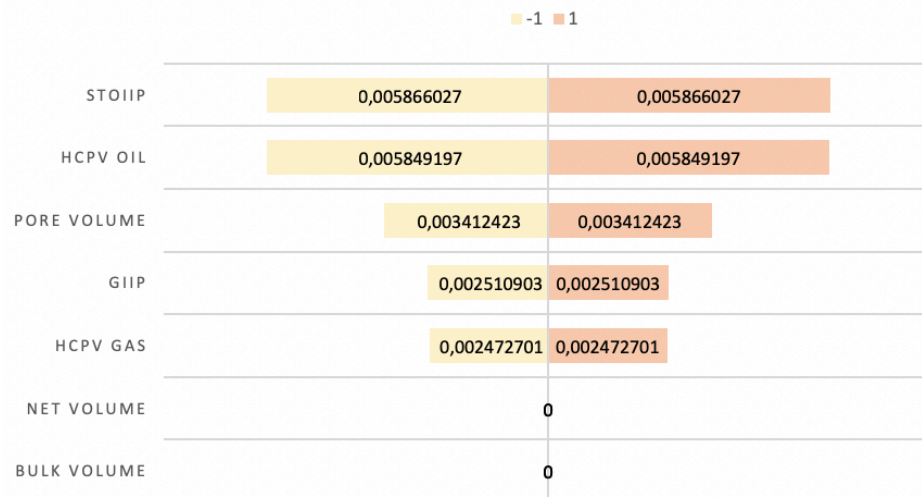
LAYERING



MOST OF VS MID POINT PICK



NORMAL VS ASYMMETRIC DISTRIBUTION

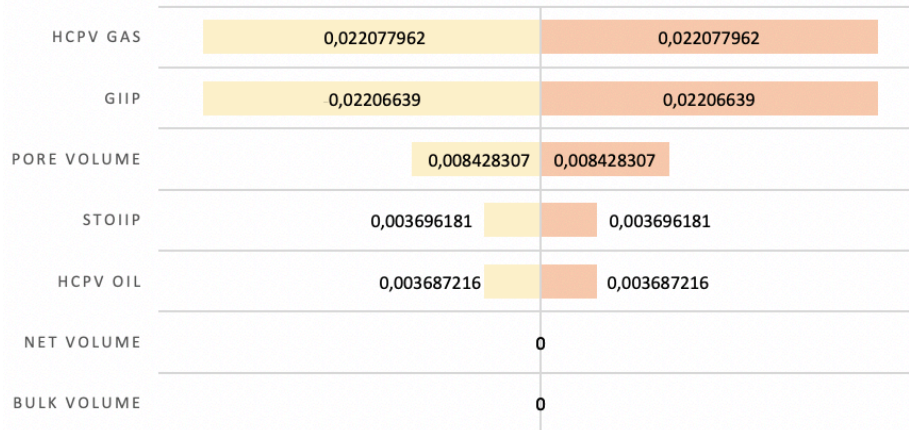


SATURATION HEIGHT FUNCTION



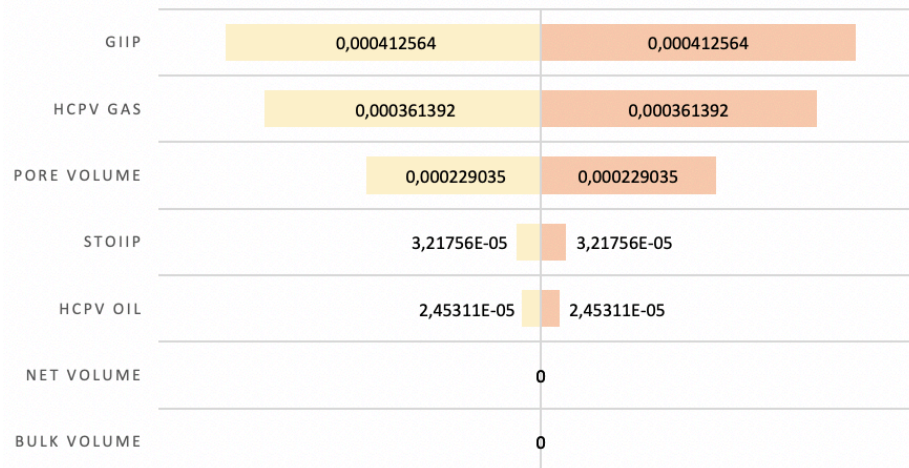
SGS VS KRIGING

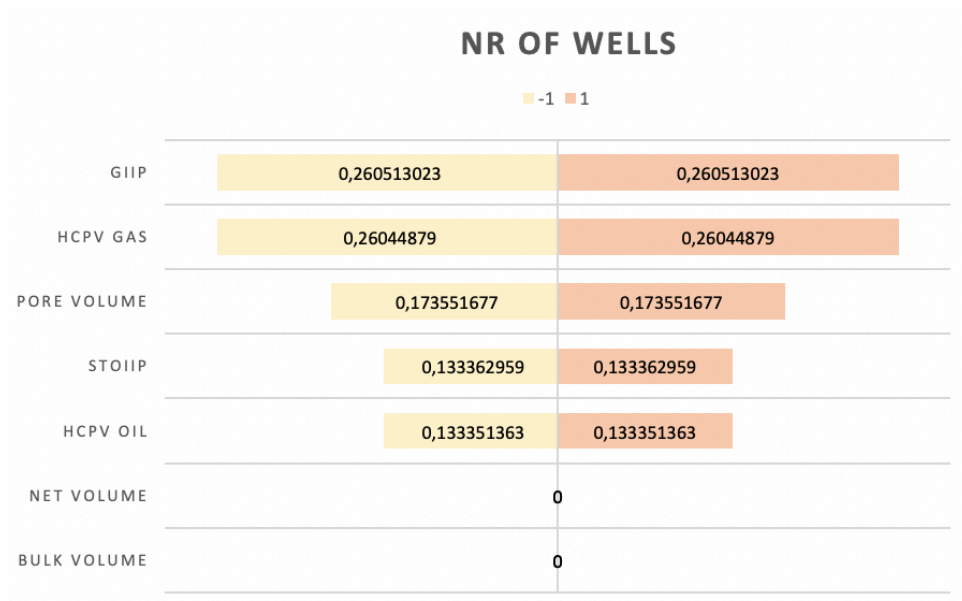
-1 1



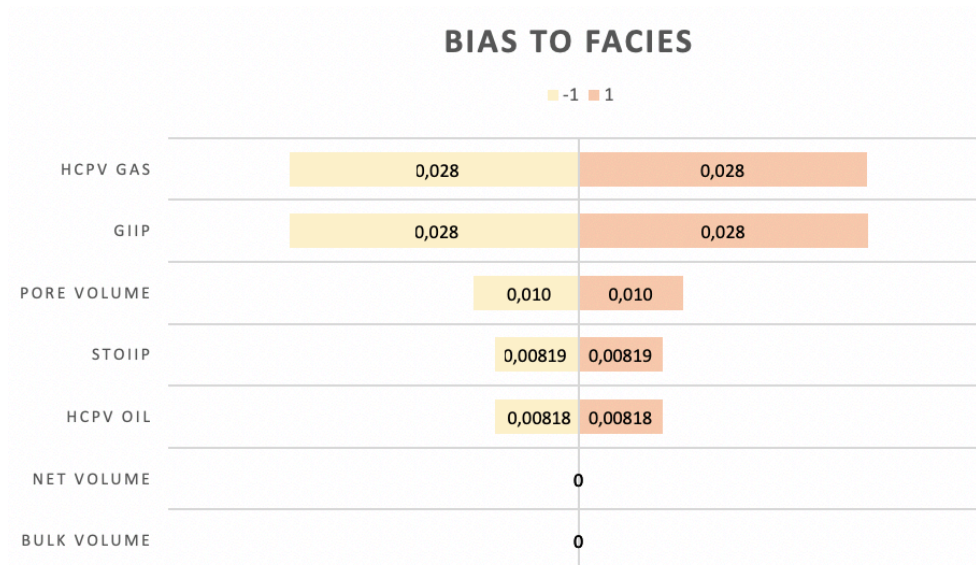
VARIOGRAM

-1 1

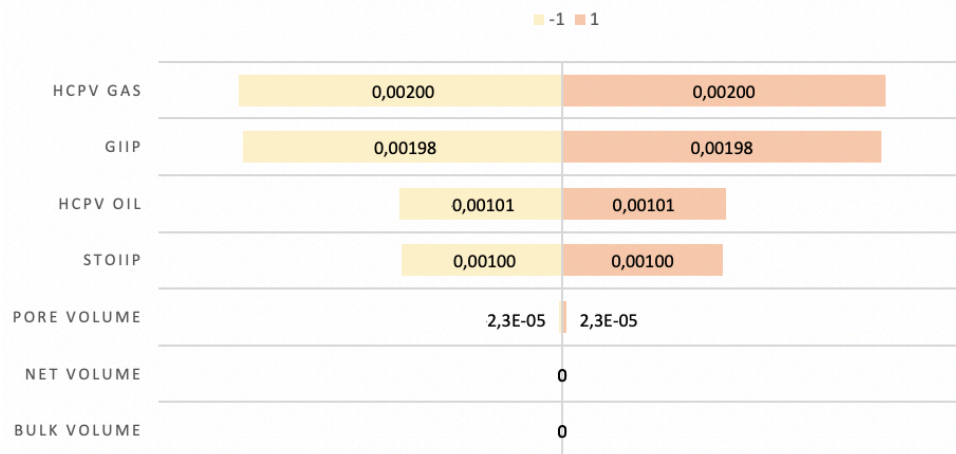




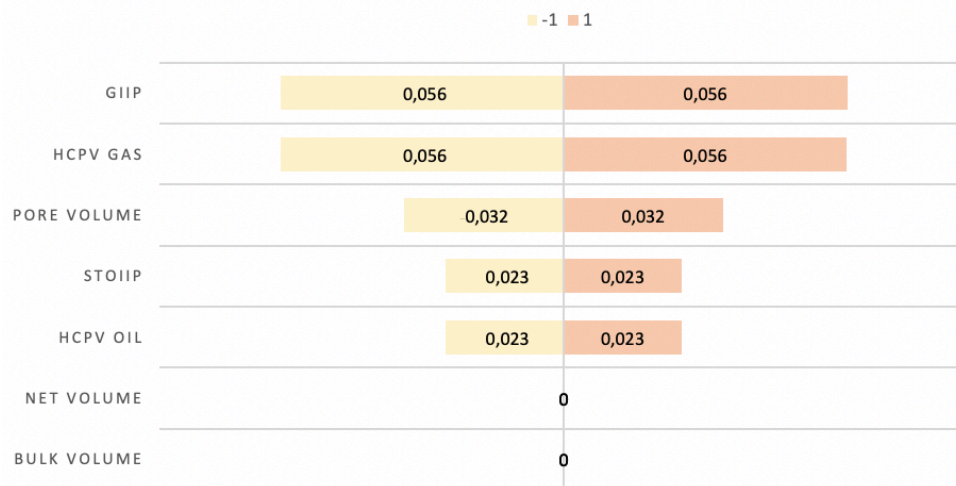
B.3 - Model 2B (Turbidite) Tornado plots of the impact of bulk volume, net volume, pore volume, HCPV oil, HCPV gas, STOIIP, and gas on each parameter



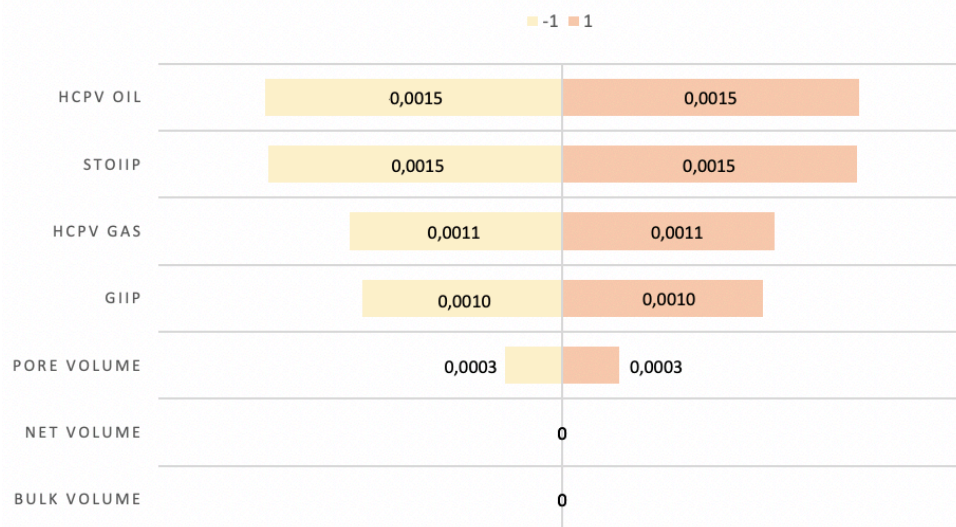
CORRELATION COEFFICIENT



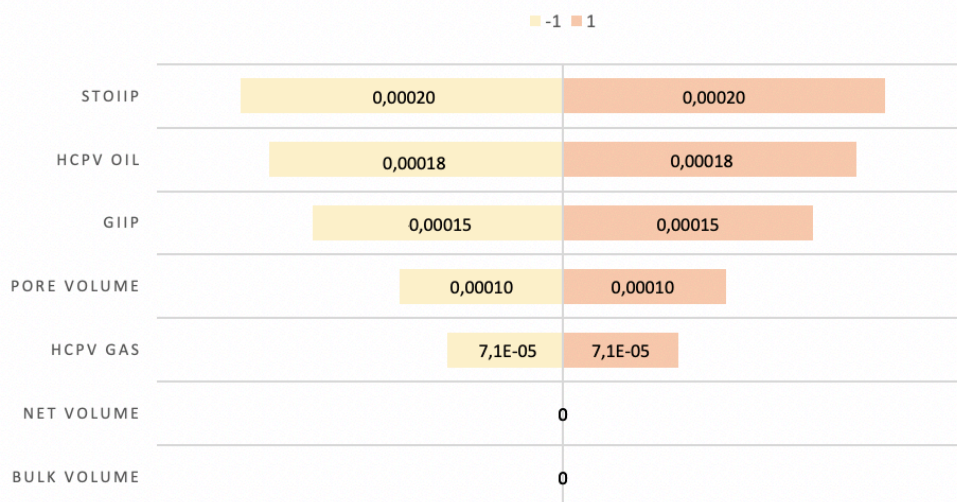
DEPTH TREND



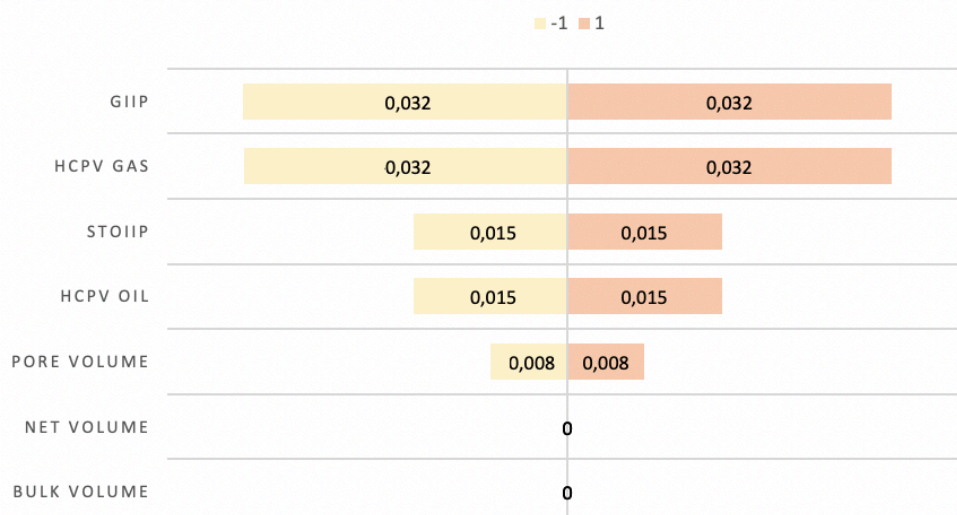
LAYERING



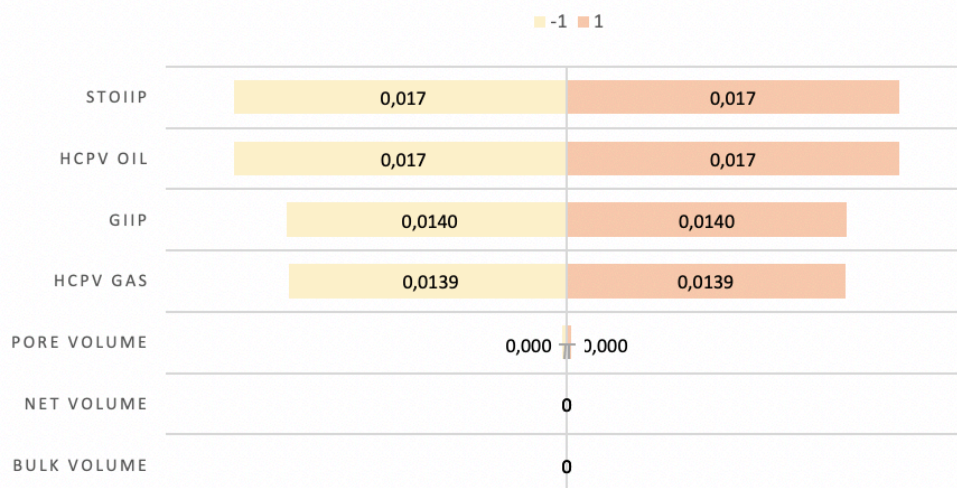
MOST OF VS MID POINT PICK



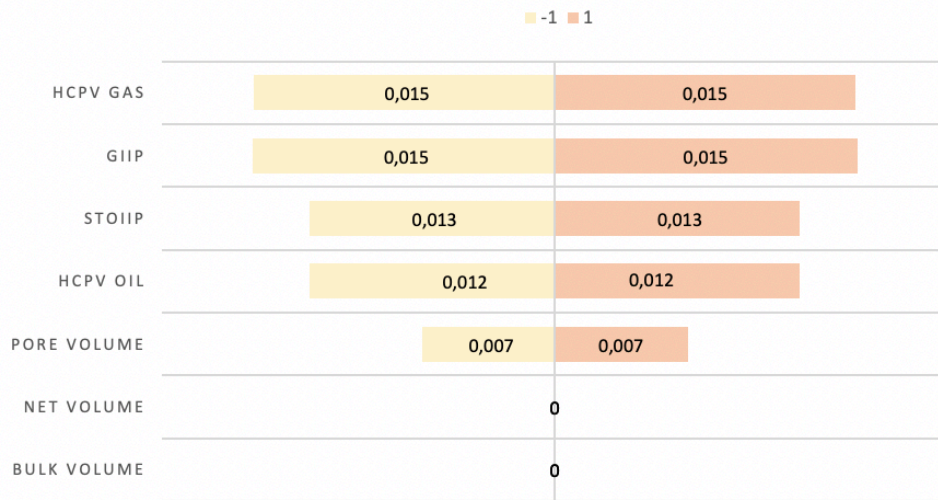
NORMAL VS ASYMMETRIC DISTRIBUTION



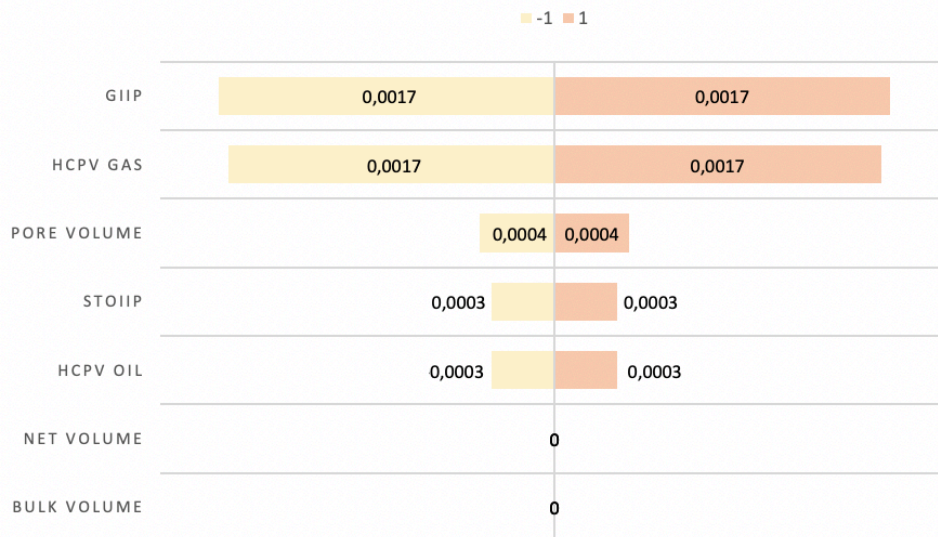
SATURATION HEIGHT FUNCTION



SGS VS KRIGING



VARIOGRAM



NR OF WELLS

